SEMI-ANALYTICAL SOLUTION FOR MULIPHASE FLUID FLOW APPLIED TO CO_2 SEQUESTRATION IN GEOLOGIC POROUS MEDIA.

A Dissertation

by

AHMED MOHAMED ANWAR SAYED MOHAMED

Submitted to the Office of Graduate Studies of
Texas A&M University
in partial fulfillment of the requirements for the degree of

DOCTOR OF PHILOSOPHY

Chair of Committee,	David Sparks
Co-Chair of Committee,	Hongbin Zhan
Committee Members,	John R. Giardino
	Mark Everett
	Hisham Nasr El-Din
Head of Department,	John R. Giardino

August 2013

Major Subject: Geology

ABSTRACT

The increasing concentration of CO_2 has been linked to global warming and changes in climate. Geologic sequestration of CO_2 in deep saline aquifers is a proposed greenhouse gas mitigation technology with potential to significantly reduce atmospheric emissions of CO_2. Feasibility assessments of proposed sequestration sites require realistic and computationally efficient models to simulate the subsurface pressure response and monitor the injection process, and quantify the risks of leakage if there is any. This study investigates the possibility of obtaining closed form expressions for spatial distribution of CO_2 injected in brine aquifers and gas reservoirs.

Four new semi-analytical solutions for CO_2 injection in brine aquifers and gas reservoirs are derived in this dissertation. Both infinite and closed domains are considered in the study. The first solution is an analysis of CO_2 injection into an initially brine-filled infinite aquifer, exploiting self–similarity and matched asymptotic expansion. The second is an expanding to the first solution to account for CO_2 injection into closed domains. The third and fourth solutions are analyzing the CO_2 injection in infinite and closed gas reservoirs. The third and fourth solutions are derived using Laplace transform. The brine aquifer solutions accounted for both Darcyian and non-Darcyian flow, while, the gas reservoir solutions considered the gas compressibility variations with pressure changes.

Existing analytical solutions assume injection under constant rate at the wellbore. This assumption is problematic because injection under constant rate is hard to maintain, especially for gases. The modeled injection processes in all aforementioned solutions are carried out under constant pressure injection at the wellbore (i.e. Dirichlet boundary condition). One major difficulty in developing an analytical or semi-analytical solution involving injection of CO_2 under constant pressure is that the flux of CO_2 at the wellbore is not known. The way to get around this obstacle is to solve for the pressure wave first as a function of flux, and then solve for the flux numerically, which is subsequently plugged back into the pressure formula to get a closed form solution of the pressure. While there is no simple equation for wellbore flux, our numerical solutions show that the evolution of flux is very close to a logarithmic decay with time. This is true for a large range of the reservoir and CO_2 properties.

The solution is not a formation specific, and thus is more general in nature than formation-specific empirical relationships. Additionally, the solution then can be used as the basis for designing and interpreting pressure tests to monitor the progress of CO_2 injection process. Finally, the infinite domain solution is suitable to aquifers/reservoirs with large spatial extent and low permeability, while the closed domain solution is applicable to small aquifers/reservoirs with high permeability.

DEDICATION

To my family

ACKNOWLEDGEMENTS

The ideas in this work are not all mine. Many people contributed on many levels. It would probably take another dissertation to fully recognize all of them, so I humbly apologize to the people who I do not have the space to thank here.

On an academic level, the biggest contributors were my advisors Hongbin Zhan and David Sparks. I sincerely thank both of them for their help and many discussions.

I also would like to thank my committee members, Dr. John R. Giardino, Dr. Hisham Naser El-Din, Dr. Mark Everett, for their guidance and support throughout the course of this research. Dr. Giardino, thank you for solving my funding problem this semester! Dr. Naser El-Din, thank you for your numerous wonderful recommendation letters! I also thank Dr. Mark Everett a lot for giving me the chance to be with him in one of his field trips.

On an emotional level, the biggest contributors were my mother, my father, and my wife. I sincerely thank them for their constant support and for understanding that good work takes a long time.

TABLE OF CONTENTS

Page

ABSTRACT……..…….…… ii

DEDICATION …….. iv

ACKNOWLEDGEMENTS……..…….…. v

TABLE OF CONTENTS…….…….…. vi

LIST OF FIGURES…….…….…. viii

LIST OF TABLES…….…… xi

1. INTRODUCTION…….……. 1

   1.1 Motivation and Background ……..…….....……... 1
   1.2 Objectives ……. 7
   1.3 Organization …….. 8

2. PRESSURE BUILDUP IN INFINTE BRINE AQUIFERS DURING CO_2 SEQUESTRATION UNDER CONSTANT INJECTION PRESSURE……. 9

   2.1 Introduction ……..... 9
   2.2 Conceptual and Mathematical Model …… 11
   2.3 Solution Development ……..... 15
   2.4 Results and Discussion ……...…… 39
   2.5 Summary and Conclusions…….. 48

3. PRESSURE BUILDUP IN BRINE CLOSED AQUIFERS DURING CO_2 SEQUESTRATION UNDER CONSTANT INJECTION PRESSURE……. 50

   3.1 Introduction ……... 51
   3.2 Conceptual Model ……..…… 56
   3.3 Mathematical Model …….. 59
   3.4 Solution Development …… 62
   3.5 Results and Discussion ……...…… 78

4. PRESSURE BUILDUP DURING CO_2 INJECTION THROUGH FULL-PENETRATING WELLS IN INFINITE AND CLOSED GAS RESERVOIR. 87

4.1 Introduction ……...…. 87
4.2 Conceptual Model ……..…… 91
4.3 Mathematical Model …….. 95
4.4 Solution Development …… 99
4.5 Results and Discussion ……..……. 103

5. SUMMARY AND CONCLUSIONS ……..... 113

5.1 Contributions …….. 116
5.2 Future Work ……... 116

NOMENCLATURE……..... 118

REFERENCES……..... 124

LIST OF FIGURES

Page

Fig. 2.1 Schematic diagram of CO_2 injection into brine aquifer under constant pressure…….. 12

Fig. 2.2 Plot of dimensionless flux vs. dimensionless time for 100 different combinations of α and γ……. 28

Fig. 2.3 Plot of numerically-determined dimensionless flux vs. time, along with a best-fit logarithmic approximation for a system α=0.009 and γ=0.1……..... 29

Fig. 2.4 Contours of the slope parameter, a_1, in (2-66) for a range of values of α and γ……... 31

Fig. 2.5 Contours of the slope parameter, a_0, in (2-66) for a range of values of α and γ……... 32

Fig. 2.6 The slope values from Fig. 2.4 plotted as a surface vs. α and γ , and a fitted polynomial in α and γ (points)…… 33

Fig. 2.7 The slope values from Fig. 2.5 plotted as a surface vs. α and γ , and a fitted polynomial in α and γ (points).……..... 34

Fig. 2.8 Pressure vs. radial distance at 10 year intervals after the beginning of pumping……. 41

Fig. 2.9 Change in pressure over a 5 year period vs. radial distance, for 4 different periods (2015-2010, 2020-2015, 2040-2035, and 2080-2075)…….. 42

Fig. 2.10 Predicted pressure buildup as a function of time at specific radial distances (r= 25 m, 100 m, 1000 m, 3000 m, and 4000 m)……... 43

Fig. 2.11 Cumulative pressure difference as a function of radial distance…….. 45

Fig. 2.12 Predicted cumulative injected CO_2 volume as a function of time……. 47

Fig. 2.13 Predicted cumulative injected CO_2 mass as a function of time……. 48

Fig. 3.1	Schematic diagram of CO_2 injection into closed brine aquifer under constant pressure……..	58
Fig. 3.2	Plot of a schematic diagram shows pseudosteady state conditions in radial flow system…….	66
Fig. 3.3	Predicted pressure vs. radial distance at different times for different years since injection begins ……..	80
Fig. 3.4	Predicted pressure increases over 3 different 5-year periods (2015-2010, 2025-2010, and 2030-2010) as a function of radial distance…..	81
Fig. 3.5	Comparison of predicted pressure buildup as a function of time at specific radial distances (r= 25 m, 100 m, 1000 m, 3000 m, and 4000 m)…….……..	82
Fig. 3.6	Pressure increase after 100 years of pumping as a function of radial distance……..	84
Fig. 3.7	Expected cumulative injected CO_2 mass vs. time……..……	85
Fig. 3.8	Expected cumulative injected CO_2 volume vs. time…….…….	86
Fig. 4.1	Schematic diagram of CO_2 injection into gas reservoir under constant pressure at the wellbore…….	94
Fig. 4.2	Predicted pressure buildup as a function of radial distance at different times (infinite reservoir)……	105
Fig. 4.3	Expected pressure buildup vs. time at specific radial distances (r= 25 m, 100 m, 1000 m, 3000 m, and 4000 m).....……..	106
Fig 4.4	Pressure increase over five different 5-year periods (0-5, 5-10, 10-15, 15-20, 20-25 years after beginning of injection) as a function of radial distance. The position of the peak difference, which changes in time, shows the progression of the diffusing pressure front…..……	107
Fig. 4.5	Cumulative pressure buildup as a function of radial distance……..	108
Fig. 4.6	Predicted injection rate at the wellbore vs. time……	110

Fig. 4.7 Calculated cumulative injected CO_2 volume vs. time……..…. 111

Fig. 4.8 Calculated cumulative injected CO_2 mass vs. time……..……. 112

LIST OF TABLES

		Page
Table 2.1	Polynomial coefficients of the slope and the intercept with 95% confidence bounds…….	34
Table 2.2	Summary of goodness of fit of the slope, the intercept and the flux, shows SSE (sum of squared errors), R^2 (the correlation coefficient), and RMSE (residual mean squared error)…….	35
Table 2.3	Geometrical and physical properties of the storage formation, initial and boundary conditions, and injection pressure used in computations…….	40
Table 3.1	Model parameters used in closed brine aquifer calculations…..…….	79
Table 4.1	The coefficients a_n range of values [*Mukhopadhyay et al.* 2012].……	96
Table 4.2	Input data used in gas reservoir computations.....	104

1. INTRODUCTION

1.1 Motivation and Background

The continued use of fossil fuel, including coal, to power the generation of electricity since the industrial revolution has released huge amounts of CO_2 to the atmosphere. These emissions have led to a significant increase of CO_2 concentration in the atmosphere. Pre-industrial CO_2 concentrations were around 280 parts per million in volume (ppmv). Since then, CO_2 concentration has increased to 392 ppmv in 2011, increasing at a rate of 2.0 ppm/year during the last decade. Current predictions are that CO_2 emissions will continue increasing at similar rates over the coming years. Now there is almost a scientific agreement that there is a direct relationship between anthropogenic CO_2 emission and climate change. Large power plants among other stationary sources of emissions are responsible for significant amounts of emissions. However, recent technologies can offer a good possibility to reduce the emissions from these stationary sources through carbon capture and sequestration (CCS). Although, CCS is a temporally solution to the CO_2 emission problem, it offers the use of carbon-based energy sources and the control of CO_2 emissions simultaneously [*Krey and Riahi* 2009; *Meinshausen et al.* 2011; *MIT* 2007]. CCS will remain the only available current solution to CO_2 emissions problem, until an economically feasible carbon-free energy alternative can be developed and deployed.

CCS consists of three stages; CO_2 capture, CO_2 transport, and then the injection and storage in deep geological formations. Various types of geological formations have high potentiality for CO2 storage. These include un-minable coal seams, depleted oil and gas reservoirs and deep confined saline aquifers [*Bachu* 2000, 2008; *Bachu and Celia* 2009; *Birkholzer and Zhou* 2009; *Gale* 2004; *Gunter et al.* 1997; *Hepple and Benson* 2005; *Holloway* 2005; *IPCC* 2005, 2007a, 2007b, 2007c; *Metz et al.* 2005; *Oldenburg* 2006; *Vilarrasa et al.* 2013; *Vilarrasa et al.* 2010b]. Of these three main subsurface formations, confined saline deep aquifers have received particular attention due to their high CO_2 storage capacity and wide availability throughout the world [*Gasda et al.* 2004; *Gasda et al.* 2009; *Nordbotten and Celia* 2006a, 2006b; *Nordbotten et al.* 2005b].

The geo-sequestered CO_2 has to be in a supercritical state (i.e. pressures greater than 72. 8 atm and temperatures above 30.978 °C) to ensure effective storage (high CO_2 density). Supercritical CO_2 has a density of about 467.6 kg/m^3 which allows significantly greater quantities to be sequestered than if it existed in the gas-phase [*Holloway and Savage* 1993; *Van der Meer* 1992]. Conditions that support the existence of supercritical CO_2 should be present at depths greater than about 800 m where pressure and temperature would be above the critical point of CO_2. Although,supercritical CO_2 reaches relatively high densities, its density and viscosity still remain lower than the density of the resident brine [*Bachu* 2003]. Thus, CO_2 will tend to show significant gravity override and float on the top of brine under the cap rock.

Injection of CO_2 into deep geological formations is achieved by creating a pressure difference between the fluids in the injection well and the formation fluids. A larger pressure differential will clearly force CO_2 more rapidly to invade the formation and replace its fluids. This may reduce the time and cost needed to complete the injection process. However, large injection rates can seriously raise the pressure in the storage formation and cause damage to the formation creating hydraulic fractures or rejuvenating old ones. Accordingly, the spatial and temporal distribution of pressure buildup in the formation is serious process and needs to be monitored. Obviously it depends on the rate of injection, the permeability, porosity, thickness of the storage formation, and the presence of faults or permeability barriers through the storage formation.

The analysis of CCS problem always involves some set of computational models to provide a mathematical description of the problem. These models can have many purposes, but eventually they have to answer some practical questions about the injection system. These questions include the size of the CO_2 plume, the spatial extent of pressure-perturbation, the possibility of leakage of fluids out of the injection formation, and the long-term fate of the injected CO_2. Answers to these questions require models; the general approach to model CCS systems is to write standard conservation equations of fluid flow and transport. Then couple these equations with material-dependent constitutive relationship to build up a system of coupled nonlinear partial differential equations. These equations can be solved numerically in three dimensions. However, the

level of numerical discretization is always limited by two factors; the available computing power and the available information about the injection system before the time of injection. These limitations have motivated the development of a new set of analytical, semi-analytical and approximate solutions of CCS problem.

Analytical solutions, including the ones that will be developed here, are based on certain simplifying assumptions regarding the underlying processes. Consequently, the predictions from an analytical solution are likely to be less accurate than those based on elaborate numerical simulations using extensive site-specific information. However, these analytical solutions often prove useful in providing guidelines, particularly before the start of the actual injection process, when very little about the storage formation has been ascertained.

Over the years, a large number of analytical and semi-analytical solutions have been developed for flow of gases through porous and permeable formations. More recently and with immediate relevance to subsurface injection of CO_2, Saripalli and McGrail [2002] developed semi-analytical solutions for modeling deep well injection of CO_2 into brine formations. Also, Nordbotten and Celia [2005b] provided a similarity solution for CO_2 injection into brine aquifers. Nordbotten and Celia [2005b] solution overlooked both the formation and fluid compressibility, however, they mentioned in their article some hints on how systems that are slightly compressible can be handled. As observed latter by Mathias et al. [2009a], a limitation of these semi-analytical solutions

is that they are developed assuming that both the geological formations and the fluids are incompressible and developed an approximate similarity solution describing the spatial and temporal distribution of pressure resulting from CO_2 injection in brine aquifers. These pressure buildup results were latter used for assisting in selection of CO_2 sequestration sites by Mathias et al. [2009b] and developing an explicit approximate solution for estimating pressure buildup due to injection of CO2 into closed brine aquifers of finite radial extent [*Mathias et al.* 2011]. Other analytical solutions have also been obtained for estimating risks of pressure buildup resulting from CO_2 injection [*Oruganti et al.* 2011] and for pressure buildup in overlying formations [*Zeidouni et al.* 2009].

Although Al-Hussainy et al. [1966] has mentioned that compressibility of gases, whether behaving ideally or otherwise, is a function of pressure, some of these previous works [*Mathias et al.* 2009a; *Mathias et al.* 2009b; *Zhou et al.* 2009] have assumed that the gas compressibility is constant and independent of pressure. In some of those studies [*Mathias et al.* 2009a; *Mathias et al.* 2009b], it has been further assumed that the gas compressibility is comparable to the compressibility of water. Vilarrasa et al. [2010b], has noted that CO_2 compressibility is one to two orders magnitude larger than that of the rock or water. In addition, Vilarrasa et al. [2010b] investigated the impact of CO_2 compressibility on CO_2 storage and proposed a method to account for compressibility effects and viscosity variations. Vilarrasa et al. [2010b], however, applied it to the analytical solutions of Nordbotten et al. [2005b] and Dentz and

Tartakovsky [*Dentz and Tartakovsky* 2009a, 2009b] without actually specifying a relationship (such as an equation of state) between density (or, compressibility) and pressure. Instead, they iteratively solved a non-linear integral equation to obtain the mean density within a plume volume. Mukhopadhyay et al. [2012]showed that a solution can be obtained through specification of a suitable equation of state. Moreover, their conceptual model accounts for the partial penetration of the injection well.

All the analytical or semi-analytical solutions described above pertain to pressure buildup resulting from CO_2 injection in either brine aquifers or gas reservoirs under constant injection rate. However, injection of gases under constant rates is almost always impossible to maintain. Following Wiese and Mathias [2010], the focus of this study is to develop a semi-analytical solution to predict the spatial and temporal nature of CO_2 extent and the pressure buildup under constant pressure injection, which is more appropriate from the practical perspective. One major difficulty in developing an analytical or semi-analytical solution involving injection of CO_2 under constant pressure is that, the flux of CO_2 at the wellbore is not known. The flux can be solved for numerically by iteration, but we demonstrate that we can write a close analytic approximation for wellbore flux.

The solutions developed here are not formation specific, and thus are more general in nature than formation-specific empirical relationships. Additionally, the

solutions then can be used as the basis for designing and interpreting pressure tests to monitor the progress of CO_2 injection process.

1.2 Objectives

The objective of this study is to derive a closed form solution for the problem of CO_2 sequestration in brine aquifers using the method of matched asymptotic expansion. The solution will be extended to include both infinite-acting and closed aquifers. Large time approximation of this solution will be derived to account for inertial effects using the Forchheimer equation. Another objective of the study is to develop an approximate solution for CO_2 injection in gas reservoirs using Laplace transform. The gas compressibility variation with pressure will be considered. By allowing for injection rate to vary with time in all aforementioned cases, this study improves on previous work by not requiring injection under constant rate, which is practically inconvenient. These solutions can be used to rapidly calculate the pressure buildup during injection, as well as, the rate of pressure falloff once injection stops. It is applicable for both open and closed systems. In addition, it can be used as the basis for designing and interpreting pressure tests as a method of monitoring the progress of CO_2 injection operations. Both solutions are simple to evaluate making them easy to implement in commonly available spreadsheet type software.

1.3 Organization

The dissertation is organized into five sections. Section 2 gives solutions for the spread of the gas phase that occurs when CO_2 is injected into an initially brine-filled aquifer of infinite extent. Section 3 describes a similar problem in a finite aquifer, which requires a different analytic approach. Section 4 applies a third semi-analytic technique to study injection into gas reservoirs, in which the compressibility of the gas is explicitly taken into account. This dissertation is ended with a brief summary and several conclusions in section 5.

2. PRESSURE BUILDUP IN INFINTE BRINE AQUIFERS DURING CO_2 SEQUESTRATION UNDER CONSTANT INJECTION PRESSURE

2.1 Introduction

Geologic sequestration of CO_2 in deep saline aquifers is a proposed greenhouse gas mitigation technology with potential to significantly reduce atmospheric emissions of CO_2 from large, stationary point sources such as fossil fuel burning power plants. Deep saline aquifers are particularly attractive since they have little value as water sources due to their high salt content. Deep saline aquifers are also considered to have the largest sequestration capacity [*IPCC* 2007c], estimated from 10,000 to 200,000 billion tons [*Bruant et al.* 2002]. Aquifers currently being studied for CO_2 storage include the Mt. Simon in the Illinois Basin [*Zhou et al.* 2009], the Frio along the Gulf Coast of Texas [*Hovorka et al.* 2001], the Johansen under the North Sea [*Bergmo et al.* 2011], and the Nisku in the Alberta Basin in western Canada [*Michael et al.* 2010].

Though CO_2 injection in brine aquifers is an existing technology, the few currently operating projects are much smaller in scale than what is being proposed for greenhouse gas control. For example, the In Salah project injects approximately 1.2 million tons per year (Mt/yr) of CO_2 [*Wright* 2007], while a single 500 MW coal generated power plant produces about 3.8 Mt/yr [*Rao and Rubin* 2002]. The pressure increase due to injection must be kept below a fracture pressure limit to avoid fracturing the caprock above the storage aquifer, which would lead to leakage of CO_2 back to the

atmosphere. Assessment of any proposed sequestration site requires realistic, computationally efficient models to simulate the subsurface pressure response and the size of the plume extent. Computer simulations are an essential tool for assessing the feasibility of CCS projects. Such simulations are used to predict the magnitude and spatial extent of the subsurface pressure increase due to injection as well as model the evolution of the injected CO_2 plume and monitor the injection process. However, they require significant computational efforts and tremendous amount of input data which might not be available as a priori.

Analytical solutions are more convenient in terms of implementation, especially at the beginning of CCS operation, when data about the injection site is limited. They are also efficient in terms of computational cost, as they can be accessible using spreadsheet software. Nevertheless, the derivation of analytical solutions gives rise to many limiting restrictions with regards to boundary conditions, simulated processes and/or input parameters.

An important analytical solution for assessing CCS potential in brine aquifers was introduced by Nordbotten et al. [2005b] describing the migration of a CO_2 plume front under constant injection rate of CO_2 into a homogeneous and confined aquifer. Mathias et al. [2009a] built on this work by evaluating an integral expression for pressure buildup and incorporating the presence of fluid and rock compressibility. However, in most situations, injection pressure should be maximized to ensure the

highest possible injection rate that does not exceed the fracture pressure of the storage formation; therefore a constant pressure boundary is preferred. Later Wiese and Mathias [2010] extended the solution of Mathias et al. [2009a] further, and applied a constant injection pressure. However, they did not provide a closed form solution for either the flux at the wellbore or for the pressure distribution function. This work describes the development of an approximate closed form solution for CO_2 injection under constant injection pressure.

2.2 Conceptual and Mathematical Model

Figure 2.1 shows the schematic diagram of CO_2 injection into an infinite, confined brine aquifer. We assume axisymmetry about the wellbore, with the origin of the cylindrical coordinate system at the aquifer base; the *z* axis is vertical and positive upward and through the center of the well; the *r* axis is radially horizontal. The injection well is fully penetrating the aquifer vertically and is perforated along the entire thickness of the aquifer H [L]. The top and bottom of the aquifer are impermeable for both CO_2 and brine flow. The injection process is running under a known constant pressure, P_o [$ML^{-1}\ T^{-2}$], at the wellbore, instead of constant injection rate. In other words, the injection rate is allowed to vary with time during the injection process.

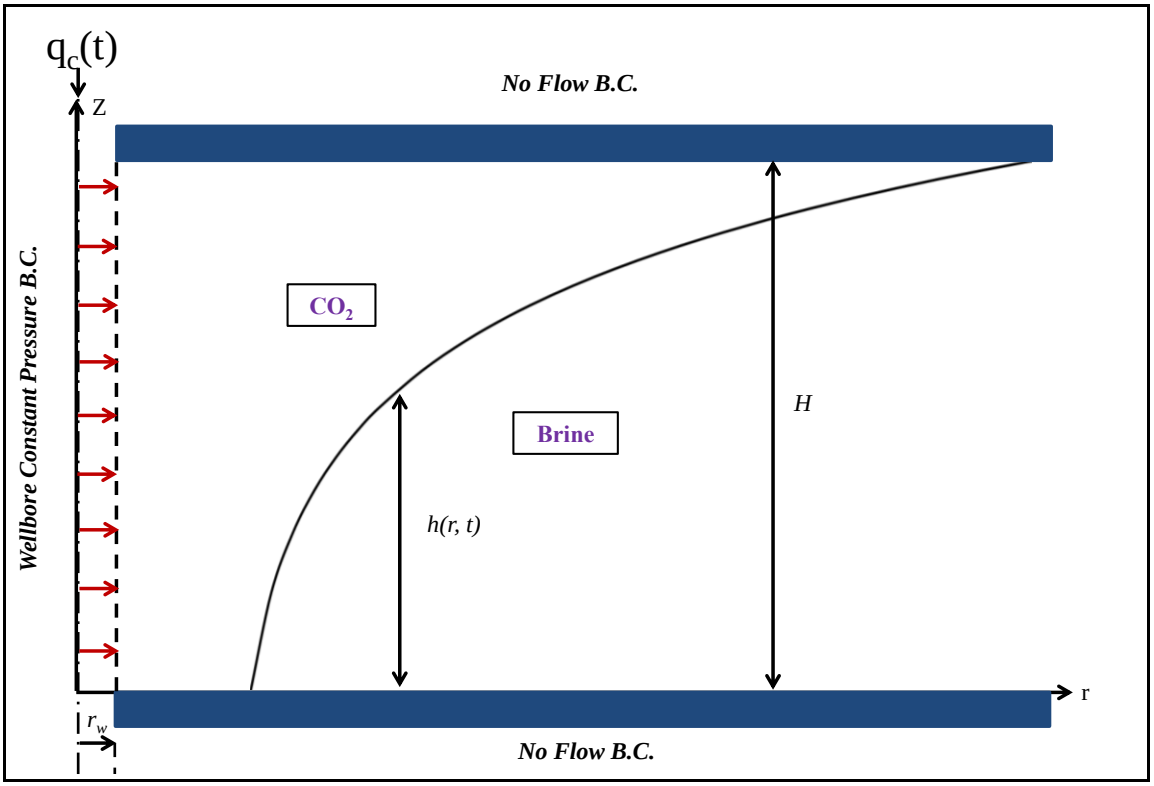

Figure 2.1: Schematic diagram of CO_2 injection into brine aquifer under constant pressure.

In this problem we assume that neither the pressure perturbation nor the invading CO_2 front reach the lateral boundaries of the aquifer during the time of interest; therefore we can treat the aquifer as of infinite radial extent. Following Nordbotten et al. [2005a], the interface between the injected CO_2 and the brine is assumed to be sharp and located at an elevation, h [L], above the base of the aquifer. CO_2 have lower density than brine, and is assumed to stay on the upper side of the interface, while brine only will be on the lower side. Capillary pressure is ignored, and the pressure, P [$ML^{-1}T^{-2}$], is assumed to be in vertical equilibrium over the entire thickness, H, of the aquifer. In other words,

because the lateral extent of the aquifer is much greater than its thickness, we can assume that most of the gradients in pressure are horizontal. Therefore, the vertical pressure gradient is ignored; this may not significantly affect the pressure build up in the proposed study, since the well is screened along the total aquifer thickness. Relative permeability and viscosity are assumed to be constant and uniform within both the CO_2 and the brine zones. The two fluids and the porous formation are both assumed to have a small compressibility that does not vary with pressure [*Mathias et al.* 2009a]. Detailed discussions concerning the theoretical basis of these assumptions are presented by Nordbotten et al. [2005a], Dentz and Tartakovsky [2009b], and Gasda et al. [2009].

Based on the aforementioned conceptual model and the mass balance principle, two equations for flow of carbon dioxide and brine under isothermal conditions can be described as follows:

$$-\frac{1}{r}\frac{\partial}{\partial r}\left[r\rho_c(H-h)q_c\right]=\frac{\partial}{\partial t}\left[\phi\rho_c(H-h)\right], \tag{2-1}$$

$$-\frac{1}{r}\frac{\partial}{\partial r}\left[r\rho_w h q_w\right]=\frac{\partial}{\partial t}\left[\phi\rho_w h\right], \tag{2-2}$$

where q_c [LT^{-1}] and q_w [LT^{-1}] are the fluxes of CO_2 and brine, respectively, and are assumed to be related to the radial pressure gradient through Forchheimer's equation [*Forchheimer* 1901], as follows:

$$-\frac{\partial P}{\partial r}=\frac{\mu_c}{k}q_c+b\rho_c q_c|q_c|, \tag{2-3}$$

$$-\frac{\partial P}{\partial r}=\frac{\mu_w}{k}q_w+b\rho_w q_w|q_w|, \tag{2-4}$$

where t [T] is time, ϕ [-] is porosity, r [L] is the radial distance from the center of the injection well, k [L2] is absolute permeability, b [L-1] is the Forchheimer parameter, and ρ_c [ML^{-3}] and ρ_w [ML^{-3}], μ_c [$ML^{-1}T^{-1}$] and μ_w [$ML^{-1}T^{-1}$] are the densities and viscosities of the CO_2 and brine, respectively. Equations (2-1) and (2-3) hold in the CO_2 region, $(z>h(r,t))$, while equations (2-2) and (2-4) hold in the brine region, $(z<h(r,t))$. The following initial and boundary conditions constrain the problem as follow:

$$P(r\geq r_w,t=0)=0, \tag{2-5}$$

$$h(r\geq r_w,t=0)=H, \tag{2-6}$$

$$P(r=r_w,t>0)=P_o, \tag{2-7}$$

$$rq_w(r=r_w,t>0)=0, \tag{2-8}$$

$$P(r\to\infty,t>0)=0, \tag{2-9}$$

$$h(r\to\infty,t>0)=H, \tag{2-10}$$

$$P(r\geq 0,t=0)=0. \tag{2-11}$$

Derivatives of density and porosity will be converted to derivatives of pressure, by substituting the compressibilities [$M^{-1}LT^2$] for the storage formation, CO_2 and brine [*Bear* 1979]:

$$C_f=\frac{1}{\phi}\left(\frac{d\phi}{dP}\right),$$

$$C_c = \frac{1}{\rho_c}\left(\frac{d\rho_c}{dP}\right),$$

$$C_w = \frac{1}{\rho_w}\left(\frac{d\rho_w}{dP}\right).$$

Then we assume that the fluids and geological formation are sufficiently rigid such that C_f, C_c, C_w, ϕ, ρ_c, and ρ_w are essentially constant. This assumption has been used extensively in the hydrogeology literature when describing the specific storage coefficient, $S_s = \phi\rho_w g\left(C_f + C_w\right)$ [L^{-1}] in confined aquifers, where g [LT^{-2}] is the gravitational constant.

2.3 Solution Development

2.3.1 Non-dimensionlization

The system is scaled by defining the following dimensionless parameters

$$r_D = \frac{r}{r_w}, \qquad h_D = \frac{h}{H}, \qquad P_D = \frac{P}{P_o}, \qquad t_D = \frac{KP_o t}{\phi\mu_c r_w^2},$$

$$q_{cD} = \frac{\mu_c r_w q_c}{KP_o}, \qquad q_{wD} = \frac{\mu_w r_w q_w}{KP_o}, \quad \alpha = P_o\left(C_f + C_w\right), \qquad \beta = \frac{b\rho_c P_o k^2}{\mu_c^2 r_w},$$

$$\gamma = \frac{\mu_c}{\mu_w}, \qquad \sigma = \frac{\rho_c}{\rho_w}, \text{ and} \qquad \varepsilon = \frac{C_c - C_w}{C_f + C_w}.$$

Rewriting the system in dimensionless form leads to

$$\left[1 + \varepsilon\left(1 - h_D\right)\right]\alpha\frac{\partial P_D}{\partial t_D} = -\frac{1}{r_D}\frac{\partial}{\partial r_D}\left[r_D\left(\left(1 - h_D\right)q_{cD} + h_D q_{wD}\right)\right], \tag{2-12}$$

$$\frac{\partial h_D}{\partial t_D} = -\frac{1}{r_D}\frac{\partial}{\partial r_D}\left(r_D h_D q_{wD}\right) - \alpha h_D \frac{\partial P_D}{\partial t_D}, \tag{2-13}$$

$$-\frac{\partial P_D}{\partial r_D} = q_{cD} + \beta q_{cD}\left|q_{cD}\right|, \tag{2-14}$$

$$-\frac{\gamma \partial P_D}{\partial r_D} = q_{wD} + \frac{\gamma\beta}{\sigma} q_{wD}\left|q_{wD}\right|, \tag{2-15}$$

$$P_D\left(r_D \geq 1, t_D = 0\right) = 0, \tag{2-16}$$

$$P_D\left(r_D \to \infty, t_D > 0\right) = 0, \tag{2-17}$$

$$P\left(r_D = 1, t_D > 0\right) = 1, \tag{2-18}$$

$$q_{wD}\left(r_D = 1, t_D > 0\right) = 0, \tag{2-19}$$

$$h_D\left(r_D \to \infty, t_D > 0\right) = 1, \tag{2-20}$$

$$h_D\left(r_D \geq 1, t_D = 0\right) = 1. \tag{2-21}$$

2.3.2 Boltzmann transformation

Following Mathias et al. [2009a], we will derive an approximate solution of the system described by equations (2-12) through (2-21), by approximating the well boundary as $r_D \approx 0$. Then we apply the Boltzmann transform to reduce the non-dimensional system of governing partial differential equations to a system of ordinary differential equations (ODEs) in a single similarity variable, $\chi = \frac{r_D^2}{t_D}$ as follows:

$$\left[1 + \varepsilon\left(1 - h_D\right)\right]\alpha \frac{dP_D}{d\chi} = -\frac{4}{\chi}\frac{d}{d\chi}\left[\left[\left(1 + \left(\gamma - 1\right)h_D\right)\chi\right]\frac{dP_D}{d\chi}\right], \tag{2-22}$$

$$\frac{dh_D}{d\chi} = -\frac{4\gamma}{\chi}\frac{d}{d\chi}\left(h_D \chi \frac{dP_D}{d\chi}\right) - \alpha h_D \frac{dP_D}{d\chi}, \tag{2-23}$$

$$-\chi \frac{dP_D}{d\chi} = q_{cD}, \tag{2-24}$$

$$-\gamma \chi \frac{dP_D}{d\chi} = q_{wD}, \tag{2-25}$$

$$P_D(\chi \to 0) = 1, \tag{2-26}$$

$$P_D(\chi \to \infty) = 0, \tag{2-27}$$

$$h_D(\chi \to 0) = 0, \tag{2-28}$$

$$h_D(\chi \to \infty) = 1. \tag{2-29}$$

2.3.3 Solution approximation without inertial flow

Now, we seek a solution for the reduced ODEs system by the method of matched asymptotic expansions [*Kevorkian* 2000]. In this approach, we will find analytic solutions for pressure and interface height in a region that is relatively close to the well ("inner region"), P_D^i and h_D^i respectively, and a second solution for the far region, P_D^o and h_D^o respectively. Then we choose integration constants in these solutions to match them at intermediate distances. The inner region contains CO_2 and the CO_2/brine interface, whereas the outer region contains brine only.

Inner solution

In the inner region, there are two very different velocities of propagation: the velocity of the invading material front and the much faster velocity of the acoustic wave. The term $\alpha \frac{\partial P_D}{\partial t_D}$ in equations (2-24) and (2-25) accounts for the pressure variation moving through the fluids at the speed of the acoustic wave. Since this is much faster than the speed of CO_2/brine interface, we can assume that P_D is always at equilibrium, so this term is small and can be neglected. By letting $\alpha \frac{\partial P_D}{\partial t_D}$ goes to zero, equations (2-22) and (2-23) can be further simplified to the following:

$$-\frac{4}{\chi}\frac{d}{d\chi}\left[\left[\left(1+(\gamma-1)h_D^i\right)\right]\chi\frac{dP_D^i}{d\chi}\right]+O(\alpha)=0, \tag{2-30}$$

$$\frac{dh_D^i}{d\chi}=-\frac{4\gamma}{\chi}\frac{d}{d\chi}\left[h_D^i\chi\frac{dP_D^i}{d\chi}\right]+O(\alpha). \tag{2-31}$$

From equation (2-30) above, we have

$$\left[\chi\frac{dP_D^i}{d\chi}\right]=\left[\frac{-c}{1+(\gamma-1)h_D^i}\right]+O(\alpha), \tag{2-32}$$

where *c* is equal to half of undermined dimensionless flux at the wellbore. Substituting equation (2-32) into equation (2-31) leads to

$$\frac{dh_D^i}{d\chi}=-\frac{4\gamma}{\chi}\frac{d}{d\chi}\left[\frac{-ch_D^i}{\left(1+(\gamma-1)h_D^i\right)}\right]+O(\alpha), \tag{2-33}$$

which can be simplified to

$$\frac{\chi}{4\gamma} = \frac{d}{dh_D^i}\left[\frac{-ch_D^i}{\left(1+(\gamma-1)h_D^i\right)}\right] + O(\alpha). \tag{2-34}$$

Solving equation (2-34) for h_D^i yields

$$h_D^i = O(\alpha) + \begin{cases} 0 & ; \quad \chi \le 4\gamma c \\ \dfrac{1}{\gamma-1}\left(\sqrt{\dfrac{4\gamma c}{\chi}} - 1\right) & ; \quad 4\gamma c < \chi < \dfrac{4c}{\gamma}. \\ 1 & ; \quad \chi \ge \dfrac{4c}{\gamma} \end{cases} \tag{2-35}$$

Equation (2-35) can be used to track the radial extent of the plume away from the injection well over time. Note above that the values of χ that mark the divisions within the inner region depend on the flux at the wellbore that will change with time. The top part of the CO_2/brine interface at any given time is always at distance of $\frac{1}{\gamma}$ times the distance of the bottom part of the interface. So the brine+CO_2 region gets wider with time, and the interface becomes more horizontal. Multiplying equation (2-35) by $(\gamma-1)$, and then adding $+1$, we have

$$1+(\gamma-1)h_D^i = O(\alpha) + \begin{cases} 1 & ; \quad \chi \le 4\gamma c \\ \sqrt{\dfrac{4\gamma c}{\chi}} & ; \quad 4\gamma c < \chi < \dfrac{4c}{\gamma}. \\ \gamma & ; \quad \chi \ge \dfrac{4c}{\gamma} \end{cases} \tag{2-36}$$

Substituting equation (2-36) back into equation (2-32) gives

$$\chi \frac{dP_D^i}{d\chi} = O(\alpha) + \begin{cases} -c & ; \quad \chi \le 4\gamma c \\ -\sqrt{\frac{c\chi}{4\gamma}} & ; \quad 4\gamma c < \chi < \frac{4c}{\gamma} \\ -\frac{c}{\gamma} & ; \quad \chi \ge \frac{4c}{\gamma} \end{cases}. \tag{2-37}$$

From equation (2-37) we can solve for P_D^i as follows:

$$P_D^i = O(\alpha) + \begin{cases} -c\ln(\chi) + c_1 & ; \quad \chi \le 4\gamma c \\ -\sqrt{\frac{c\chi}{4\gamma}} + c_2 & ; \quad 4\gamma c < \chi < \frac{4c}{\gamma} \\ -\frac{c}{\gamma}\ln(\chi) + c_3 & ; \quad \chi \ge \frac{4c}{\gamma} \end{cases}, \tag{2-38}$$

where c_1, c_2, c_3 are integration constants to be determined.

Now, let us simplify equation (2-83)by expressing c, c_2, c_3 in terms of c_1. At very small distance near the well and from equation (2-83) we have

$$P_D^i = -c\ln(\chi) + c_1, \tag{2-39}$$

Substituting $\chi = \frac{r_D^2}{t_D}$ and $r_D = 1$ (i.e. at $r = r_w$ and $P_D^i = 1$) into equation (2-93), we have

$$c = \frac{1 - c_1}{\ln(t_D)}. \tag{2-40}$$

Similarly, we can solve for c_2, c_3 in terms of c_1 by applying the continuity principles at the interface between the different regions. This gives us

$$c_2 = c\left[-\ln(4\gamma c)+2\right]+c_1, \tag{2-41}$$

$$c_3 = \frac{-2c}{\gamma}+c\left[-\ln(4\gamma c)+2\right]+c_1+\frac{c}{\gamma}\left|\ln\left(\frac{4c}{\gamma}\right)\right|. \tag{2-42}$$

Substituting equations (2-40) through (2-42) into equation (2-83) yields

$$P_D^i \approx c_1+\begin{cases} -c\ln(\chi) & ;\quad \chi \le 4\gamma c \\ -\sqrt{\dfrac{c\chi}{4\gamma}}+c\left[-\ln(4\gamma c)+2\right] & ;\quad 4\gamma c < \chi < \dfrac{4c}{\gamma}. \\ -\dfrac{c}{\gamma}\ln(\chi)+c\left[-\ln(4\gamma c)+2\right]-\dfrac{c}{\gamma}\left[-\ln\left(\dfrac{4c}{\gamma}\right)+2\right] & ;\quad \chi \ge \dfrac{4c}{\gamma} \end{cases} \tag{2-43}$$

This analytical solution of h_D^i and P_D^i is similar to Nordbotten et al. [2005a], Nordbotten and Celia [2006b], and Mathias et al. [2009a], except that the flux of CO_2 in our solution (c) is undetermined yet. The solution divides the aquifer into three regions: the region of $\chi \le 4\gamma c$ near the wellbore filled only with CO_2, the zone of $4\gamma c < \chi < \dfrac{4c}{\gamma}$ in the middle that has a layer of CO_2 above a layer of brine, and finally the zone of $4\chi > \dfrac{4c}{\gamma}$ far away from the wellbore, filled only with brine.

Outer solution

Since the outer region is occupied by brine only (i.e. $h_D = 1$ in the outer region), as indicated by equation (2-35), so we only need to solve for the pressure, P_D^o, in that

region. To develop an outer solution for pressure wave perturbation in this region, we apply the scaling transform $\psi = \alpha\chi$ to equation (2-22), and we obtain

$$\left[1+\varepsilon\left(1-h_D\right)\right]\alpha^2 \frac{dP_D^o}{d\psi} = -\frac{4}{\psi}\alpha^2 \frac{d}{d\psi}\left[\left[\left(1+\left(\gamma-1\right)h_D\right)\psi\right]\frac{dP_D^o}{d\psi}\right]. \tag{2-44}$$

By letting $\varepsilon \to 0$ and $h_D = 1$, and then rearranging equation (2-44) we have

$$-\frac{1}{4\gamma}\psi\frac{dP_D^o}{d\psi} = \frac{d}{d\psi}\left[\psi\frac{dP_D^o}{d\psi}\right]. \tag{2-45}$$

Solving equation (2-45), we obtain

$$\psi\frac{dP_D^o}{d\psi} = c_4 \exp\left(\frac{-\psi}{4\gamma}\right). \tag{2-46}$$

Substituting $u = \dfrac{\psi}{4\gamma}$ into equation (2-46) yields

$$u\frac{dP_D^o}{du} = c_4 e^{-u}, \tag{2-47}$$

where c_4 is an integration constant. Now we can solve for P_D^o in the outer region as follows:

$$\int dP_D^o = c_4 \int_U^\infty \frac{e^{-u}}{u} du, \tag{2-48}$$

where $\int_U^\infty \dfrac{e^{-u}}{u} du = E_1(u) = -E_i(-u)$ is the exponential integral function [*Abramowitz and Stegun* 1965] and is approximated as follows:

$$E_1(u) = -\delta - \ln|u| + \sum_{n=1}^{\infty} \frac{(-1)^{n+1}}{nn!} u^n,$$

where ($\delta \approx 0.5772$ is Euler's constant). If we restricted our attention to positive values of *u* and assumed that *u* is small (i.e. for values of $\chi < \frac{10\gamma}{\alpha}$), then the exponential integral can be approximated as follows:

$$E_1(u) = -E_i(-u) = -\delta - \ln(u). \tag{2-49}$$

From equation (2-48) we have

$$P_D^o = c_4 E_1(u) + c_5, \tag{2-50}$$

where c_5 is an integration constant to be determined.

In this region P_D^o and c_5 go to zero as ψ goes to infinity, and the solution to equation (2-52) reduces to the Theis solution [*Theis* 1935] as follows:

$$P_D^o = c_4 E_1(u). \tag{2-51}$$

Substituting equation (2-49) into equation (2-51) leads to

$$P_D^o = c_4[-\delta - \ln u] + O(u), \tag{2-52}$$

or

$$P_D^o = c_4\left[-\delta - \ln\left(\frac{-\psi}{4\gamma}\right)\right] + O\left(\frac{-\psi}{4\gamma}\right). \tag{2-53}$$

Substituting $\psi = \alpha\chi$ back into equation (2-53) and expanding around α leads to

$$P_D^o = c_4\left[-\delta - \ln(\chi) + \ln\left(\frac{4\gamma}{\alpha}\right)\right] + O(\alpha). \tag{2-54}$$

Now, we have a solution for the pressure perturbation in the outer region, where c_4 is an integration constant to be determined. The integration constants c_4 and c_1 can be determined by matching asymptotically both the inner and outer solution, and this can be done by setting

$$\lim_{\substack{\alpha\to 0 \\ \psi \text{ is fixed}}} P_D^i = \lim_{\substack{\alpha\to 0 \\ \chi \text{ is fixed}}} P_D^o \,. \tag{2-55}$$

In other words, the outer limit of the inner solution is equal to the inner limit of the outer solution. Comparing equations (2-43) with equation (2-54), we obtain

$$c_1 = \frac{c}{\gamma}\left[\ln\left(\frac{\gamma^2}{\alpha c}\right) - \delta + 2\right] - c\left[-\ln(4\gamma c) + 2\right] \quad , \tag{2-56}$$

$$c_4 = \frac{c}{\gamma} \quad . \tag{2-57}$$

Substituting equation (2-56) and (2-57) into equations (2-43) and (2-54), respectively, leads to

$$P_D^i \approx \begin{cases} -c\ln\left(\dfrac{\chi}{4\gamma c}\right)-\dfrac{c}{2}+\dfrac{2c}{\gamma}-\dfrac{c}{\gamma}\left[\ln\left(\dfrac{\alpha c}{\gamma^2}\right)+\delta\right] & ; \quad \chi \le 4\gamma c \\ -\sqrt{\dfrac{c\chi}{4\gamma}}+\dfrac{2c}{\gamma}-\dfrac{c}{\gamma}\left[\ln\left(\dfrac{\alpha c}{\gamma^2}\right)+\delta\right] & ; \quad 4\gamma c < \chi < \dfrac{4c}{\gamma}, \\ -\dfrac{c}{\gamma}\left[\ln\left(\dfrac{\chi c}{4\gamma}\right)+\delta\right] & ; \quad \chi \ge \dfrac{4c}{\gamma} \end{cases} \tag{2-58}$$

$$P_D^o \approx \frac{c}{\gamma}\left[\ln\left(\frac{4\gamma}{\alpha}\right)-\ln(\chi)-\delta\right]. \tag{2-59}$$

Equations (2-58) and (2-59) show the solution for pressure in inner region and outer region, respectively. Note that both solutions are still dependent on the flux at the wellbore.

Composite solution

We can construct the composite solution by asymptotically matching the inner and outer solution. In other words, we add the inner and outer solution together, and then subtract the common terms in the overlap domain. The common term in the overlap domain is equal to the inner limit of the outer solution or the outer limit of the inner solution as follows:

$$F(\chi,c)=\frac{c}{\gamma}E_1\left(\frac{\alpha\chi}{4\gamma}\right)=-\frac{c}{\gamma}\left[\ln\left(\frac{\alpha\chi}{4\gamma}\right)+\delta\right]=-\frac{c}{\gamma}\left[\ln\left(\frac{e^{\delta}\alpha\chi}{4\gamma}\right)\right]. \tag{2-60}$$

Based on equation (2-62), we obtain

$$P_D = P_D^i + P_D^o + \frac{c}{\gamma}\left[\ln\left(\frac{\alpha\chi}{4\gamma}\right)+\delta\right], \tag{2-61}$$

$$h_D = h_D^i + h_D^o - 1 = h_D^i \,, \tag{2-62}$$

$$P_D \approx \begin{cases} -c\ln\left(\dfrac{\chi}{4\gamma c}\right) - \dfrac{c}{2} + \dfrac{2c}{\gamma} + F\left(\dfrac{4c}{\gamma}\right); & \chi \le 4\gamma c \\ -\sqrt{\dfrac{c\chi}{4\gamma}} + \dfrac{2c}{\gamma} + +F\left(\dfrac{4c}{\gamma}\right) & ; \quad 4\gamma c < \chi < \dfrac{4c}{\gamma}, \\ F(\chi, c) & ; \quad \chi \ge \dfrac{4c}{\gamma} \end{cases} \tag{2-63}$$

where $F\left(\dfrac{4c}{\gamma}\right) = -\dfrac{c}{\gamma}\left\lfloor \ln\left(\dfrac{\alpha c}{\gamma^2}\right) + \delta \right\rfloor$.

Finally, we solve for the constant c, by rewriting the inner solution for pressure in terms in of r_D and t_D as follows:

$$P_D = c\left\lfloor \ln(4\gamma t_D) + \frac{1}{\gamma}\ln\left(\frac{\gamma^2}{\alpha}\right) + \left(\frac{-\delta+2}{\gamma}\right) - 2 \right\rfloor + \ln(c)\left\lfloor \frac{c\gamma - c}{\gamma} \right\rfloor \quad , \tag{2-64}$$

setting $P_D(r_D = 1) = 1$ (i.e. reverting back to the original boundary condition at the wellbore), this results in a transcendental equation for c (half the flux at the wellbore):

$$f(c) = c\left\lfloor \ln(4\gamma t_D) + \frac{1}{\gamma}\ln\left(\frac{\gamma^2}{\alpha}\right) + \left(\frac{-\delta+2}{\gamma}\right) - 2 \right\rfloor + \ln(c)\left\lfloor \frac{c\gamma - c}{\gamma} \right\rfloor - 1 = 0 \,. \tag{2-65}$$

Wellbore flux is a function of the dimensionless time, and only two dimensionless parameters: the ratio of the two fluid viscosities, γ, and the scaled wellbore pressure, α. An exact solution for the flux at any time requires an iterative

numerical method. We can find the roots of equation (2-65) to determine c, and then plug it back into equations (2-63) and (2-35) to solve explicitly for pressure and elevation at any time from the start of injection and any distance from the injection well. We have done this for a large range of the two parameters in equation (2-65): α ranging from 0.0001 to 0.009, and γ ranging from 0.001 to 0.1. Figure 2.2 shows the evolution of c with t_D for all of these different solutions. The time ranges in Figure 2.2 corresponds to a scaled from one second to 100 years. This plot, as well as curve fits to each individual solution, show that the evolution of c is very close to a logarithmic decay with time. One example numerical solution for c along with the best fit curve is shown in Figure 2.3.

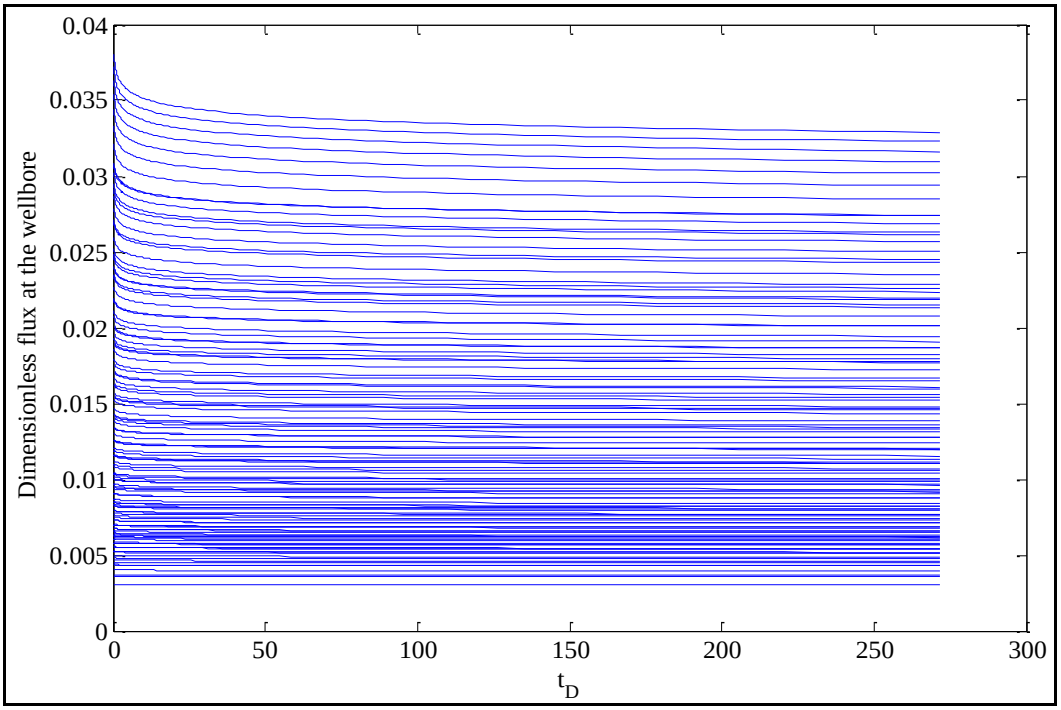

Figure 2.2: Plot of dimensionless flux vs. dimensionless time for 100 different combinations of α and γ.

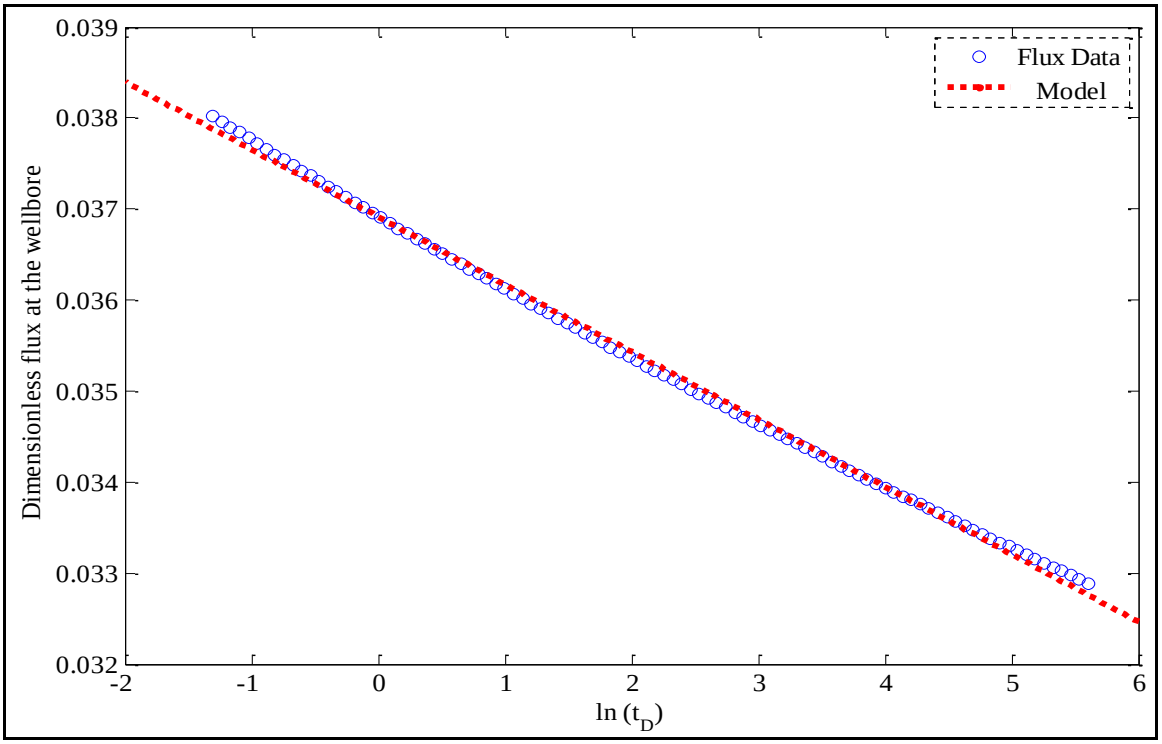

Figure 2.3: Plot of numerically-determined dimensionless flux vs. time, along with a best-fit logarithmic approximation for a system α=0.009 and γ=0.1.

All of the curves in Figure 2.2 can be fitted very well by the model

$$c = a_0 + a_1 4 \ln(t_D), \tag{2-66}$$

where, a_0 and a_1 are the slope and the intercept. For the example shown in Figure 2.3, a_0 and a_1 are equal to 0.037 and -0.00074, respectively. The values of the slope and intercept will vary with the parameters α or γ. To delineate the relationship of a_0 and a_1 with the parameters in the problem, we used MATLAB to determine the best fit logarithmic function to each of the c vs. t_D curves in Figure 2.2. Figures 2.4 and 2.5

show that the slope and intercept vary smoothly as α and γ change. Two surfaces are constructed to show the variations of slop, intercept versus the parameters α and γ changes, and then two polynomials, equations (2-67) and (2-68), are fitted to the surfaces to capture those relationships as shown by Figure 2.6 and Figure 2.7, respectively.

$$f_1(\alpha,\gamma) = a_{00} + a_{10}\alpha + a_{01}\gamma + a_{11}\alpha\gamma + a_{02}\gamma^2, \tag{2-67}$$

$$f_2(\alpha,\gamma) = a_{00} + a_{10}\alpha + a_{01}\gamma + a_{11}\alpha\gamma + a_{20}\alpha^2, \tag{2-68}$$

where $f_1(\alpha,\gamma)$ and $f_2(\alpha,\gamma)$ are the functions of the slope and intercept, respectively. The values of coefficients of the polynomials, a_{ii} (where $i = 0,1,2$), and the goodness of fit are summarized in Tables 2.1 and 2.2.

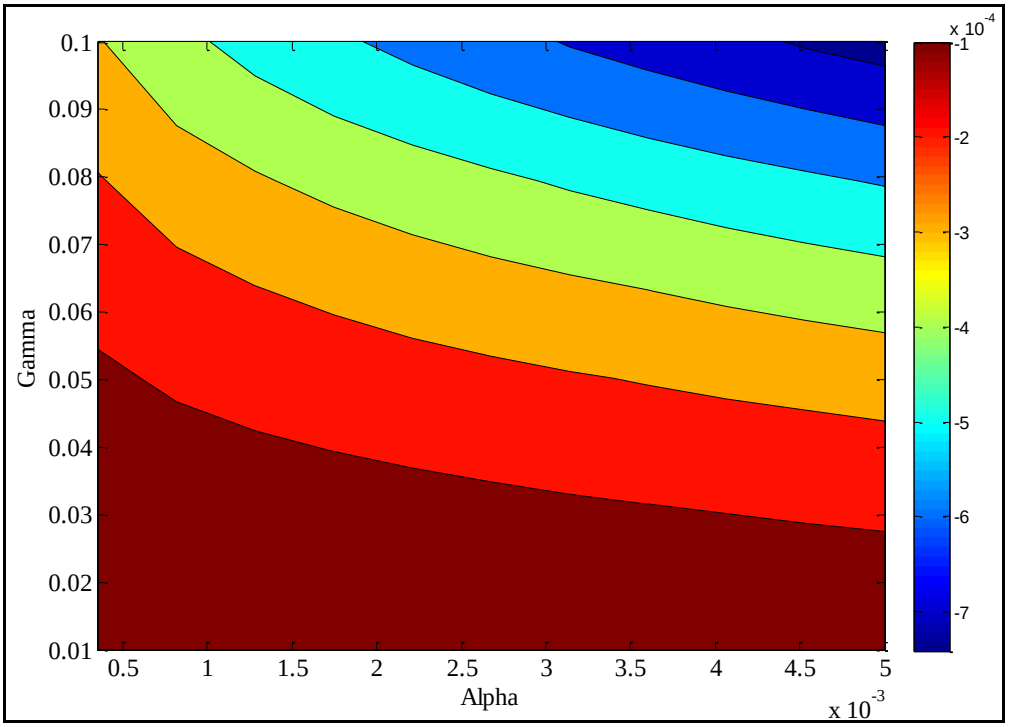

Figure 2.4: Contours of the slope parameter, a_1, in (2-66) for a range of values of α and γ.

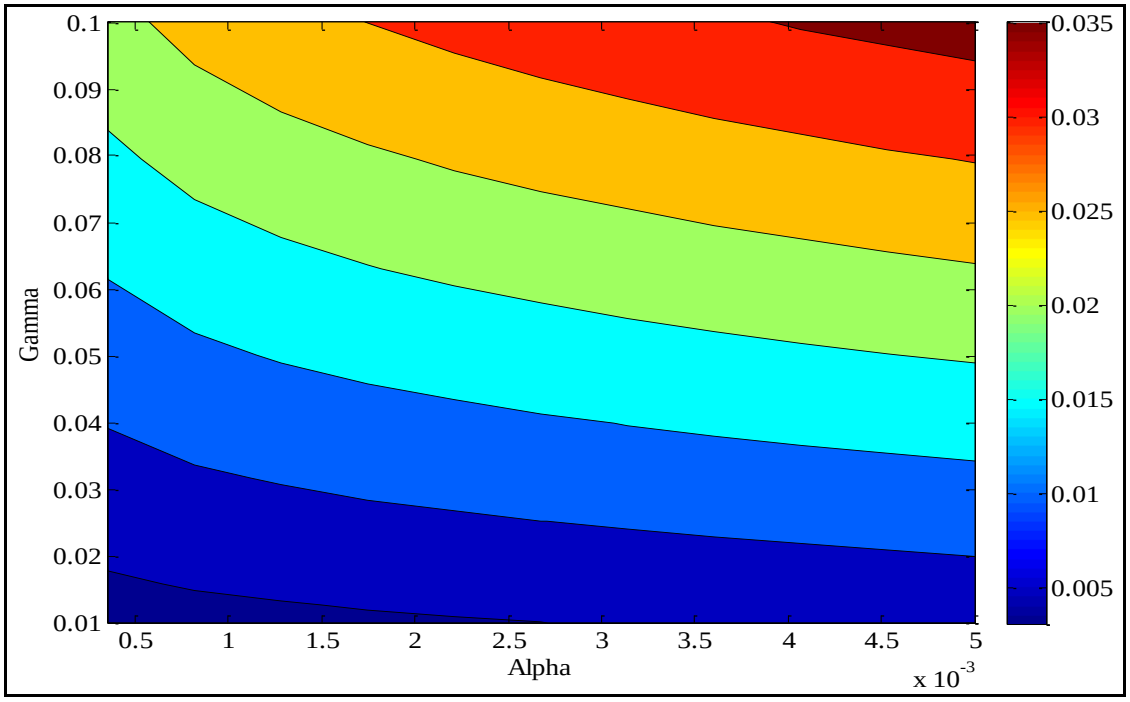

Figure 2.5: Contours of the slope parameter, a_0, in (2-66) for a range of values of α and γ.

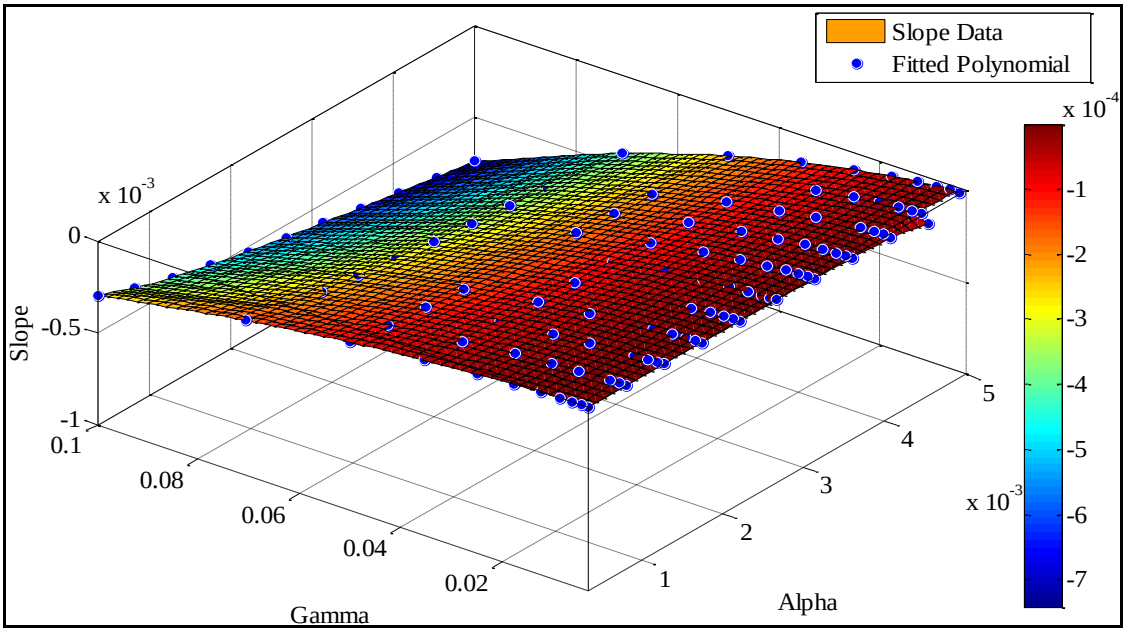

Figure 2.6: The slope values from Fig. 2-4 plotted as a surface vs. α and γ , and a fitted polynomial in α and γ (points).

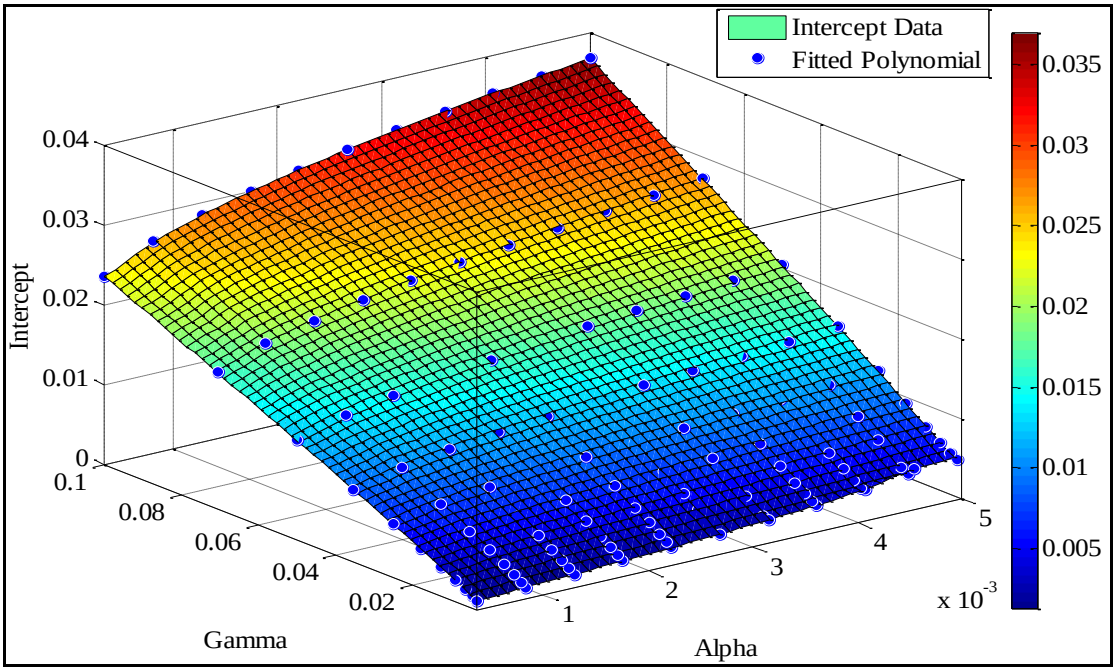

Figure 2.7: The slope values from Fig. 2-5 plotted as a surface vs. α and γ , and a fitted polynomial in α and γ (points).

Table 2.1: Polynomial coefficients of the slope and the intercept with 95% confidence bounds.

Polynomial coefficient	Slope	Intercept
a_{00}	-1.238 E-005	-5.617 E-005
a_{10}	4.25 E-003	1.190
a_{01}	1.011 E-003	2.434 E-001
a_{11}	-8.708 E-001	21.43
a_{20}	0.000	-126.30

Table 2.2: Summary of goodness of fit of the slope, the intercept and the flux, shows *SSE* (sum of squared errors), R^2 (the correlation coefficient), and *RMSE* (residual mean squared error).

Goodness of fit	Slope	Intercept	flux
SSE	1.518 E-008	1.703 E-005	1.233 E-012
R^2	9.957 E-001	9.983 E-001	1.000
RMSE	1.149 E-005	3.848 E-004	1.122 E-007

Now we can construct the final solution for the domain of infinite extent with non-inertial effects when $r_{wD} \to 0$, $\varepsilon \to 0$, and $\alpha << 1$ as follows:

$$P_D \approx \begin{cases} -c\ln\left(\dfrac{\chi}{4c\gamma}\right) - 2c + \dfrac{2c}{\gamma} - \dfrac{c}{\gamma}\left[\ln\left(\dfrac{c\alpha}{\gamma^2}\right) + \delta\right]; & \chi \le 4\gamma c \\ -\sqrt{\dfrac{c\chi}{\gamma}} + \dfrac{2c}{\gamma} - \dfrac{c}{\gamma}\left[\ln\left(\dfrac{c\alpha}{\gamma^2}\right) + \delta\right] & ; 4\gamma c < \chi < \dfrac{4c}{\gamma}, \\ -\dfrac{c}{\gamma}\left[\ln\left(\dfrac{\alpha\chi}{4\gamma}\right) + \delta\right] & ; \chi \ge \dfrac{4c}{\gamma} \end{cases} \tag{2-69}$$

where

$$c \approx \left[1.2\alpha + 0.24\gamma + 21.4\alpha\gamma\right] + 10^{-3}\left[-0.1 + 4.2\alpha + \gamma - 870\alpha\gamma\right]4\ln\left(t_D\right). \tag{2-70}$$

2.3.4 Solution approximation with inertial flow

Following Roose et al. [2001], we can include the nonlinear inertial terms provided we focus only on large times after injection begins. Roose et al. [2001] introduce new dimensionless time and distance, defined by

$$t_D = \frac{\tau}{\beta^2},\ r_D = \frac{\lambda}{\beta},\ \chi = \frac{\lambda^2}{\tau},\ \eta = \alpha\chi, \tag{2-71}$$

where β is a dimensionless parameter that depends on the Forcheimer parameter. For $\beta << 1$, τ and λ are auxiliary variables defined as above.

Outer solution

Now we seek a solution in the far field in terms of similarity variable $\chi = \frac{\lambda^2}{\tau}$.

Note that in the previous section, inner region included all of the CO_2 plus some of the brine. Now the outer region includes all of the brine plus some CO_2, and inner region contains CO_2 only. Substituting equation (2-71) into equation (2-12) leads to

$$\frac{dP_D^o}{d\eta} = -\frac{4}{\eta}\frac{d}{d\eta}\left[\left(1+(\gamma-1)h_D^o\right)\eta\frac{dP_D^o}{d\eta}\right]. \tag{2-72}$$

Solving for P_D^o when $h_D = 1$ leads to

$$P_D^o = c_6 E_1\left(\frac{\alpha\chi}{4\gamma}\right) + O(\alpha,\beta^2), \tag{2-73}$$

where c_6 is an integration constant. At $h_D \neq 1$, we revert equation (2-72) back into χ coordinate, and obtain

$$\left[\chi\frac{dP_D^O}{d\chi}\right] = \left[\frac{c}{1+(\gamma-1)h_D^o}\right] + O\left(\alpha,\beta^2\right). \tag{2-74}$$

Similarly, we can substitute equation (2-74) into equation (2-13), and have

$$\frac{dh_D}{d\chi} = -\frac{4\gamma}{\chi}\frac{d}{d\chi}\left[h_D\chi\frac{dP_D^o}{d\chi}\right] + O\left(\alpha,\beta^2\right). \tag{2-75}$$

Substituting equation (2-74) into equation (2-75) gives

$$-\frac{\chi}{4\gamma}=\frac{c}{\left[\left(1+(\gamma-1)h_D^o\right)\right]^2}+O\left(\alpha,\beta^2\right). \tag{2-76}$$

Solving equation (2-76) for the interface elevation, h_D^o, yields

$$h_D^o\approx\begin{cases}0 & ;\quad \chi\le 4\gamma c\\ \dfrac{1}{\gamma-1}\left(\sqrt{\dfrac{4\gamma c}{\chi}}-1\right) & ;\quad 4\gamma c<\chi<\dfrac{4c}{\gamma}\\ 1 & ;\quad \chi\ge\dfrac{4c}{\gamma}\end{cases}. \tag{2-77}$$

Substituting equation (2-77) into equation (2-74), and then solving for P_D^o gives

$$P_D^o\approx c_7\begin{cases}-c\ln(\chi)+-2c+\dfrac{2c}{\gamma}-\dfrac{c}{\gamma}\left[\ln\left(\dfrac{c\alpha}{\gamma^2}\right)+\delta\right]+c\ln(4c\gamma) & ;\quad \chi\le 4\gamma c\\ -\sqrt{\dfrac{c\chi}{\gamma}}+\dfrac{2c}{\gamma}-\dfrac{c}{\gamma}\left[\ln\left(\dfrac{c\alpha}{\gamma^2}\right)+\delta\right] & ;\quad 4\gamma c<\chi<\dfrac{4c}{\gamma},\\ -\dfrac{c}{\gamma}\left[\ln\left(\dfrac{\alpha\chi}{4\gamma}\right)+\delta\right] & ;\quad \chi\ge\dfrac{4c}{\gamma}\end{cases} \tag{2-78}$$

where c_7 is another integration constant.

For the inner solution, where the CO_2 phase exists only near the well (i.e. "λ" is so small and h_D=0), it is better to revert back to the variable r_D, so that the inner limit process is described by

$$\alpha\beta^2\frac{\partial P_D^i}{\partial\tau}=-\frac{1}{r_D}\frac{\partial}{\partial r_D}\left(r_D q_{cD}\right)\text{ and }\lim_{r_D\to 1}r_D q_{cD}=c, \tag{2-79}$$

where "q_{cD}" satisfies $q_{cD} + \beta q_{cD}^2 = -\dfrac{dP_D^i}{dr_D}$, (2-80)

where $\beta << 1$. In equation (2-80), we used full derivatives instead of partial derivatives, because the solution here is to be derived at large times (i.e. the pressure is independent on time, and changes with radial distance only). Substituting equation (2-79) into equation (2-80), and then solve for P_D^i, we obtain

$$P_D^i \approx \frac{4\beta c^2}{\sqrt{t_D \chi}} - 2c\ln\left(\sqrt{t_D \chi}\right) + c\ln\left(4ct_D\gamma\right) - 2c + \frac{2c}{\gamma} - \frac{c}{\gamma}\left[\ln\left(\frac{c\alpha}{\gamma^2}\right) + \delta\right]. \quad (2\text{-}81)$$

Composite solution

Matching the inner and outer solutions asymptotically yields

$$P_D \approx -c\ln\left(\frac{\chi}{4c\gamma}\right) - 2c + \frac{2c}{\gamma} + \frac{4c^2\beta}{\sqrt{t_D \chi}} - \frac{c}{\gamma}\left[\ln\left(\frac{c\alpha}{\gamma^2}\right) + \delta\right]. \quad (2\text{-}82)$$

Now we can construct the final solution for the domain of infinite extent with inertial effects when $r_{wD} \to 0$, $\varepsilon \to 0$, $t_D >> \dfrac{\beta^2}{2\gamma}$, and $\alpha << 1$ as follows:

$$P_D \approx \begin{cases} -c\ln\left(\dfrac{\chi}{4c\gamma}\right) - 2c + \dfrac{2c}{\gamma} - \dfrac{c}{\gamma}\left[\ln\left(\dfrac{c\alpha}{\gamma^2}\right) + \delta\right] + \left(\dfrac{\beta}{\sqrt{t_D\chi}}\right) & ;\ \chi \le 4\gamma c \\ -\sqrt{\dfrac{c\chi}{\gamma}} + \dfrac{2c}{\gamma} - \dfrac{c}{\gamma}\left[\ln\left(\dfrac{c\alpha}{\gamma^2}\right) + \delta\right] & ;4\gamma c < \chi < \dfrac{4c}{\gamma}, \\ -\dfrac{c}{\gamma}\left[\ln\left(\dfrac{\alpha\chi}{4\gamma}\right) + \delta\right] & ;\ \chi \ge \dfrac{4c}{\gamma} \end{cases} \quad (2\text{-}83)$$

or in terms of r_D and t_D the solution can be expressed as follows:

$$P_D \approx \begin{cases} -c\ln\left(\frac{r_D^2}{4c\gamma\, t_D}\right) - 2c + \frac{2c}{\gamma} - \frac{c}{\gamma}\left[\ln\left(\frac{c\alpha}{\gamma^2}\right) + \delta\right] + \left(\frac{\beta}{r_D}\right); r_D \le \sqrt{4\gamma c t_D} \\ -\sqrt{\frac{cr_D^2}{\gamma\, t_D}} + \frac{2c}{\gamma} - \frac{c}{\gamma}\left[\ln\left(\frac{c\alpha}{\gamma^2}\right) + \delta\right] & ; \sqrt{4\gamma c t_D} < r_D < \sqrt{\frac{4ct_D}{\gamma}} \\ -\frac{c}{\gamma}\left[\ln\left(\frac{\alpha r_D^2}{4\gamma\, t_D}\right) + \delta\right] & ; r_D \ge \sqrt{\frac{4ct_D}{\gamma}} \end{cases} \quad (2\text{-}84)$$

2.4 Results and Discussions

We apply the solution scheme described above to a specific example aquifer, where the injection pressure, initial and boundary conditions, and the formation properties (thickness, perforation thickness, permeability and porosity) are summarized in Table 2.3. The injection process continues for one hundred years, starting in the year 2010 and ended in 2110. The pressure buildup across the entire aquifer is shown at five year intervals in Figure 2.8. During the entire injection period, there are large pressure gradients within 250 m of the well, and then gradients are much lower at larger distances. It also shows that the rate of pressure buildup decreases with time, with the late time pressure curves (i.e. after the year 2080) stacking nearly on top of one another.

Table 2.3: Geometrical and physical properties of the storage formation, initial and boundary conditions, and injection pressure used in computations.

Parameter	Value
A	315 km^2
T	55[C^o]
C_c	7.2 E-005 [bar^{-1}]
C_f	7.2 E-005 [bar^{-1}]
H	100[m]
k	10 E-14 [m^2]
P_o	13 [kpa]
p_i	11 [kpa]
r_w	0.2 [m]
t	100 [year]
μ_c	4.6 E-10-5 [pa s]
μ_w	9.6 E-10-4 [pa s]
ρ_c	610 [kg m^{-3}]
ρ_w	1139 [kg m^{-3}]
ϕ	0.3 [-]

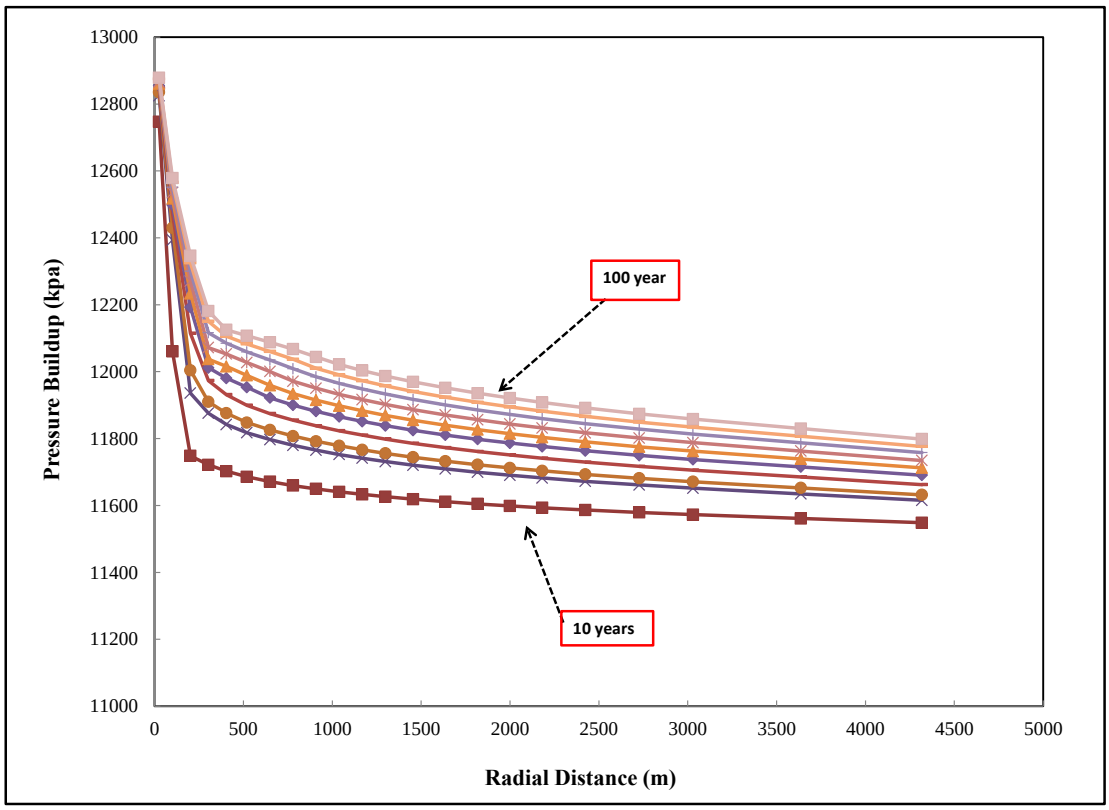

Figure 2.8: Pressure vs. radial distance at 10 year intervals after the beginning of pumping.

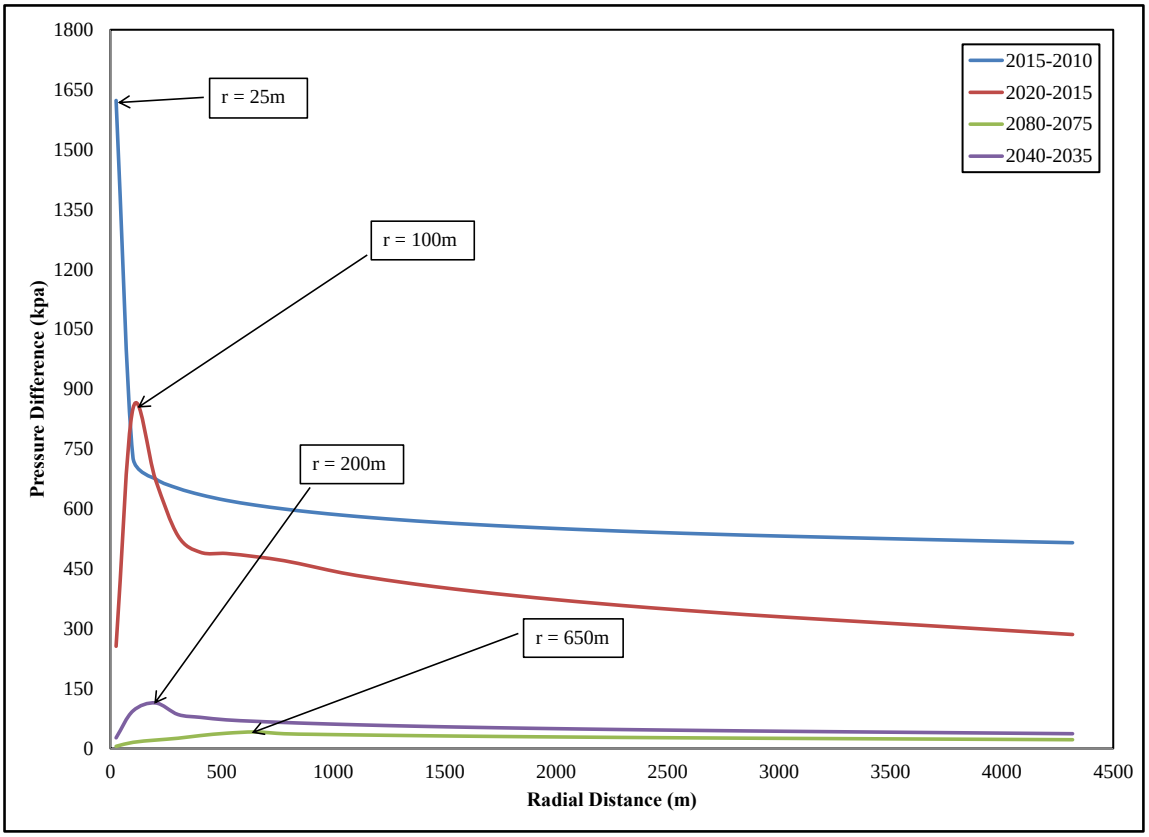

Figure 2.9: Change in pressure over a 5 year period vs. radial distance, for 4 different periods (2015-2010, 2020-2015, 2040-2035, and 2080-2075).

Figure 2.9 shows the difference between calculate reservoir pressures separated by 5 years in time; this difference therefore is approximately proportional to the rate of change of pressure. At any given time, the maximum rate of pressure increase will occur at some distance from the wellbore. The decrease in amplitude and increase in radial distance with time demonstrates the front of pressure diffusing outward from the wellbore as time evolves. The rate of pressure difference between the years 2015-2010 is largest very near the well at r=5m.While between the years 2035-2040 the peak rate of change is found at r=100m. Then it is shifted to be at r=250m between the years 2040-

2035, and then it kept migrating and attenuating away from the well to be at *r*= 700m between the years 2070-2085. This is because each pressure perturbation wave starts very strong nearby the wellbore, and then as it migrates away from the wellbore it attenuates and changes its location. In other words, the pressure perturbation wave starts with very sharp and high peak, and then diffuses with radial distance away from the well as time evolves.

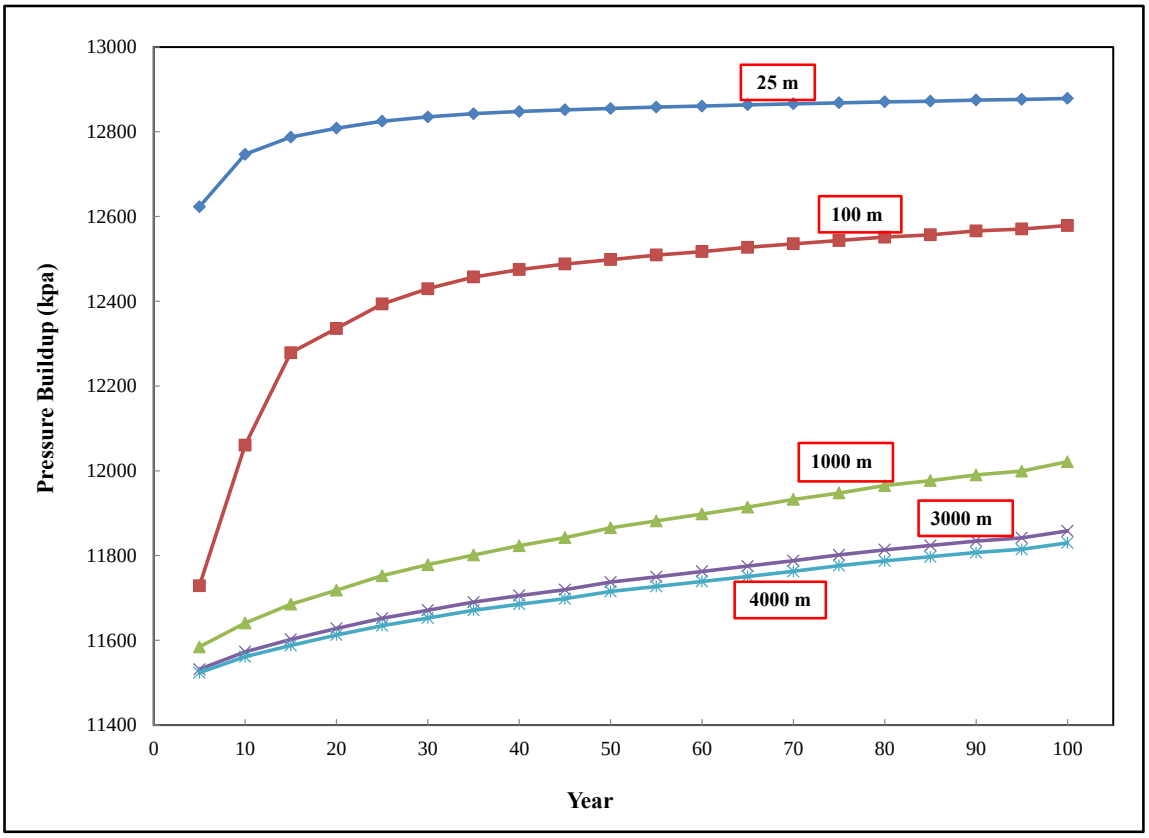

Figure 2.10: Predicted pressure buildup as a function of time at specific radial distances (r= 25 m, 100 m, 1000 m, 3000 m, and 4000 m).

Figure 2.10 shows the results of pressure build up at five different radial locations (r = 25, 100, 1000, 3000, and 4000m). These locations are selected to compare the pressure buildup at close (i.e. r=25 and 100m), intermediate (i.e. r= 1000 and 3000m) and at far (i.e. r=4000m) distance from the well. The pressure increased by 1622 kpa at r=25m by the end of the first five years of injection (2010-2015), then the increase dropped down to be 125 kpa in the second five years and kept going down to increase with 10 kpa till the year 2050, and finally the increase was reduced to be 5kpa every ten years till the end of injection process. While at distance r=100 the pressure profile increased with 730 kpa in the first five years, and kept increasing with 330 and 220 kpa during the second and third five years (i.e. 2020-2015 and 2025-2020), respectively, and then fallen down increase with 15 kpa. The last three curves (i.e. at r=1000, 3000, and 4000m) follow the same pattern, started to increase rapidly at the first ten years with about 500 kpa, and then kept increasing with a smaller rate of about 30 kpas till the end of injection.

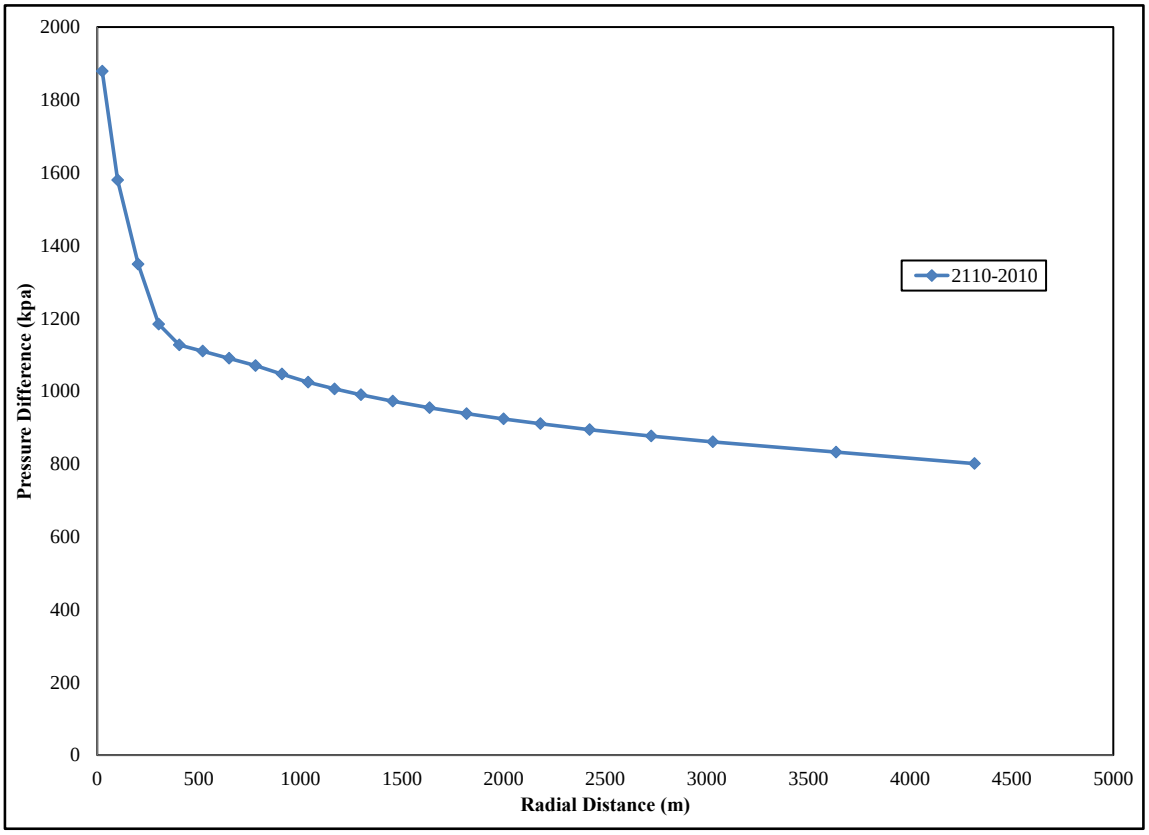

Figure 2.11: Cumulative pressure difference as a function of radial distance.

Figure 2.11 confirms the results obtained from Figures 2.8, 2.9, and 2.10 that the pressure gradient increases nearby the wellbore and decrease with increasing the radial distance from the wellbore. The pressure gradient starts very high near the wellbore and then keeps decreasing away from the wellbore.

The cumulative injection volume, N_I, can be defined as follows

$$N_I = \int_0^t q_c(r = r_w, \tau) d\tau \,. \tag{2-85}$$

Using equations (2-69) and (2-70) together with equation (2-85), we can calculated the cumulative injected volume of CO_2 over the injection period as shown in Figure 2.12. Then we can calculate the cumulative CO_2 injected mass during the injection process as follows:

by definition, the universal law of gas is

$$PV = nRT, \tag{2-86}$$

where V is the volume of CO_2, R is gas constant, T is the temperature, P is the pressure, and n is the number of moles. From equation (2-86) we can calculate the n, then having the molecular weight of CO_2 we can calculate the mass of injected CO_2 as shown in Figure 2.13.

Figures 2.12 and 2.13 show the cumulative injected volume (in cubic meter) and mass (in megaton) during the injection process, respectively. It can be seen that the two curves have the same pattern; they keep increasing from the star till the end of the hundred year injection.

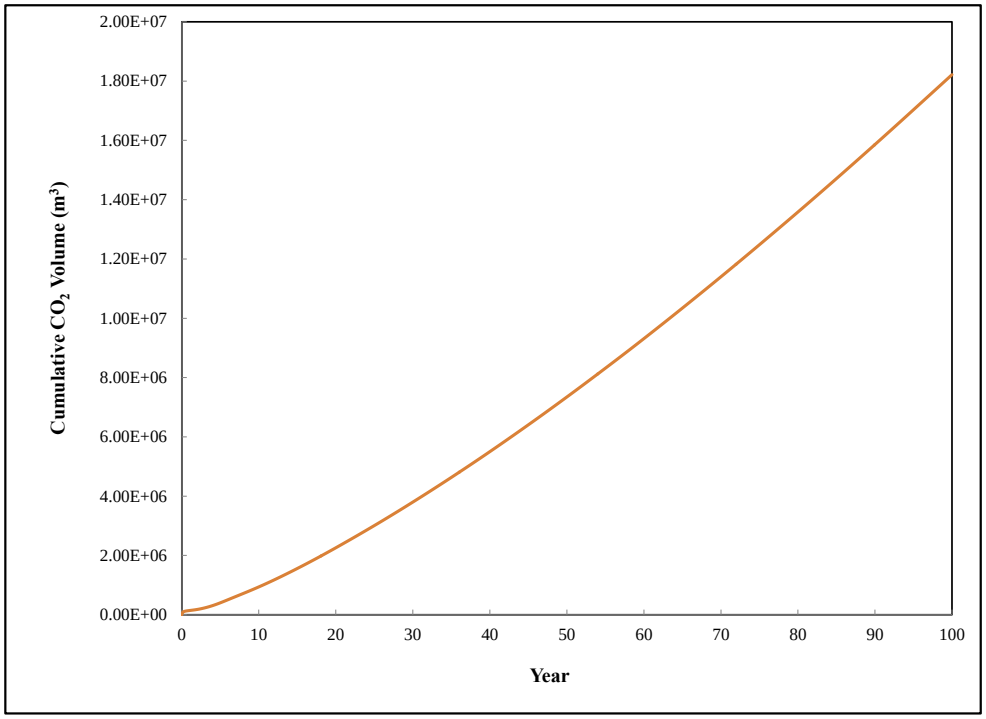

Figure 2.12: Predicted cumulative injected CO_2 volume as a function of time.

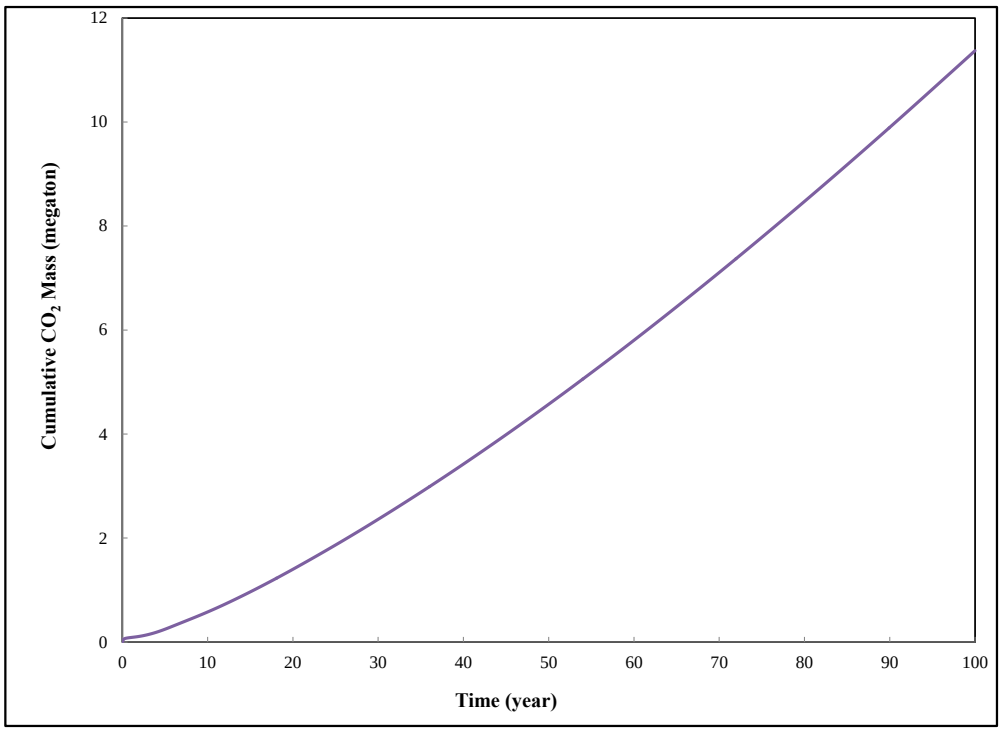

Figure 2.13: Predicted cumulative injected CO_2 mass as a function of time.

2.5 Summary and Conclusions

The governing equations for CO2 injection into a slightly compressible brine aquifer with a vertical pressure equilibrium assumption were presented. The problem was first solved for non-inertial flow. By assuming an infinitesimal well radius and applying a similarity transform, the problem reduced to two ordinary differential equations. An assumption of small compressibility (i.e. α goes to zero) was then invoked and an analytical solution obtained using the method of matched asymptotic expansions (The small α approximation). The pressure distribution in equation (2-63) was first obtained as a function of the wellbore flux. Then, a closed form solution for the wellbore

flux was obtained as in equation (2-72). Wellbore flux was found to be a function of the dimensionless time, and only two dimensionless parameters: the ratio of the two fluid viscosities, γ, and the scaled wellbore pressure, α. An exact solution for the flux at any time required an iterative numerical method. We have done this for a large range of the two parameters in equation (2-65): α ranging from 0.0001 to 0.009, and γ ranging from 0.001 to 0.1. The evolution of the wellbore flux was also found to be very close to a logarithmic decay with time. The resulting pressure distribution can be obtained by evaluating equation (2-63) in conjunction with equation (2-72). The corresponding CO2-brine interface elevation can be obtained from equation (2-35). On the basis of the above, a solution for flow with inertial effects was obtained using Forchheimer equation and applying the method of matched asymptotic expansion with a large time assumption (the large time approximation), the pressure distribution formula is described by equation (2-84).

Considering that the solutions were derived under constant injection pressure, the new solutions are more practical and can be used safely without hitting the fracture pressure of the storage formation. Given the likely scale of the CCS effort required over the coming years, this new method provides the basis for fast and cost-effective screening to quickly identify those sites that will be suitable for the injection procedure. The two approximate solutions derived in this article are highly appropriate for the kinds of spreadsheet software that will probably be used for this purpose.

3. PRESSURE BUILDUP IN BRINE CLOSED AQUIFERS DURING CO_2 SEQUESTRATION UNDER CONSTANT INJECTION PRESSURE

Over the past 20 years, the concept of permanently storing (i.e. sequestering) carbon dioxide (CO_2) in geologic media (e.g. brine aquifers) has gained increasing attention as part of important technology option of carbon capture and storing (CCS) within a portfolio of options aimed at reducing anthropogenic emissions of greenhouse gases to the earth's atmosphere.

Although high injection rates can minimize the cost of injection, it can result in huge formation damage if it leads to pressures that fracture the formation or overlying caprock. Optimal injection rate has to remain within the safe pressure limits. Accordingly, a robust monitoring of the transient pressure buildup characteristics resulting from CO_2 sequestration in brine aquifers is compulsory.

While numerical simulations can provide reliable pressure buildup predictions, they require extensive knowledge about the formation, which is not available at the start of the injection process. There have been simple analytical and semi-analytical techniques to support monitoring the pressure buildup, however they are all assuming constant injection rate. Geo-sequestration injection more commonly occurs at a constant wellbore CO_2 pressure, with the input rate decreasing as the CO_2 front penetrates into the formation. Therefore, a new model predicting pressure buildup resulting from CO_2 sequestration under constant pressure injection is required. The solution derived in

Section 2 is useful for very large reservoirs where permeability is small. In this section, the approximate solutions of Section 2 are extended to account for formations of finite radial extent, leading to an approximate analytical solution that is accurate over the entire domain of practical interest.

We formulate the problem in terms of a CO_2 potential that facilitates solution in horizontal layers. We find that when CO_2 is injected under a constant pressure in a fully-penetrating well, CO_2 advances initially uniformly through the entire aquifer. With time, the CO_2 advances more rapidly along the top of the reservoir than the bottom, so that the plume does not necessarily occupy the whole thickness of the aquifer. Both CO_2 plume position and fluid pressure is described by the solution derived in this section. Therefore, this solution facilitates quick evaluations of the CO_2 plume position and fluid pressure distribution when injecting supercritical CO_2 in a deep closed saline aquifer.

3.1 Introduction

In the year 1950, Charles Keeling initiated a program of ongoing measurements of atmospheric CO_2 emissions. The measured data shows annual cycles of variability superimposed on a monotonic increase over the half-century of measurements. Atmospheric concentration of CO_2 in the late 1950's was around 315 parts per million (ppm), while today's concentration has grown to about 385 ppm. The data when combined with ice core data also shows stable atmospheric concentration of CO_2 to be 280 ppm over the last 1000 years. The increase over the 280 ppm occurred after the start

of the industrial revolution and increased over time. This increase above the natural CO_2 level is regarded to be driven by anthropogenic emission [*IPCC* 2007a, 2007b, 2007c].

Practical solutions to the carbon problem will necessarily involve modifications to the underlying engineering systems that have created the problem, while maintaining an expected standard of living. Such solutions require both modifications to existing technologies and development of fundamentally new technologies.

In this study, we will focus on analysis of one such technology, which is referred to as Carbon Capture and Storage (CCS). CCS is a critical enabling technology for carbon-free electricity from fossil fuels [*IEA* 2007; *IPCC* 2005, 2007a, 2007b, 2007c; *Pacala and Socolow* 2004; *Sheppard and Socolow* 2007]. Among the possible formations available for storage, deep saline aquifers have the largest capacity [*IPCC* 2005] and are relatively ubiquitous. There are some studies provided a useful review summarizing different modeling approaches [*Schnaar and Digiulio* 2009] and other ones provided a good overview of the current state of scientific knowledge on CO2 storage in saline aquifers and experience from existing storage operations [*Michael et al.* 2009; *Michael et al.* 2010]. Many others solved the CO_2 problem over large spatial scales [*Nordbotten et al.* 2005a; *Nordbotten* 2004; *Nordbotten and Celia* 2006b; *Nordbotten et al.* 2004; *Nordbotten et al.* 2008]. There are some example applications for such problem introduced in different studies [*Bachu and Celia* 2009; *Celia et al.* 2006; *Kavetski et al.* 2006; *Nordbotten et al.* 2005b].

The injected CO_2 is driven into the formation by the pressure gradients generated by the pressure at the well, with its flow paths modified by capillarity and the associated relative permeability functions as well as heterogeneities in formation properties [*IPCC* 2005; *Johnson et al.* 2004]. The flow is also affected significantly by the strong density difference between the brine and CO_2, which leads to a buoyancy-driven upward movement of CO_2 that produces strong gravity segregation. This strong buoyant drive is one of the most important characteristics of the system because it gives a clear macroscopic spatial structure to the fluids. Buoyancy is also a major driving force in potential leakage scenarios, thereby highlighting the importance of the caprock formation above the injection formation. This buoyant segregation is a key element in approaches that allow simplifications to mathematical models for these systems [*Nordbotten and Celia* 2011], and we take full advantage of this in the model that we present later in this work.

In order to design an appropriate model for a particular problem, it is important to consider the spatial and temporal scales involved, and how the physical processes and parameters of the system relate to these scales. Important scales include those associated with the domain, system parameters, and physical processes; and those associated with the solution to the problem [*Nordbotten and Celia* 2011]. The largest spatial scale considered for geological storage of CO_2 is the length scale of the aquifer system into which the injection occurs, which is on the order of a few kilometers or more. This scale is important, as diverse issues such as capacity estimates, liability, and computational

domains all relate to this scale. The vertical extent of the formation is self - explanatory, and is usually on the order of ten to several hundred meters. Finally, three of the largest length scales are defined as scales associated with the solution of the problem: the plume extent during injection, the extent of pressure perturbations associated with the injection, and the overall migration distance including postinjection migration [*Nordbotten and Celia* 2011].

The full equations for CO_2 storage in three dimensions are too complex, both in terms of parameters and processes, to readily admit analytical solutions. Many assumptions have to be made to simplify the equations such that analytical and semi-analytical solutions can be obtained [*Celia and Nordbotten* 2009; *Celia and Nordbotten* 2011]. In contrast, several of the vertically integrated macroscale models have a sufficiently simple structure that analytical solutions can be obtained for relevant problems. These solutions serve three purposes. By themselves, analytical solutions provide insight into the interplay among different processes and parameters in the problem. Together with numerical approximations, analytical solutions are valuable from the perspective of verification and benchmarking. Finally, analytical solutions serve as building blocks for fast algorithms.

In this article we present an approximate analytical solution for two–phase flow problems. The solution is on analysis of CO_2 injection into an initially brine-filled closed aquifer, exploiting self–similarity and matched asymptotic expansion. The solution

developed in this work is based on a set of analytical and semi-analytical solutions for CO_2 injection [*Mathias et al.* 2009a; *Mathias et al.* 2011; *Nordbotten et al.* 2005a; *Nordbotten and Celia* 2006b; *Wiese and Mathias* 2010] and more closely on the solution we derived in section 2.

We will consider the problem of injection into a deep permeable saline aquifer that is bounded above and below by low–permeability cap-rock formations and is initially filled with brine. We will assume injection from a single vertical well, although the processes governing the system are essentially independent of the orientation of the injection wells. We also assume that the brine is the wetting fluid, and the injected CO_2 is the non-wetting fluid. Therefore, displacement of brine by CO_2 is a drainage process, while displacement of CO_2 by brine is an imbibition process. Injection of CO_2 into the formation is achieved by raising the pressure of CO_2 in the wellbore to a value above the entry pressure for the formation material and limited by requirements to remain below the estimated fracture pressure of the formation and caprock.

The injection process will take place at relatively high pressures, so that near the injection well, the system will tend to have wetting fluid close to, or at, its residual saturation, S_r. Therefore, we expect the region close to the well that is invaded by CO_2 to have brine at residual saturation (i.e. immobile phase). In regions close to the well, dry CO_2 will continually displace the wet CO_2 and in so doing will evaporate some of the residual brine. Eventually, the water in the residual brine will all evaporate, and the only

fluid remaining in the pore space will be dry CO_2 (along with some precipitated salts from the evaporated brine). This creates an expanding region of dry CO_2 in the vicinity of the injection well [*Nordbotten and Celia* 2011]. However, we will ignore the evaporation process of brine near the wellbore and will consider both the residual brine and CO_2 to coexist in this region.

3.2 Conceptual Model

Injection into a confined aquifer defines the first major time period of a CO_2 storage operation. During this period, advective two-phase flow dominates the system, while the dip of the aquifer, dissolution, and mineral reactions are expected to have minimal influence on the solution and will be ignored. Therefore, we simplify the system by assuming a horizontal aquifer with immiscible and slightly incompressible fluids. We also use the Dupuit pressure reconstruction to average the vertical pressure [*Gasda et al.* 2011]. The Dupuit assumption assigns a pressure field such that flows perpendicular to the aquifer boundaries are ignored; this means that flows in the *z*-direction are neglected. In other words, the vertical equilibrium assumption is essentially an assumption of negligible flow in the vertical direction (i.e. flow perpendicular to the formation is negligible, which is denoted as the Dupuit assumption).

We consider injection into a confined homogeneous and isotropic aquifer with constant fluid properties, where the injection takes place at a constant pressure through a single vertical well. We assume the problem has a radial symmetry.

Figure 3.1, shows the schematic diagram of CO_2 injection into infinite confined brine aquifer. The cylindrical coordinate system is set as follow: the origin of the coordinate is at the aquifer base; the *z* axis is vertical and positive upward and through the center of the well; the *r* axis is radially horizontal. The injection well is fully penetrating the aquifer vertically and is perforated along the entire thickness of the aquifer *H* [L]. The top and bottom of the aquifer are impermeable for both CO_2 and brine flow. The injection process is running under a known constant pressure, P_0 [$ML^{-1}\ T^{-2}$], at the wellbore, instead of constant injection rate. In other words, the injection rate is let to vary with time during the injection process. The lateral boundary is of finite radial extent and was assumed to be no flow boundary. Following Nordbotten [2005a], the interface is assumed to be sharp and located at an elevation, *h* [L], above the base of the aquifer. CO_2 has lower density than brine, and is assumed to stay with residual (immobile) brine on the upper side of the interface, while mobile brine only will be on the lower side. Capillary pressure is ignored, and the pressure, *P* [$ML^{-1}\ T^{-2}$], is assumed to be in vertical equilibrium over the entire thickness of the aquifer. In other words, the vertical pressure gradient is ignored, which may not significantly affect the pressure buildup in the proposed study, since the well is screened along the entire aquifer thickness. Saturation, relative permeability, and viscosity are assumed to be constant and uniform within both the CO_2 and the brine zones. The two fluids and the porous formation are assumed to have small compressibility each that does not vary with pressure [*Mathias et al.* 2009a; *Mathias et al.* 2011]. Detailed discussions concerning

the theoretical basis of these assumptions are presented in many previous studies [*Dentz and Tartakovsky* 2009a, 2009b; *Gasda et al.* 2009; *Nordbotten et al.* 2005b].

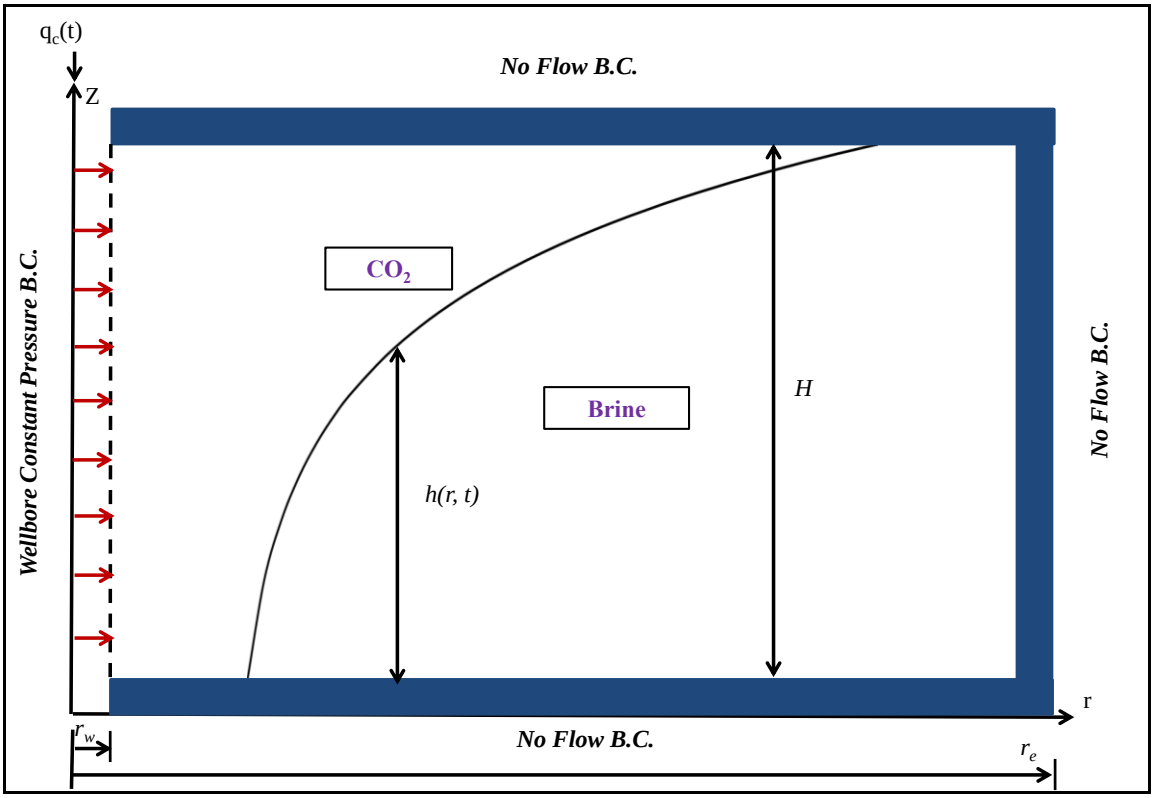

Figure 3.1: Schematic diagram of CO_2 injection into closed brine aquifer under constant pressure.

3.3 Mathematical Model

Based on the conceptual model described above and the mass balance, we write the partial differential equation for the fluid pressures, *P*, and the interface elevation, *h*, initial and boundary conditions for the system in radial coordinates as follows:

$$\Delta t\left[2\pi r\Delta z q_c\,\rho_c(H-h)\big|_r - 2\pi r\Delta z q_c\,\rho_c(H-h)\big|_{r+\Delta r}\right] = \quad , \tag{3-1}$$
$$(1-S_r)\left[2\pi r\Delta r\Delta z\phi\,\rho_c(H-h)\big|_{t+\Delta t} - 2\pi r\Delta r\Delta z\phi\,\rho_c(H-h)\big|_t\right]$$

$$\Delta t\left[2\pi r\Delta z q_w\,\rho_w h\big|_r - 2\pi r\Delta z q_w\,\rho_w h\big|_{r+\Delta r}\right] = \tag{3-2}$$
$$(1-S_r)\left[2\pi r\Delta r\Delta z\phi\,\rho_w h\big|_{t+\Delta t} - 2\pi r\Delta r\Delta z\phi\,\rho_w h\big|_t\right],$$

where h [L] is the elevation of CO_2/brine interface, r [L] is the radial distance from the center of the injection well, z [L] is the vertical distance from the bottom of the storage formation, S_r [-] residual saturation of brine, t [T] is time, ϕ [-] is porosity, k [L^2] is absolute permeability, q_c [LT^{-1}] is the CO_2 flux, q_w [LT^{-1}] is the brine flux, ρ_c [ML^{-3}] is the density of CO_2, ρ_w [ML^{-3}] is the density of brine, μ_c [$ML^{-1}T^{-1}$] is the viscosity of CO_2, μ_w [$ML^{-1}T^{-1}$] is the viscosity of brine, Δr, Δz and Δt are infinitesimal changes in radial distance, vertical distance, and time, respectively. At the limit $\Delta r, \Delta z, \Delta t \to 0$, equations (3-1) and (3-2) can be written as

$$(1-S_r)\frac{\partial}{\partial t}\left[\phi\rho_c(H-h)\right] = -\frac{1}{r}\frac{\partial}{\partial r}\left[r\rho_c(H-h)q_c\right], \tag{3-3}$$

$$(1-S_r)\frac{\partial}{\partial t}\left[\phi\rho_w h\right] + S_r\frac{\partial}{\partial t}\left[\phi\rho_w H\right] = -\frac{1}{r}\frac{\partial}{\partial r}\left[r\rho_w h\,q_w\right]. \tag{3-4}$$

The fluxes q_c and q_w are assumed to be related to the radial pressure gradient through the Forchheimer's equation [*Forchheimer* 1901], as follows:

$$-\frac{\partial P}{\partial r}=\frac{\mu_c}{k_r K}q_c+b_r b\rho_c q_c|q_c|, \tag{3-5}$$

$$-\frac{\partial P}{\partial r}=\frac{\mu_w}{K}q_w+b\rho_w q_w|q_w|. \tag{3-6}$$

Where b [L^{-1}] is the Forchheimer's parameter, the factors k_r [-] and b_r [-] are the relative permeability and relative Forchheimer's parameters, respectively, for the CO_2, representing the fact that the irreducible brine saturation is occupying the CO_2 region together with the invading phase (i.e. CO_2). This will reduce the transmissivity of the CO_2 [*Bennion and Bachu* 2008]. Relative permeability and relative Forchheimer's parameters for the brine are not required in this article, because the aquifer is assumed to be initially fully saturated with brine before the injection of CO_2 starts.

The following initial and boundary conditions are constraining our problem as follow:

$$P(r\geq r_w, t=0)=0 \quad , \tag{3-7}$$

$$h(r\geq r_w, t=0)=H, \tag{3-8}$$

$$P(r=r_w, t>0)=P_0, \tag{3-9}$$

$$rq_c(r=r_e, t>0)=0, \tag{3-10}$$

$$rq_w(r=r_e, t>0)=0, \tag{3-11}$$

$$rq_w(r=r_w, t>0)=0. \tag{3-12}$$

Substituting the compressibilities [$M^{-1}LT^2$] for the geological formation, CO_2 and brine $C_f = \frac{1}{\phi}\left(\frac{d\phi}{dP}\right)$, $C_c = \frac{1}{\rho_c}\left(\frac{d\rho_c}{dP}\right)$, and $C_w = \frac{1}{\rho_w}\left(\frac{d\rho_w}{dP}\right)$, respectively [*Bear* 1979], we obtain

$$\left[(H-h)(C_f + C_c)\frac{\partial P}{\partial t} - \frac{\partial h}{\partial t}\right]\phi\rho_c(1-S_r) = -\frac{1}{r}\frac{\partial}{\partial r}\left[r\rho_c(H-h)q_c\right], \tag{3-13}$$

$$\left[(C_f + C_w)\left(\frac{S_r H}{(1-S_r)} + h\right)\frac{\partial P}{\partial t} + \frac{\partial h}{\partial t}\right]\phi\,\rho_w(1-S_r) = -\frac{1}{r}\frac{\partial}{\partial r}\left[rh\rho_w q_w\right]. \tag{3-14}$$

Then, we assume that the fluids and geological formation are sufficiently rigid such that $C_f, C_c, C_w, \phi, \rho_c$, and ρ_w are essentially constant. This assumption has been used extensively in the water resources literature when describing the specific storage coefficient, $S_s = \phi\rho_w g(C_f + C_w)$ [L^{-1}] in confined aquifers, where g [LT^{-2}] is the gravitational constant. Rewriting the system using the above assumption leads to:

$$\begin{aligned}\phi\rho_c(1-S_r)(C_f + C_w)\left[\left(\frac{H}{1-S_r}\right) + (H-h)\left(\frac{C_c - C_w}{C_f + C_w}\right)\right]\frac{\partial P}{\partial t}, \\ = -\frac{1}{r}\frac{\partial}{\partial r}\left[r\left((H-h)\rho_c q_c + hq_w\right)\right]\end{aligned} \tag{3-15}$$

$$\phi(1-S_r)\frac{\partial h}{\partial t} = -\frac{1}{r}\frac{\partial}{\partial r}\left[rhq_w\right] - \phi(C_f + C_w)\left[S_r H + (1-S_r)h\right]\frac{\partial P}{\partial t}. \tag{3-16}$$

3.4 Solution Development

3.4.1 Non-dimensionalization

The system to be analyzed can be simplified further by defining the following dimensionless parameters

$$r_D = \frac{r}{r_w}, \qquad r_{eD} = \frac{r_e}{r_w}, \qquad h_D = \frac{h}{H}, \qquad t_D = \frac{KP_0 t}{(1-S_r)\phi\mu_c r_w^2},$$

$$P_D = \frac{P}{P_o}, \qquad q_{cD} = \frac{\mu_c r_w q_c}{k_r K P_0}, \quad q_{wD} = \frac{\mu_w r_w q_w}{k_r K P_0}, \qquad \alpha = \frac{P_0(C_f + C_w)}{k_r(1-S_r)},$$

$$\beta = \frac{b_r b \rho_c P_0 k_r^2 K^2}{\mu_c^2 r_w}, \quad \gamma = \frac{\mu_c}{k_r \mu_w}, \qquad \sigma = \frac{b_r \rho_c}{\rho_w}, \text{ and} \qquad \varepsilon = (1-S_r)\frac{C_c - C_w}{C_f + C_w}.$$

Re-writing equations from (3-5) to (3-14) in dimensionless form leads to

$$[1+\varepsilon(1-h_D)]\alpha\frac{\partial P_D}{\partial t_D} = -\frac{1}{r_D}\frac{\partial}{\partial r_D}[r_D((1-h_D)q_{cD} + h_D q_{wD})], \tag{3-17}$$

$$\frac{\partial h_D}{\partial t_D} = -\frac{1}{r_D}\frac{\partial}{\partial r_D}(r_D h_D q_{wD}) - \alpha[S_r + (1-S_r)h_D]\frac{\partial P_D}{\partial t_D}, \tag{3-18}$$

$$-\frac{\partial P_D}{\partial r_D} = q_{cD} + \beta q_{cD}|q_{cD}|, \tag{3-19}$$

$$-\gamma\frac{\partial P_D}{\partial r_D} = q_{wD} + \frac{\gamma\beta}{\sigma}q_{wD}|q_{wD}|, \tag{3-20}$$

associated with the following initial and boundary conditions:

$$P_D(r_D \geq 1, t_D = 0) = 0, \tag{3-21}$$

$$h_D\left(r_D \geq 1, t_D = 0\right) = 1, \tag{3-22}$$

$$P\left(r_D = 1, t_D > 0\right) = 1, \tag{3-23}$$

$$q_{cD}\left(r_D = r_{eD}, t_D \geq 0\right) = 0, \tag{3-24}$$

$$q_{wD}\left(r_D = 1, t_D > 0\right) = 0, \tag{3-25}$$

$$q_{wD}\left(r_D = r_{eD}, t_D > 0\right) = 0. \tag{3-26}$$

In section 2, it has been shown that the final solution for domains of infinite extent when $r_{wD} \to 0$, $r_{eD} \to \infty, \varepsilon \to 0$, $t_D >> \dfrac{\beta^2}{2\gamma}$, and $\alpha << 1$ is described as follows:

$$P_D \approx \begin{cases} -c\ln\left(\dfrac{\chi}{4c\gamma}\right) - 2c + \dfrac{2c}{\gamma} - \dfrac{c}{\gamma}\left[\ln\left(\dfrac{c\alpha}{\gamma^2}\right) + \delta\right] + \left(\dfrac{\beta}{\sqrt{t_D\chi}}\right) & ; \quad \chi \leq 4\gamma c \\ -\sqrt{\dfrac{c\chi}{\gamma}} + \dfrac{2c}{\gamma} - \dfrac{c}{\gamma}\left[\ln\left(\dfrac{c\alpha}{\gamma^2}\right) + \delta\right] & ; \quad 4\gamma c < \chi < \dfrac{4c}{\gamma}. \\ -\dfrac{c}{\gamma}\left[\ln\left(\dfrac{\alpha\chi}{4\gamma}\right) + \delta\right] & ; \quad \chi \geq \dfrac{4c}{\gamma} \end{cases}$$

Let

$$F_D\left(\chi, c\right) = -\frac{c}{\gamma}E_1\left(\frac{\alpha\chi}{4\gamma}\right) \approx -\frac{c}{\gamma}\left[\ln\left(\frac{\alpha\chi}{4\gamma}\right) + \delta\right] = -\frac{c}{\gamma}\left[\ln\left(\frac{e^{\delta}\alpha\chi}{4\gamma}\right)\right], \tag{3-27}$$

we obtain

$$P_D \approx \begin{cases} -c\ln\left(\dfrac{\chi}{4c\gamma}\right) - 2c + \dfrac{2c}{\gamma} - F_D\left(\dfrac{4c}{\gamma}\right) + \left(\dfrac{\beta}{\sqrt{t_D\chi}}\right) & ; \quad \chi \le 4\gamma c \\ -\sqrt{\dfrac{c\chi}{\gamma}} + \dfrac{2c}{\gamma} - F_D\left(\dfrac{4c}{\gamma}\right) & ; \quad 4\gamma c < \chi < \dfrac{4c}{\gamma}, \\ F_D(\chi, c) & ; \quad \chi \ge \dfrac{4c}{\gamma} \end{cases} \tag{3-28}$$

where $\chi = \dfrac{r_D^2}{t_D}$ and E_1 denote the E_n function with n = 1, which is related to the exponential integral function, $E_i(\chi)$, via $E_1(\chi) = -E_1(-\chi)$.

The equation for a single-phase fluid of density, ρ_c, viscosity, μ_w, and radially flows in steady state conditions in a formation with finite radial extent r_e can be described as follows [*Dake* 1978]:

$$P = \frac{r_w \mu_w q_c(r = r_w, t)}{k} \ln\left(\frac{r_e}{r}\right). \tag{3-29}$$

Applying the dimensionless transformation, we have

$$P_D = \frac{2c}{\gamma}\ln\left(\frac{r_e}{r}\right) = \frac{2c}{\gamma}\ln\left(\frac{r_e^2}{r^2}\right)^{\frac{1}{2}} = -\frac{c}{\gamma}\ln\left(\frac{r_D^2}{r_{eD}^2}\right), \tag{3-30}$$

combining equations (3-27) and (3-30) and setting $P_D = F_D(\chi, c)$ gives:

$$\left(\frac{r_D^2}{r_{eD}^2}\right) = \left(\frac{e^{\delta}\alpha r_D^2}{4\gamma t_D}\right), \text{ and } \; t_D = t_{eD} = \frac{\alpha r_{eD}^2 e^{\delta}}{4\gamma}, \tag{3-31}$$

where t_{eD} is the time required by the perturbed pressure wave to hit the outer boundary of the domain r_{eD}. Following Mathias et al. [2011], we calculated the time span required

by the pressure wave to reach the outer boundary of the domain. Recalling that the injection process in our case is running under constant pressure at the wellbore (i.e. the flux at the wellbore in not known). However, we still can solve for the time span by using the flux formula developed previously in section 2. Equation (3-31) shows that the time span t_{eD} needed to reach that boundary is proportional to the squared distance between the injection well and the outer boundary, as well as, the total compressibility of the formation and the fluid, and the injection pressure at the wellbore. Although, equation (3-28) was derived for infinite domains only, it can be used for finite domains as long as the injection time is less than t_{eD}, calculated by equation (3-31).

3.4.2 Pseudo-steady state solution in a radial system for single phase flow

Physical consideration

As in section 2, an outer region, $r > r_i$, is assumed to consist of only a single phase. To solve for this region with a closed boundary conditions, we will introduce the simplification that the pressure in this region is in a pseudo-steady-state. The physical concept of pseudosteady state is defined as the condition where the pressure at all points in the reservoir changes at the same rate, so that the flux becomes independent of time, as illustrated by Figure 3.1. This condition is applicable to a reservoir which has been under injection for a sufficient period of time so that the effect of the outer boundary has been felt. In terms of radial flow model, it is considered that the well is surrounded by a

solid “brick wall” outer boundary which prevents the flow of fluids outside the reservoir, accordingly, at the outer boundary $\frac{\partial P(r_e,t)}{\partial t}=0$.

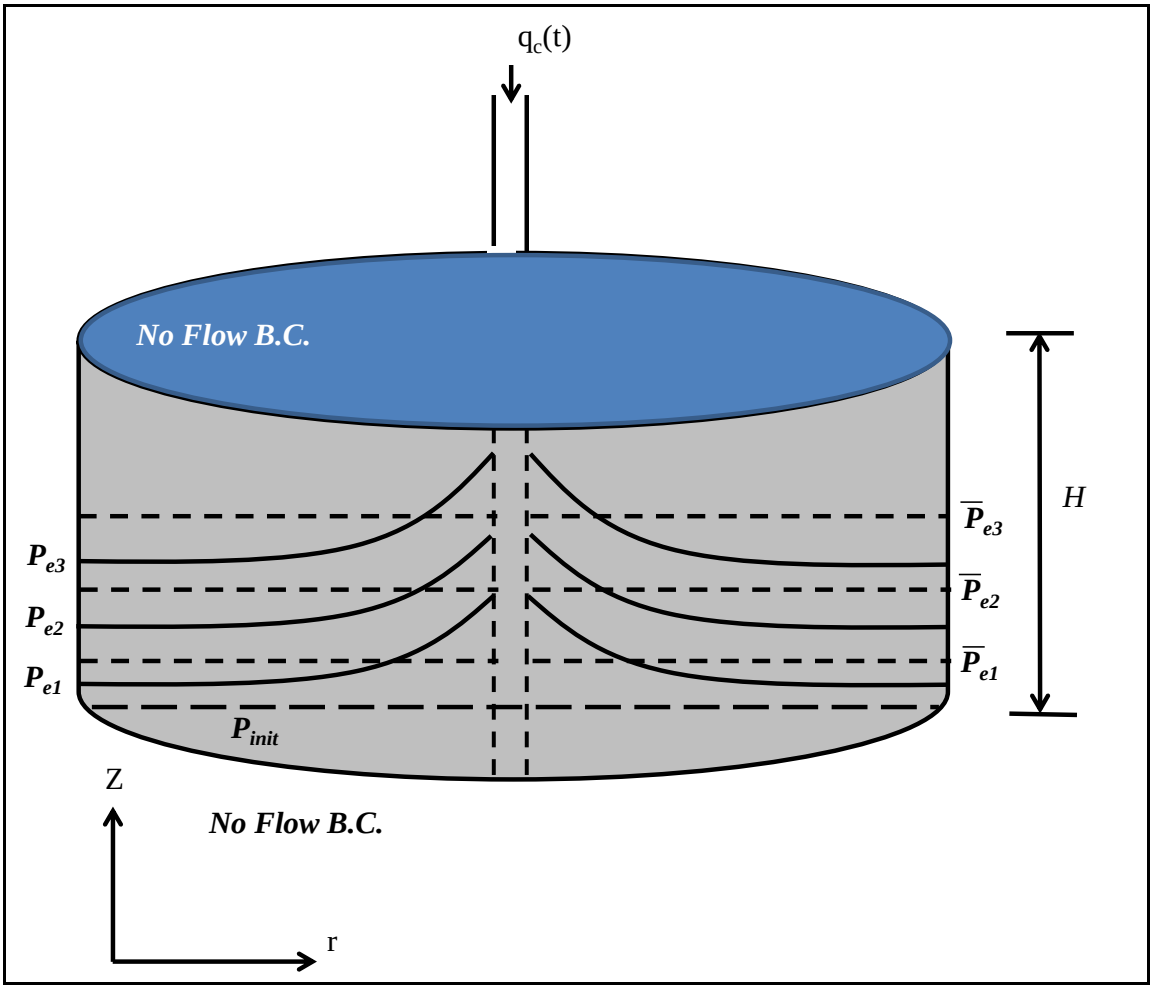

Figure 3.2: Plot of a schematic diagram shows pseudosteady state conditions in radial flow system.

Where P_{init} is the initial reservoir pressure; P_{e1}, P_{e2} and P_{e3} are the pressure at the reservoir boundary at times t_1, t_2, and t_3; $\overline{P}_{e1}$, $\overline{P}_{e2}$, $\overline{P}_{e3}$ are the average reservoir pressure at times t_1, t_2, and t_3, respectively.

Mathematical model

Now consider radial single-phase flow of a fluid with density, ρ_c, and viscosity, μ_w, in a closed formation of outer boundary "r_e". The governing partial differential equation for flow in porous media is called the diffusivity equation. The diffusivity equation for a slightly compressible liquid is given as

$$\frac{1}{r}\frac{\partial}{\partial r}\left[r\frac{\partial P}{\partial r}\right] = \frac{\phi\mu_w C_t}{k}\frac{\partial P}{\partial t} \quad , \tag{3-32}$$

where C_t is the total compressibility and is defined as $C_t = C_f + C_c$. The significant assumptions made in equation (3-32) are:

1. Slightly compressible liquid (i.e. constant compressibility)
2. Constant fluid viscosity
3. Single-phase liquid flow
4. Gravity and capillary pressure are neglected
5. Constant permeability
6. Horizontal radial flow (i.e. no vertical flow).

The system is subjected to the following boundary and initial conditions,

$$P(r_i < r < r_e, t = 0) = 0, \tag{3-33}$$

$$P(r = r_i, t > 0) = P_0, \tag{3-34}$$

$$q_c(r = r_e, t \geq 0) = 0, \tag{3-35}$$

where P_0 and r_i [L] are the injection constant pressure, and the radius of injection well in the case of single phase flow. After sufficient time has been passed for the outer boundary to be felt, the system will develop a pseudo-steady state. Then, the change in pressure with time becomes more or less uniform, so that the right hand side of equation (3-32) can be approximate as constant. The values of that constant can be obtained from a simple material balance relationship using the definition of compressibility. Once the reservoir reached the pseudo-steady state condition, each injection well in the reservoir will inject into its own no-flow boundary quite independently of the other wells. For this condition $\frac{dP(r,t)}{dt}$ must be approximately constant throughout the entire reservoir otherwise flow would occur across the boundaries causing a re-adjustment in their positions until stability was eventually achieved. In this case a simple technique can be applied to determine the volume average reservoir pressure.

The average aquifer pressure, $\overline{P}$ [MLT^{-2}], is controlled by a material balance using the compressibility definition as follows:

$$\overline{P} = P_{init} + \frac{2\pi H r_i}{C_t V} N_I, \tag{3-36}$$

where $\overline{P}$ [MLT^{-2}] is the average aquifer pressure, P_{init} [MLT^{-2}] is the initial aquifer pressure, $C_t = \frac{1}{V}\frac{dV}{dP}$ [M^{-1}LT^2] is the total compressibility for a cylindrical aquifer with fluid volume [L^3] , $V = AH\phi$, and cross-sectional area [L^2], $A = \pi\left(r_e^2 - r_i^2\right)$. N_I is the cumulative integrated injection rate into the aquifer (proportional to the total injected volume), and is defined as follows:

$$N_I = \int_0^t q_w(r = r_i, \tau)d\tau\,, \tag{3-37}$$

therefore, $\frac{dN_I}{dt} = q_w(r = r_i, t)$.

Taking the derivative of equation (3-36) with respect to time

$$\frac{d\overline{P}}{dt} = \frac{2\pi Hr_i}{VC_t} q_w(r = r_i, t)\,, \tag{3-38}$$

under the pseudo-steady state assumption,

$$\frac{dP}{dt} = \frac{d\overline{P}}{dt} = \frac{2\pi Hr_i}{VC_t} q_w(r = r_i, t)\,. \tag{3-39}$$

Substituting equation (3-39) into equation (3-32) (note that partial derivatives are now expressed as ordinary derivatives), we have

$$\frac{1}{r}\frac{d}{dr}\left[r\frac{dP}{dr}\right] = \frac{2\pi Hr_i\phi\mu_w}{Vk} q_w(r = r_i, t)\,. \tag{3-40}$$

Let

$$G(t) = \frac{2\pi Hr_i\phi\mu_w\, q_w(r = r_i, t)}{Vk}\,. \tag{3-41}$$

Substituting equation (3-41) into equation (3-40) and integrating, we obtain

$$G\frac{r}{2}+\frac{c_1}{r}=\frac{dP}{dr}. \tag{3-42}$$

Evaluating equation (3-42) at the outer boundary, $\frac{d}{dr}\left[P(r,t)\right]_{r_e}=0$, leads to

$$\frac{G}{2}r_e+c_1\frac{1}{r_e}=0, \tag{3-43}$$

where c_1 is an integration constant. Solving for c_1, we obtain

$$c_1=-\frac{G}{2}r_e^2. \tag{3-44}$$

Substituting equation (3-44) back into equation (3-42), multiplying through by dr, and integrating both sides across the entire aquifer radius (i.e. using separation of variable) leads to

$$\int_{P_i}^{P_r}dP=-\frac{G}{2}\int_{r_i}^{r}\left[\frac{r_e^2}{r}-r\right]dr, \tag{3-45}$$

evaluating the integration of equation (3-45), we obtain

$$P_r-P_i=-\frac{G}{2}\left[r_e^2\ln(r)\Big|_{r_i}^{r}-\frac{r^2}{2}\Big|_{r_i}^{r}\right]=\frac{G}{2}\left[r_e^2\ln\left(\frac{r_i}{r}\right)+\frac{1}{2}\left(r^2-r_i^2\right)\right]. \tag{3-46}$$

Substituting equation (3-41) into equation (3-46) gives

$$P_r-P_i=\frac{\pi Hr_i\phi\mu_w q_c}{Vk}\left[r_e^2\ln\left(\frac{r_i}{r}\right)+\frac{1}{2}\left(r^2-r_i^2\right)\right]. \tag{3-47}$$

Now, equation (3-47) can be written in dimensionless form as

$$P_{rD} - P_{iD} = \frac{\pi r_i r_e^2 q_{cD}(t_D)}{A\gamma r_w}\left[\ln\left(\frac{r_{iD}}{r_D}\right) + \frac{1}{2}\frac{\left(r_D^2 - r_{iD}^2\right)}{r_{eD}^2}\right].$$

Substituting $A = \pi\left(r_e^2 - r_i^2\right)$ into equation (3-47) and solving for P_r, we have

$$P_r = P_i + \frac{r_i \mu_w q_c}{k r_w}\left[\left(\frac{r_e^2}{r_e^2 - r_i^2}\right)\ln\left(\frac{r_i}{r}\right) + \frac{1}{2}\left(\frac{r^2 - r_i^2}{r_e^2 - r_i^2}\right)\right], \tag{3-48}$$

which can be rewritten in dimensionless form as

$$P_{rD} = P_{iD} + \frac{r_{eD} q_{cD}(t_D)}{\gamma}\left[\ln\left(\frac{r_i}{r}\right) + \frac{1}{2}\left(\frac{r^2 - r_i^2}{r_e^2}\right)\right]. \tag{3-49}$$

Development of $\overline{P}_r - P_i$ relationship

Now we will develop a relationship between the average aquifer pressure, $\overline{P}_r$, and the wellbore injection pressure, P_i. By definition, the average aquifer pressure is given by

$$\overline{P}_r = \frac{\int_{r_i}^{r} P_r dV}{\int_{r_i}^{r} dV}, \tag{3-50}$$

for a cylindrical aquifer, we have

$$V = \phi\pi H\left(r^2 - r_i^2\right), \text{ and } \quad dV = 2\phi\pi H r dr. \tag{3-51}$$

Substituting equation (3-51) into equation (3-50) gives

$$\overline{P}_r = \frac{2\pi\phi H}{\pi\phi H\left(r^2 - r_i^2\right)} \int_{r_i}^{r} P_r \, r dr \,,$$

which is reduced to

$$\overline{P}_r = \frac{2\pi}{A} \int_{r_i}^{r} P_r \, r dr \,. \tag{3-52}$$

Substituting equation (3-48) into equation (3-52) yield

$$\overline{P}_r = \frac{2\pi}{A} \int_{r_i}^{r} \left[P_i + \frac{r_i \mu_w q_c}{k} \left[\left(\frac{r_e^2}{r_e^2 - r_i^2} \right) \ln\left(\frac{r_i}{r} \right) + \frac{1}{2} \left(\frac{r^2 - r_i^2}{r_e^2 - r_i^2} \right) \right] \right] r dr \,. \tag{3-53}$$

Expanding equation (3-53) and isolating each integral as follows

$$\begin{aligned}
\overline{P}_r = {} & \frac{2}{r_e^2 - r_i^2} P_i \int_{r_w}^{r} r dr \\
& + \frac{2}{r_e^2 - r_i^2} \frac{r_i \mu_w q_w}{k} \left(\frac{r_e^2}{r_e^2 - r_i^2} \right) \int_{r_i}^{r} r \ln\left(\frac{r_i}{r} \right) dr \\
& + \frac{2}{r_e^2 - r_i^2} \frac{r_i \mu_w q_w}{k} \frac{1}{2} \left(\frac{1}{r_e^2 - r_i^2} \right) \int_{r_i}^{r} r^3 dr \\
& - \frac{2}{r_e^2 - r_i^2} \frac{r_i \mu_w q_w}{k} \frac{1}{2} \left(\frac{r_w^2}{r_e^2 - r_i^2} \right) \int_{r_i}^{r} r dr
\end{aligned} \,.$$

Evaluating each integral of equation (3-53) separately, we have

$$\int_{r_i}^{r} r dr = \frac{1}{2}\left(r^2 - r_i^2\right) \quad , \tag{3-54}$$

$$\int_{r_i}^{r} r \ln\left(\frac{r_i}{r} \right) dr = \frac{1}{2} r^2 \ln\left(\frac{r_i}{r} \right) + \frac{1}{4}\left(r^2 - r_i^2\right), \tag{3-55}$$

and

$$\int_{r_i}^{r} r^3 dr = \frac{1}{4}\left(r^4 - r_i^4\right) = \frac{1}{4}\left(r^2 + r_i^2\right)\left(r^2 - r_i^2\right). \tag{3-56}$$

Substituting equations (3-54) through (3-56) back into equation (3-53) and collecting similar terms, we obtain

$$\overline{P}_r = P_i + \frac{r_i \mu_w q_c}{k}\left[\left(\frac{r_e^2}{r_e^2 - r_i^2}\right)\left(\left(\frac{r^2}{r^2 - r_i^2}\right)\ln\left(\frac{r_i}{r}\right) + \frac{1}{2}\right) + \frac{1}{4}\left(\frac{r^2 + r_i^2}{r_e^2 - r_i^2}\right) - \frac{1}{2}\left(\frac{r_i^2}{r_e^2 - r_i^2}\right)\right]. \tag{3-57}$$

Equation (3-57) is our fundamental linking relation between the wellbore pressure and the average reservoir pressure during pseudo-steady state flow. However, $\overline{P}_r$ (the average reservoir pressure over a given radius, *r*) is of a little use. In order to obtain the average pressure of the reservoir based on the entire aquifer volume, we need to evaluate equation (3-57) at $r = r_e$ as follows

$$\overline{P} = P_i + \frac{r_i \mu_w q_C}{k}\left[\left(\frac{r_e^2}{r_e^2 - r_i^2}\right)\left(\left(\frac{r_e^2}{r_e^2 - r_i^2}\right)\ln\left(\frac{r_i}{r_e}\right) + \frac{1}{2}\right) + \frac{1}{4}\left(\frac{r_e^2 + r_i^2}{r_e^2 - r_i^2}\right) - \frac{1}{2}\left(\frac{r_i^2}{r_e^2 - r_i^2}\right)\right]. \tag{3-58}$$

Assuming $r_e >> r_i$ (i.e. the radial extent of the plume is always much smaller than that of the formation), this leads to

$$\left(\frac{r_e^2}{r_e^2 - r_i^2}\right) \approx 1, \left(\frac{r_e^2 + r_i^2}{r_e^2 - r_i^2}\right) \approx 1, \left(\frac{r_i^2}{r_e^2 - r_i^2}\right) \approx 0,$$

and the above solution reduces to the following equation

$$\overline{P} = P_i + \frac{r_i \mu_w q_c}{k}\left[\left(\ln\left(\frac{r_i}{r_e}\right) + \frac{3}{4}\right)\right]. \tag{3-59}$$

Now we can directly couple equation (3-59) with the material balance, equation (3-39), to develop a time-pressure relation for pseudo-steady state flow.

Recalling equation (3-39), we have

$$\frac{dP}{dt} = \frac{d\overline{P}}{dt} = \frac{2\pi Hr_i}{VC_t} q_w(r = r_i, t),$$

which upon integration yields an estimate of the average aquifer pressure as follows

$$\overline{P} = \frac{2\pi Hr_i}{VC_t} \int_0^t q_w(\tau) d\tau . \tag{3-60}$$

Substituting equation (3-60) into equation (3-59), we obtain the pressure at the inner boundary of the pseudo-steady state region:

$$P_i = \frac{2\pi Hr_i}{VC_t} \int_0^t q_c(\tau) d\tau - \frac{r_i \mu_w q_c}{k} \left[\left(\ln\left(\frac{r_i}{r_e}\right) + \frac{3}{4} \right) \right]. \tag{3-61}$$

3.4.3 Combining single phase solution with two phase solution

We now set r_i to be the outside edge of the two phase region. Recalling that $\chi = \frac{r_D^2}{t_D}$, and the outside edge of the two-phase region is defined by $\chi = \frac{4c}{\gamma}$, it follows that $\frac{4c}{\gamma} = \frac{r_{iD}^2}{t_D}$, and $\frac{r_i^2}{r^2} = \frac{4c}{\gamma \chi}$. Assuming that the pressure distribution in the far field regions obeys equation (3-47) (i.e. $F_D\left(\frac{4c}{\gamma}\right) = P_{iD}$), where equation (3-61) can be written in dimensional form as

$$P_{iD} = \frac{2\pi r_w^2}{\alpha A}\int_0^{t_D} q_{cD}(\tau_D)d\tau_D - \frac{q_{cD}}{\gamma}\left[\left(\ln\left(\frac{r_{iD}}{r_{eD}}\right)+\frac{3}{4}\right)\right]. \tag{3-62}$$

By substituting equation (3-62) into the part represents the outer solution (i.e. when $r_i < r < r_e$) of equation (3-28) , we can rewrite equation (3-28) as follows:

$$P_D - P_{iD} \approx \begin{cases} -2c\ln\left(\frac{r}{r_i\gamma}\right) - 2c + \frac{2c}{\gamma} + \left(\frac{\beta\, r_w}{r}\right) & ; \quad r_w \le r \le r_i\gamma \\ -\frac{2rc}{r_i\gamma} + \frac{2c}{\gamma} & ; \quad r_i\gamma < r < r_i \\ -\frac{q_{cD}(t_D)}{\gamma}\left[-\ln\left(\frac{r_i}{r}\right) + \frac{1}{2}\left(\frac{r^2 - r_i^2}{r_e^2}\right)\right] & ; \quad r_i < r < r_e \end{cases}. \tag{3-63}$$

The mean dimensionless pressure is defined by

$$\overline{P}_D - P_{iD} = \frac{2\pi}{A}\int_{r_w}^{r_e} r\left(P_D - P_{iD}\right)dr\,,$$

or

$$P_{iD} = \frac{2\pi r_w^2}{\alpha A}\int_0^{t_D} q_{cD}(r_D = 1, \tau_D)d\tau_D - \frac{2\pi}{A}\int_{r_w}^{r_e} r\left(P_D - P_{iD}\right)dr\,. \tag{3-64}$$

Substituting equation (3-63) into equation (3-64) and integrating yields

$$\begin{aligned} P_{iD} = {} & \frac{2\pi r_w^2}{\alpha A}\int_0^{t_D} q_{cD}(r_D = r_{iD}, \tau_D)d\tau_D \\ & - \frac{2\pi}{A}\left\{\beta\left(\gamma\, r_i r_w - r_w^2\right) + \left(1 + \frac{2}{\gamma^3}\right)\left(\frac{\gamma^2 r_i^2 c}{6}\right) - \frac{r_w^2}{2}\left(\ln\left(\frac{\gamma\, r_i}{r_w}\right) + \frac{2c}{\gamma} - 2c + \frac{1}{2}\right)\right. \\ & \left. + \frac{r_e^2 q_{cD}(t_D)}{\gamma}\left(\frac{3}{4} - \ln\left(\frac{r_e}{r_i}\right) - \frac{r_i^2}{r_e^2} + \frac{1}{4}\frac{r_i^4}{r_e^4}\right)\right\}. \end{aligned} \tag{3-65}$$

Now we can write $F_D(\chi,c)$ as follows:

$$F_D(\chi,c)\approx\begin{cases}-\dfrac{c}{\gamma}\ln\left(\dfrac{e^{\delta}\alpha\,\chi}{4\gamma}\right) & ;\quad t_D<t_{eD}\\ \\ P_{iD}+q_{cD}(t_D)\left[\dfrac{1}{2\gamma}\ln\left(\dfrac{4c}{\gamma\,\chi}\right)+\dfrac{(\gamma\,\chi-4c)t_D}{2\gamma^2 r_{eD}^2}\right] & ;\quad t_D>t_{eD}\end{cases}, \qquad (3\text{-}66)$$

or

$$F_D(\chi,c)\approx\begin{cases}-\dfrac{c}{\gamma}\ln\left(\dfrac{e^{\delta}\alpha\,\chi}{4\gamma}\right) & ;\quad t_D<t_{eD}\\ \\ P_{iD}+\dfrac{1}{\gamma}\left[\dfrac{q_{cD}(t_D)}{2}\left(\ln\left(\dfrac{4c}{\gamma\,\chi}\right)+\dfrac{(\gamma\,\chi-4c)t_D}{\gamma\,r_{eD}^2}\right)\right] & ;\quad t_D>t_{eD}\end{cases}. \qquad (3\text{-}67)$$

Recalling that $t_{eD}=\dfrac{e^{\delta}\alpha\,\chi}{4\gamma}$ is the time needed for the pressure wave perturbation to reach the outer boundary of the domain. Now it becomes clear that equation (3-66) is the solution of a closed domain and it is the analogue of equation (3-28).

Note that the second part of equation (3-66) is obtained by substituting $r^2=\dfrac{\gamma\,\chi}{4c}r_i^2$ and $r_i^2=\dfrac{4c\,r_w^2 t_D}{\gamma}$ (where $\dfrac{r}{r_i}=\sqrt{\dfrac{\gamma\,\chi}{4c}}$ and $\dfrac{r_i}{r_w}=\sqrt{\dfrac{4ct_D}{\gamma}}$) into the part of equation (3-60) describes the pressure propagation in the outer most region of the domain (i.e. when $r_i<r<r_e$).

Now let's evaluate P_{iD} when $t_D > t_{eD}$ assuming that $r_e >> r_i$ (i.e. the radial extent of the plume is always much smaller than that of the formation), and hence the quantities: r_i^2, $\frac{r_i^2}{r_e^2}$ and $\frac{r_i^4}{r_e^4}$ are too small and could be substituted with zero. This leads to $A = \pi r_e^2$ and equation (3-64) reduces to the following

$$P_{iD} = \frac{2\pi r_w^2}{\alpha A}\int_0^{t_D} q_{cD}(r_D = r_{iD}, \tau_D)\, d\tau_D - \frac{2\pi}{A}\left[\frac{r_e^2 q_{cD}(t_D)}{\gamma}\left(\frac{3}{4} + \frac{1}{2}\ln\left(\frac{r_i^2}{r_e^2}\right)\right)\right]. \tag{3-68}$$

Substituting $r_i^2 = \frac{4c\, r_w^2 t_D}{\gamma}$ into equation (3-67) gives

$$P_{iD} = \frac{2\pi r_w^2}{\alpha A}\int_0^{t_D} q_{cD}(r_D = r_{iD}, \tau_D)\, d\tau_D - \frac{2\pi}{A}\left[\frac{r_e^2 q_{cD}(t_D)}{\gamma}\left(\frac{3}{4} + \frac{1}{2}\ln\left(\frac{4c\, t_D}{r_{eD}^2 \gamma}\right)\right)\right], \tag{3-69}$$

or

$$P_{iD} = \frac{2\pi r_w^2}{\alpha A}\int_0^{t_D} q_{cD}(r_D = r_{iD}, \tau_D)\, d\tau_D - \frac{1}{\gamma}\left[\frac{2\pi r_e^2 q_{cD}(t_D)}{A}\left(\frac{3}{4} + \frac{1}{2}\ln\left(\frac{4c\, t_D}{r_{eD}^2 \gamma}\right)\right)\right]. \tag{3-70}$$

Substituting equation (3-69) into equation (3-66), we obtain

$$F_D(\chi, c) \approx \begin{cases} -\frac{c}{\gamma}\ln\left(\frac{\alpha\,\chi}{4\gamma e^{\delta}}\right) & ; \quad t_D < t_{eD} \\ \frac{2\pi r_w^2}{\alpha A}\int_0^{t_D} q_{cD}(r_D = 1, \tau_D)\, d\tau_D - & \\ \frac{1}{\gamma}\left[\frac{q_{cD}(t_D)}{2}\left(\ln\left(\frac{4c}{\gamma\,\chi}\right) + \frac{(\gamma\,\chi - 4c)t_D}{\gamma\, r_{eD}^2} + \frac{4\pi r_e^2}{A}\left(\frac{3}{4} + \frac{1}{2}\ln\left(\frac{4c\, t_D}{r_{eD}^2\gamma}\right)\right)\right)\right] & ; \quad t_D > t_{eD} \end{cases} . \tag{3-71}$$

Finally, we can obtain a closed form expression for P_D as follows:

$$P_D \approx \begin{cases} -c\ln\left(\dfrac{\chi}{4c\gamma}\right) - 2c + \dfrac{2c}{\gamma} - F_D\left(\dfrac{4c}{\gamma}\right) + \left(\dfrac{\beta}{\sqrt{t_D\chi}}\right) & ; \quad \chi \le 4\gamma c \\ -\sqrt{\dfrac{c\chi}{\gamma}} + \dfrac{2c}{\gamma} - F_D\left(\dfrac{4c}{\gamma}\right) & ; \quad 4\gamma c < \chi < \dfrac{4c}{\gamma}, \\ F_D(\chi, c) & ; \quad \chi \ge \dfrac{4c}{\gamma} \end{cases} \tag{3-72}$$

where

$$F_D(\chi, c) = \frac{2\pi r_w^2}{\alpha A}\int_0^{t_D} q_{cD}(r_D = 1, \tau_D)\,d\tau_D - \frac{1}{\gamma}\left[\frac{q_{cD}(r_D = 1, t_D)}{2}\left(\ln\left(\frac{4c}{\gamma\chi}\right) + \frac{(\gamma\chi - 4c)t_D}{\gamma r_{eD}^2} + \frac{4\pi r_e^2}{A}\left(\frac{3}{4} + \frac{1}{2}\ln\left(\frac{4c\,t_D}{r_{eD}^2\gamma}\right)\right)\right)\right], \tag{3-73}$$

$$F_D\left(\frac{4c}{\gamma}\right) = \frac{2\pi r_w^2}{\alpha A}\int_0^{t_D} q_{cD}(r_D = r_{iD}, \tau_D)\,d\tau_D - \frac{1}{\gamma}\left[\frac{2\pi}{A}\frac{r_e^2 q_{cD}(r_D = 1, t_D)}{\gamma}\left(\frac{3}{4} + \frac{1}{2}\ln\left(\frac{4c\,t_D}{r_{eD}^2\gamma}\right)\right)\right], \tag{3-74}$$

and $q_{cD}(r_D = 1, t_D) = 2c$, recalling that c is half of the dimensionless flux at the wellbore as defined in section 2.

3.5 Results and Discussion

We apply the solution scheme described above to a specific example aquifer, where the injection pressure, initial and boundary conditions, and the formation

properties (thickness, perforation thickness, permeability and porosity) are summarized in Table 2.3 and 3.1. The injection process continues for one hundred years, starting in the year 2010 and ended in 2110. The pressure buildup across the entire aquifer is shown at five year intervals in Figure 3.3. During the entire injection period, there are large pressure gradients within 250 m of the well, and then gradients are much lower at larger distances. It also shows that the rate of pressure buildup decreases with time, with the late time pressure curves (i.e. after the year 2070) stacking nearly on top of one another.

Table 3.1: Model parameters used in closed brine aquifer calculations.

Parameter	Value
k_r	0.6[-]
r_e	10 [km]
S_r	0.15[-]

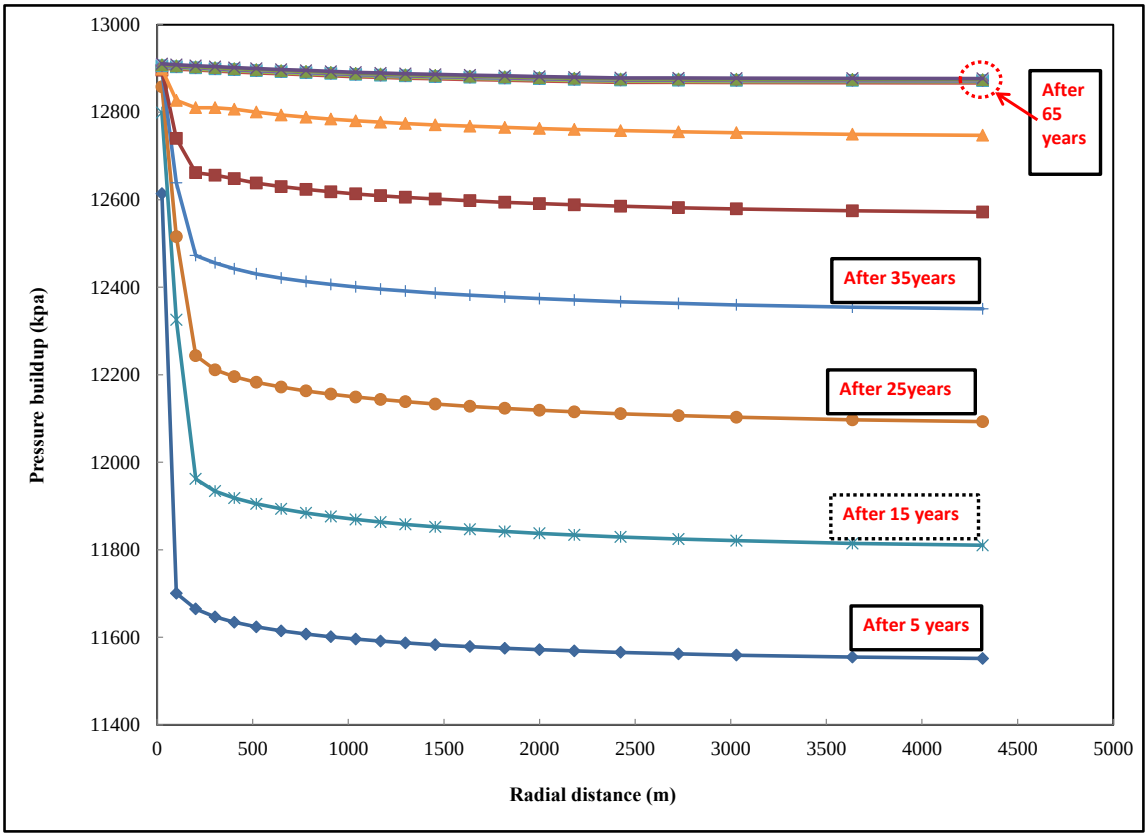

Figure 3.3: Predicted pressure vs. radial distance at different times for different years since injection begins.

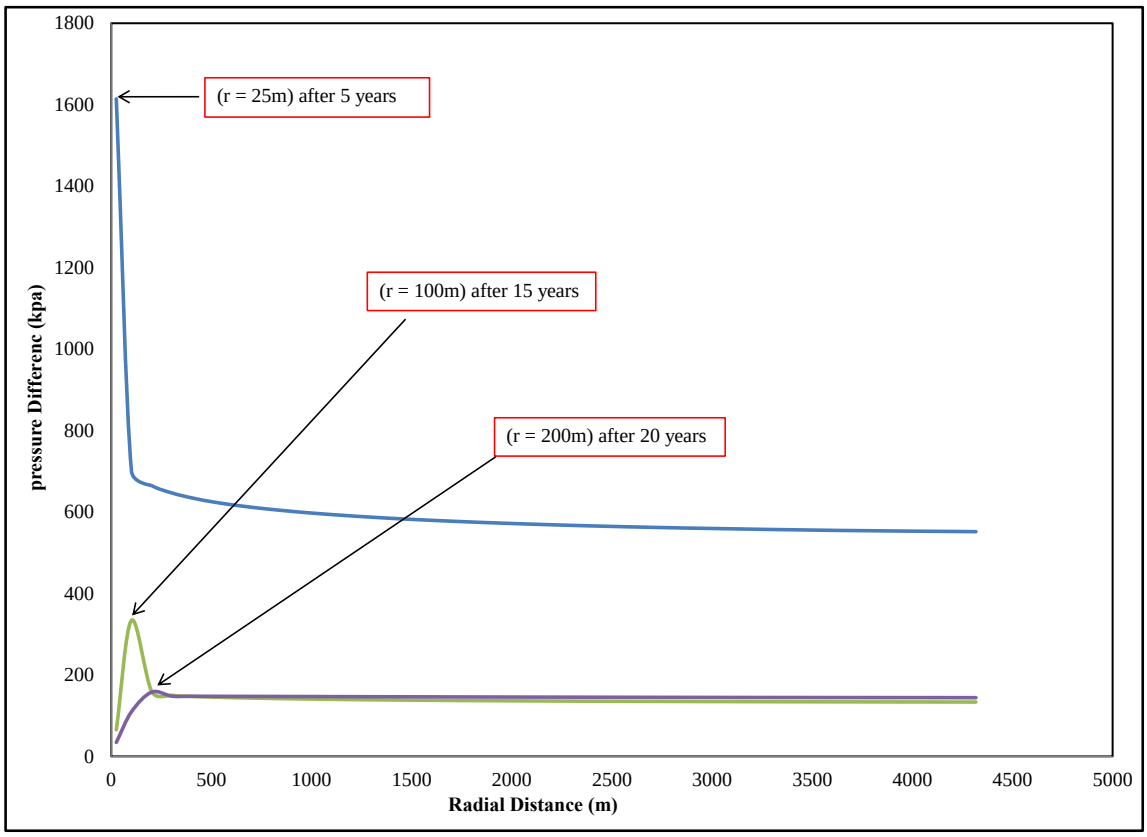

Figure 3.4: Predicted pressure increases over 3 different 5-year periods (2015-2010, 2025-2010, and 2030-2010) as a function of radial distance.

Figure 3.4 shows the difference between calculate reservoir pressures separated by 5 years in time; this difference therefore is approximately proportional to the rate of change of pressure. At any given time, the maximum rate of pressure increase will occur at some distance from the wellbore. The decrease in amplitude and increase in radial distance with time demonstrates the front of pressure diffusing outward from the wellbore as time evolves. The rate of pressure difference between the years 2015-2010 is largest very near the well at r=25m.While between the years 2025-2020 the peak rate of change is found at r=100m. Then it is shifted to be at r=200m between the years 2030-

2025, then it kept migrating and attenuating away from the well as time proceeds . This is because each pressure perturbation wave starts very strong nearby the wellbore, and then as it migrates away from the wellbore it attenuates and changes its location. In other words, the pressure perturbation wave starts with very sharp and high peak, and then diffuses with radial distance away from the well as time evolves.

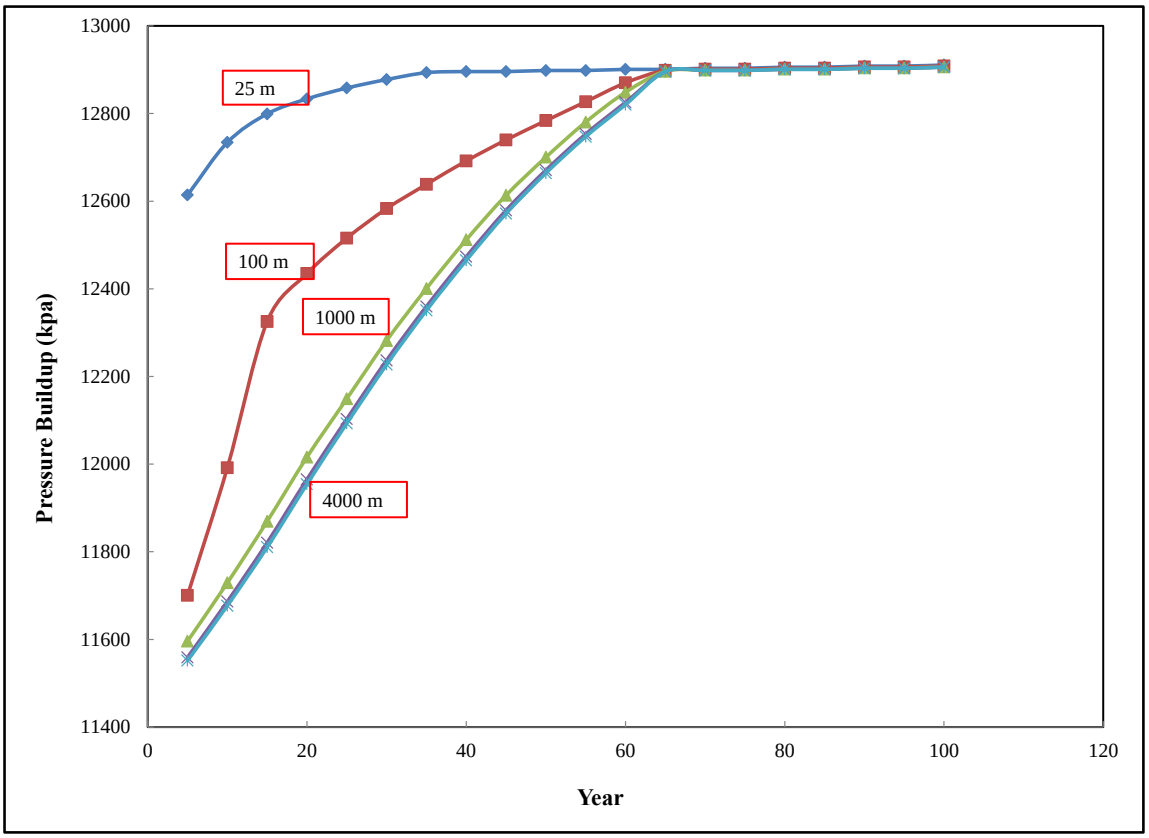

Figure 3.5: Comparison of predicted pressure buildup as a function of time at specific radial distances (r= 25 m, 100 m, 1000 m, 3000 m, and 4000 m).

Figure 3.5 shows the results of pressure build up at five different radial locations (r = 25, 100, 1000, 3000, and 4000m). These locations are selected to compare the pressure buildup at close (i.e. r=25 and 100m), intermediate (i.e. r= 1000 and 3000m) and far (i.e. r=4000m) distance from the well. The pressure increased by 1600 kpa at r=25m by the end of the first five years of injection (2010-2015), then the increase dropped down to be 120 kpa in the second five years and kept going down to increase with 65, 35 , 25, 20, and 18 kpa in the third, fourth, fifth, sixth and seventh periods, respectively. It started to level off and increase by 2.5 between the years 2060 and 2110 to possess an overall increase in pressure with 1910 kpa from the beginning till the end of injection. While at distance r=100 the pressure profile increased with 700 kpa in the first five years, and kept increasing with 330, 290, 110, 90, 80, 65, and 30 kpa every five years between the year 2015 and 2070, and started to stabilize with 2.5 kpa raise up every five years during the last 20 years of injection. The last three curves (i.e. at r=1000, 3000, and 4000m) follow the same pattern, kept their increasing rate with an average of 180 kpa till the year 2070, and then declined to increase with 2.5 kpa between the years 2070 and 2110.

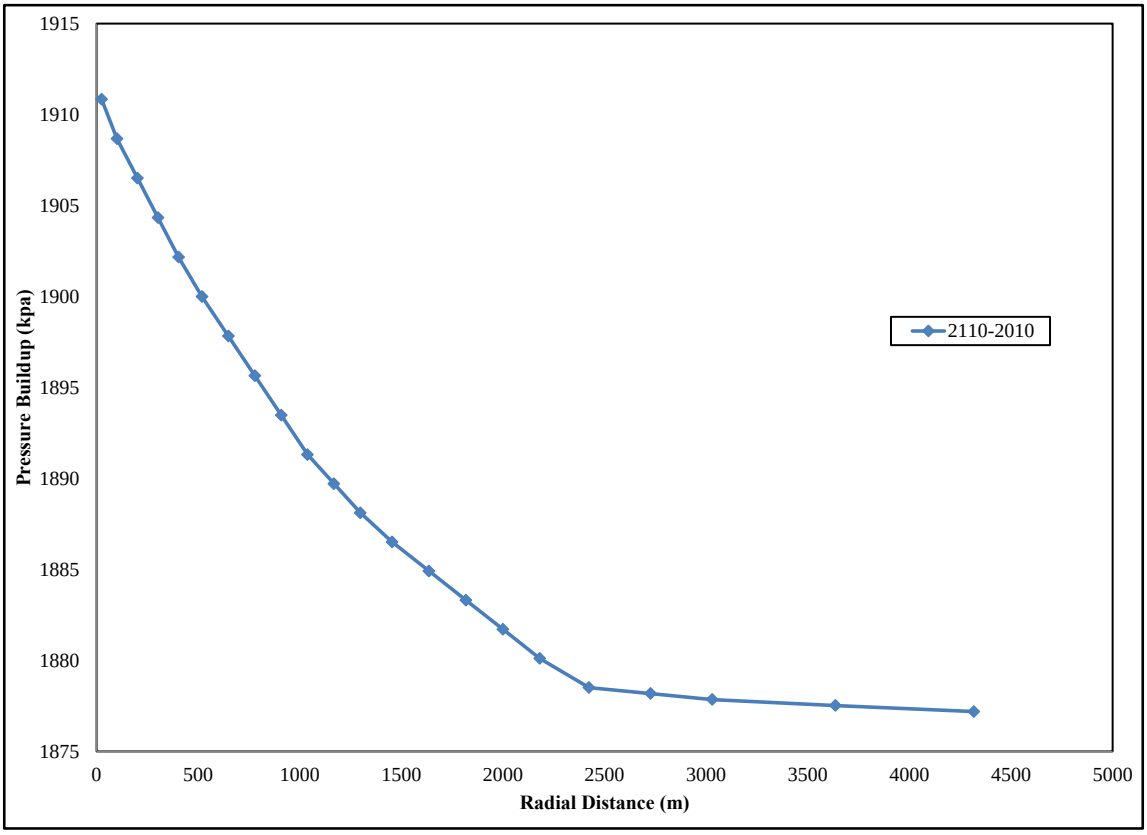

Figure 3.6: Pressure increase after 100 years of pumping as a function of radial distance.

Figure 3.6 shows essentially the same results as Figures 3.3, 3.4 and 3.5. It shows that as a consequence of injection the aquifer develops a very steep pressure gradient near to the wellbore, and as we move away from the wellbore the gradient relaxes till it levels off at the outer boundary.

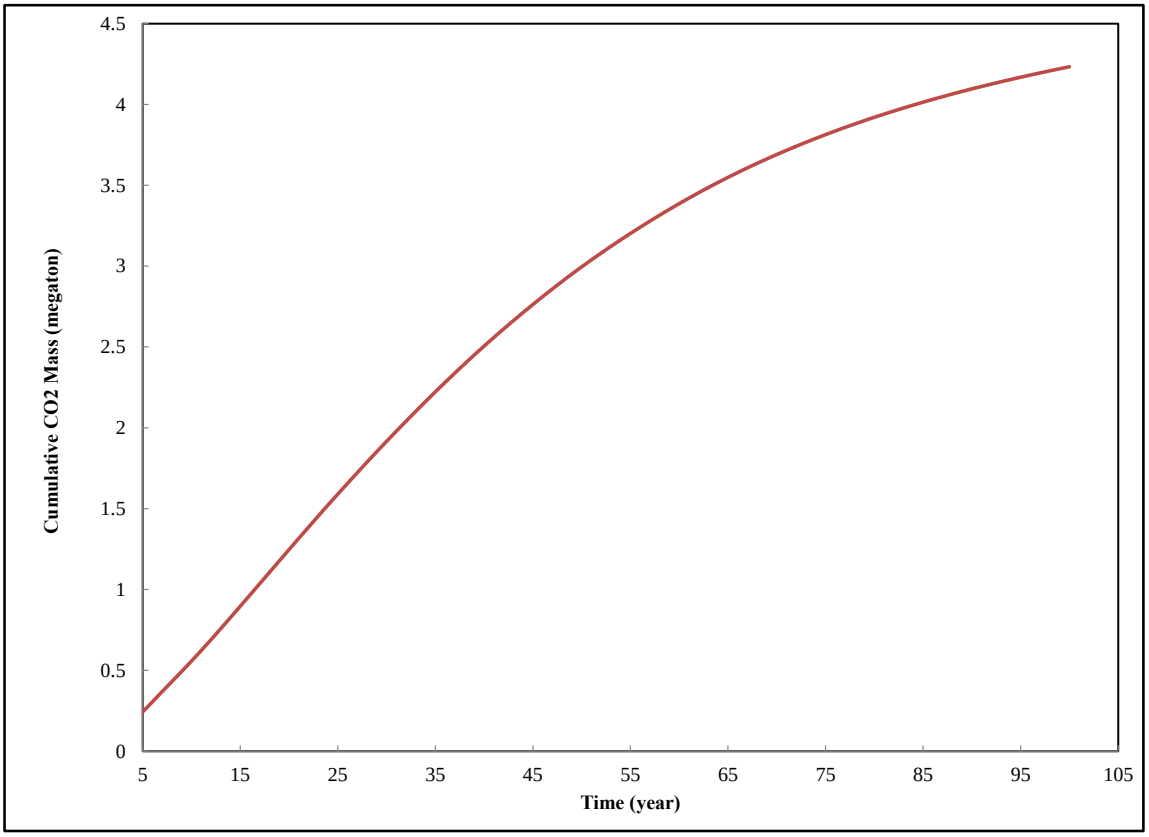

Figure 3.7: Expected cumulative injected CO_2 mass vs. time.

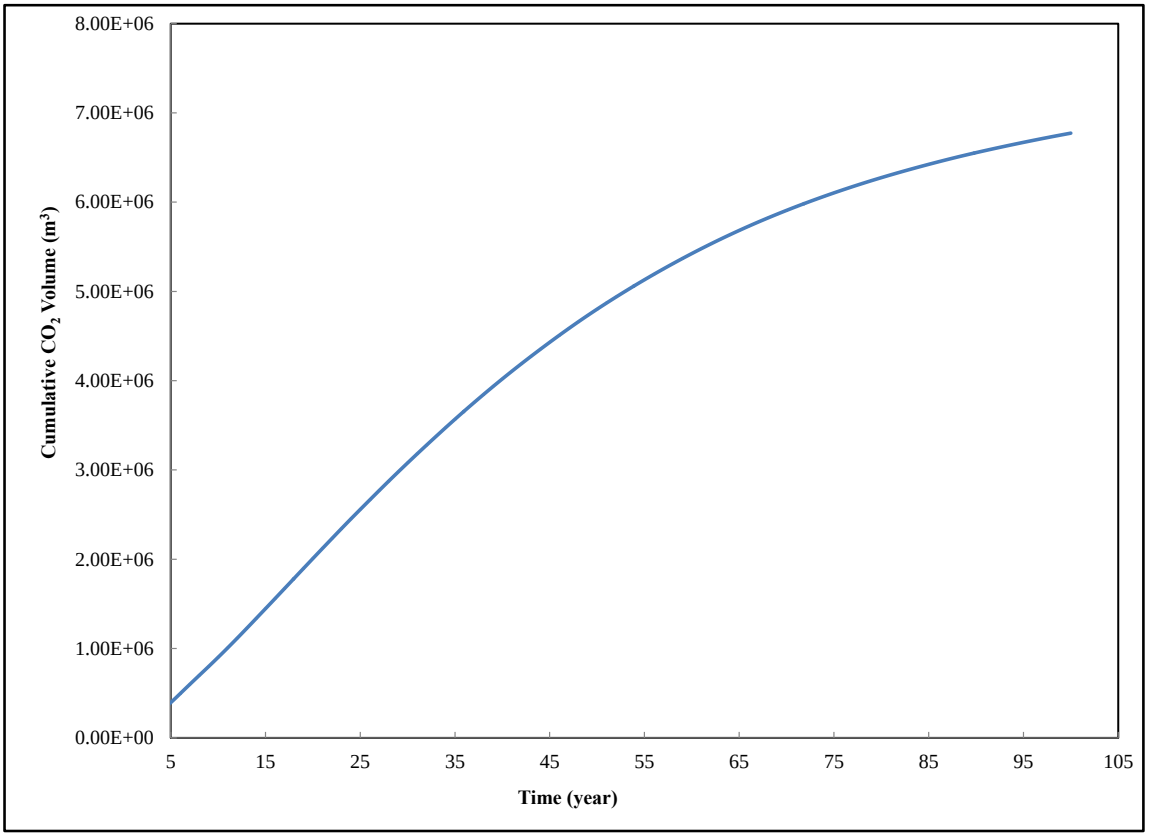

Figure 3.8: Expected cumulative injected CO_2 volume vs. time.

Following the same procedure we can calculate both the cumulative injected CO_2 volume and mass. Figures 3.7 and 3.8 show the cumulative injected volume (in cubic meter) and mass (in megaton) during the injection process, respectively. It can be seen that the two curves have the same pattern; they keep increasing from the star till the end of the hundred year injection.

4. PRESSURE BUILDUP DURING CO_2 INJECTION THROUGH FULL-PENETRATING WELLS IN INFINTE AND CLOSED GAS RESERVOIR

Among the possible formations available for CO_2 storage, deep saline aquifers have the largest capacity [*IPCC* 2005] and are relatively ubiquitous. However, because of the enormous scale of the problem, any full-scale implementation of CCS will likely require use of other geological media such as oil and gas reservoirs [*IPCC* 2005].

In this section, we develop a semi-analytical solution for the pressure evolution in depleted gas reservoirs when CO_2 is injected at a constant pressure. The solution accounts for CO_2 compressibility, and both infinite-acting and closed reservoirs are considered. The time-variable injection rate and the cumulative mass and volume of CO_2 injected during the injection period are also calculated

4.1 Introduction

Because of the uncertainty in predicting climate behavior and the need to avoid irreversible climate changes and the associated risks resulting from greenhouse effects, most of the industrialized world has committed to reduce the release of anthropogenic CO_2 into the atmosphere [*IPCC* 2005]. Carbon capture and storage (CCS) is an immediately available means of reducing CO_2 emissions into the atmosphere from major point sources, such as thermal power plants and the petrochemical industry [*IPCC* 2005].

CCS with geo-sequestration consists of three stages. The first is the CO_2 capture itself, the second is its transport and the third the injection and storage in deep geological formations. Various types of geological formations can be considered for CO_2 sequestration. These include un-minable coal seams [*Krooss et al.* 2002; *Shi and Durucan* 2005; *Stevens et al.* 1999], depleted oil and gas reservoirs [*Ferronato et al.* 2010; *Gallo et al.* 2002; *Hawkes et al.* 2005; *Li et al.* 2005; *Li* 2006; *Li et al.* 2006; *Oldenburg and Benson* 2002; *Oldenburg et al.* 2001; *Oldenburg* 2006; *Stevens et al.* 2000; *Whittaker et al.* 2004], and deep saline aquifers [*Bachu* 2000, 2008; *Birkholzer and Zhou* 2009; *Gale* 2004; *Gunter et al.* 1997; *Hepple and Benson* 2005; *Holloway* 2005; *IPCC* 2005; *Vilarrasa et al.* 2010a]. Currently, depleted or nearly depleted oil and gas reservoirs are the most appealing geological storage sites for CO_2 sequestration for the following reasons. First, the depleted reservoirs have been extensively investigated during the exploitation stage. In addition, the underground and surface infrastructure (wells, equipment and pipelines) is already available and could be used for CO_2 storage injection with, at most, minor modifications. Moreover, the injection of different gases, including CO_2, into natural gas reservoirs as a technique to enhance recovery has been widely practiced in the gas industry. The experience gained can be adapted to guide the CO_2 sequestration injection.

Accordingly, the sequestration of CO_2 in nearly depleted or even developing gas reservoirs can simultaneously reduce greenhouse gas emissions and increase gas recovery. Recovery of natural gas is highly efficient, leaving a large amount of void

space to store CO_2 [*Stevens et al.* 2001]. Also, the process has many advantages. Firstly, the CO_2 is trapped in the reservoirs in the same way gas is stored. Therefore, this method can bypass an important barrier of geological storage, long-term liability of the injected CO_2 [*Kuuskraa and Ferguson* 2008].

Secondly, gas can be recovered, supporting the economy and creating incentives for gas companies [*Kuuskraa and Ferguson* 2008], and a CO_2 sequestration market will be created that can balance out the cost of carbon capture, transportation, and storage. The size of this market is about 7,500 million tons between now and 2030 [*Kuuskraa and Ferguson* 2008].

A typical reservoir consists of a layer of permeable rock with another layer of impermeable rock above, forming a trap that can hold CO_2 inside in the same way it keeps gas [*Plasynski et al.* 2009]. One of the biggest challenging facing large-scale applications of geologic sequestration in gas fields is the lack of adequate monitoring techniques and verification to convince regulators and the public that sequestration is secure over a long term. This challenge could be overcome by developing a robust and practical monitoring technique to the sequestration process.

Different aspects of CO_2 storage in depleted gas reservoirs have been extensively studied using numerical models, including underground migration simulation [*Audigane et al.* 2007; *Johnson et al.* 2004; *Obi and Blunt* 2006; *Oldenburg et al.* 2001; *Van der*

Meer 1992], geochemical modeling [*André et al.* 2007; *Audigane et al.* 2007; *Audigane et al.* 2009; *Xu and Pruess* 2001; *Xu et al.* 2004], long-term integrity and risk assessment [*Celia et al.* 2006; *Duncan et al.* 2009].

Predictions of the CO_2 plume extent and the generated overpressure should be performed for each potential CO_2 storage site. Creating a numerical model for every one of these sites will be needed. Still, analytical solutions, which make simplifying assumptions, may help in the process of screening and decision making for initial site selection.

Some of the existing analytical solutions of the syninjection period, [*Dentz and Tartakovsky* 2009a, 2009b; *Nordbotten et al.* 2005b] and those for the post-injection period [*Hesse et al.* 2008; *Hesse et al.* 2007; *Juanes et al.* 2010], assume that CO_2 is incompressible. This assumption can induce large errors in the CO_2 plume position estimation. There is only one explicit solution (to our knowledge) for pressure buildup in a gas reservoir during the injection of compressible CO_2 [*Mukhopadhyay et al.* 2012], which assumed an infinite acting reservoir and a constant injection rate.

Existing analytical solutions assume injection at a constant rate at the wellbore. This assumption is also problematic because injection under constant rate is hard to maintain especially for gases. This leads to the objective of this study, which incorporates CO_2 compressibility and constant pressure injection in a semi-analytical

solution for the CO_2 pressure distribution in gas reservoirs. One major difficulty in developing an analytical or semi-analytical solution involving injection of CO_2 under constant pressure is that, the flux of CO_2 at the wellbore is not known. The way to get around this obstacle is to solve for the pressure wave first as a function of flux, and then solve for the flux numerically, which is subsequently plugged back into the pressure formula to get a closed form solution of the pressure.

The objective of this study is to develop an approximate solution for pressure build up during the injection of CO_2 under constant pressure into gas reservoirs through a fully penetrating well. The solution is extended to account for both infinite acting reservoirs and closed ones as well. The solution is developed using Laplace transform to obtain the solution in Laplace domain, and then invert it back into the real time domain.

4.2 Conceptual Model

Once a gas reservoir has undergone a CO_2 injection process, a supercritical CO_2 phase will replace the original hydrocarbon near the wellbore, and may fill the either the bottom or top of the reservoir, depending on the relative density of CO_2 and hydrocarbon.. There are many different mechanisms that control the migration of CO_2 in the reservoir. The most important transport mechanisms include: fluid flow under pressure gradient created by the injection process, effect of buoyancy forces resulting from the density differences between the fluids, diffusion, dispersion and fingering caused by the existence of preferential pathways due to heterogeneity of the storage

formation and differences in mobility between fluids, and transport by capillarity arising from contrast of fluids wettability [*IPCC* 2005]. Other potentially important processes include the reaction of CO_2 with mineral surfaces in the reservoir, dissolution into the original reservoir fluid, and the adsorption upon the surface of clay minerals. Following Mukhopadhyay et al [2012], we simplified the system in order to develop a closed form solution. Dispersion, mineralization, dissolution, and adsorption processes are not considered since they only become significant at times larger than the time of our interest (i.e., during injection and the following ~100 years). We also ignore capillary forces, and assume a homogeneous formation, so that the two phases remain separated by a sharp, simple boundary. . The viscosity of pure supercritical CO_2 can be significantly larger than that of pure Methane [*Oldenburg and Doughty* 2011], but for simplicity and following Mukhopadhyay et al [2012] , we assume that the viscosity of the resident gas phase is equal to that of the injected gas.

The buoyancy forces that drive vertical flow depend on the type of the in-situ fluid. Also, the magnitude of the density difference between the invading gas and the in-situ gas phase depends on formation pressure and temperature. This may lead to significant buoyancy effects between dense CO_2 and the lighter native natural gas (e.g., CH_4) [*Oldenburg and Doughty* 2011]. However, our objective is to estimate the maximum pressure buildup during injection (i.e. is near the injection well), which is dominated by viscous forces and not buoyancy forces (which are important farther away). We then exclude buoyancy from our conceptual model. This exclusion is likely

to produce a conservative estimate of the maximum extent of pressure buildup, because buoyancy drives fluids away vertically from the point of injection into the formation. Thus, the predicted pressure without buoyancy at the point of injection is larger than the actual pressure (when buoyancy is included). Additionally, when buoyancy is ignored, the model results will overestimate injection-induced horizontal migration of CO_2 (i.e., the actual near-field horizontal spreading would be slightly less when buoyancy is included).

The schematic diagram in Figure 4.1 shows the conceptual model. The reservoir is cylindrical and bounded on the top and bottom by impermeable rocks creating no flow boundary conditions. The well is vertical and fully penetrating the reservoir in the center. The flow is assumed to be horizontal and axisymmetric around the wellbore, which is justified since the buoyancy force is ignored as a vertical transport driving mechanism. The wellbore is acting as the first-type (Dirichlet) inner boundary condition, where the pressure is prescribed there.

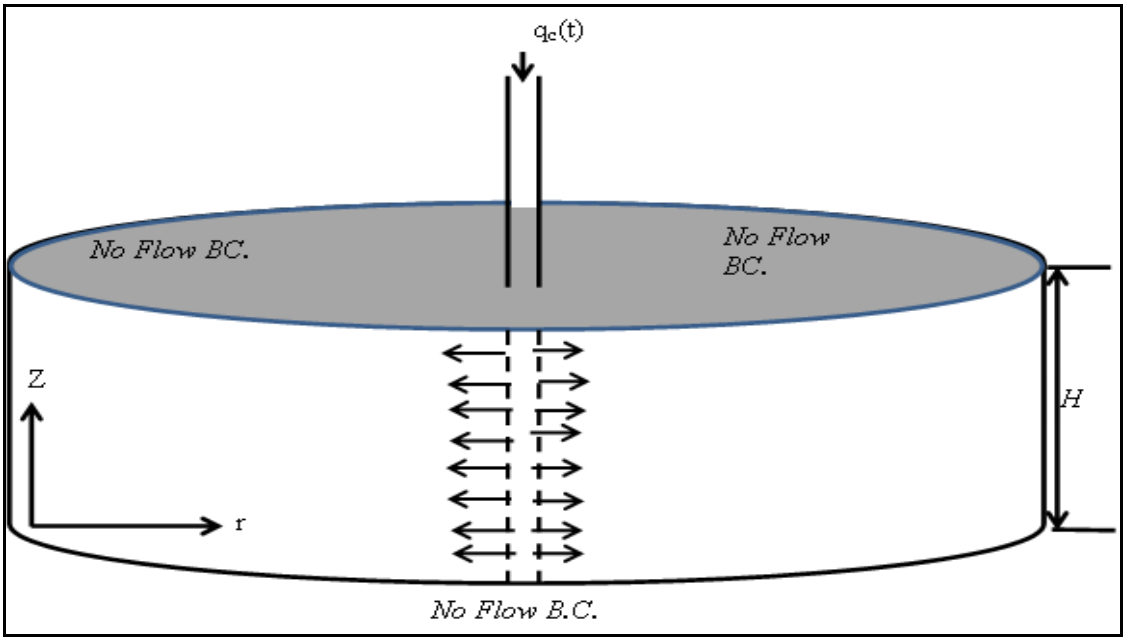

Figure 4.1: Schematic diagram of CO_2 injection into gas reservoir under constant pressure at the wellbore.

The problem will be investigated for two different outer boundary conditions: constant pressure at infinite radial distance from the injection well to simulate an infinite-acting reservoir, or no radial flow at a specific distance from the injection well to simulate a bounded reservoir. The infinite-acting reservoir refers to a problem in which time of interest is not long enough for injection from the well to interact with the boundaries of the reservoir (i.e., very large reservoirs, slow injection or relatively short times). The storage formation is assumed to be homogeneous and has a uniform initial pressure. The injection process is assumed to occur under isothermal conditions. Since the phases are assumed to be non-mixing and the capillary pressure is ignored, the pressure in the two phases is continuous at the interface, and hence we will solve for one pressure only.

4.3 Mathematical Model

Based on the conceptual model described above, the governing equation of CO_2 flow, and the initial and boundary conditions of the system can be written in radial coordinate as follows

$$-\frac{1}{r}\frac{\partial}{\partial r}\left(rq_c\rho\right)=\phi\frac{\partial P}{\partial t}, \tag{4-1}$$

$$P\left(r,0\right)=0, \tag{4-2}$$

$$P\left(r_w,t\right)=P_0, \tag{4-3}$$

$$P\left(\infty,t\right)=0, \tag{4-4}$$

$$r\frac{\partial P}{\partial r}\left(r_e,t\right)=0, \tag{4-5}$$

where r, r_w, r_e, ϕ, P, ρ, μ, and q_C are the radial distance from wellbore, injection well radius, radial distance from injection well to outer boundary, porosity of storage formation, pressure, density, viscosity, and flux of CO_2, respectively.

Assuming the CO_2 is governed by Darcy's law, we have

$$q_c=-\frac{k}{\mu}\frac{\partial P}{\partial r}, \tag{4-6}$$

where k and μ are the permeability of the formation and the dynamic viscosity of CO_2. Substituting equation (4-6) back into equation (4-1) gives

$$-\frac{1}{r}\frac{\partial}{\partial r}\left(r\rho\frac{\partial P}{\partial r}\right)=\frac{\phi\mu}{k}\frac{\partial P}{\partial t}. \tag{4-7}$$

Since we will let the gas density vary with pressure, we will need to have a relation between the density and pressure. We use Altunin's correlation to calculate density, ρ:

$$\rho = \rho_P + a_0 + a_1 P + a_2 P^2 + a_3 P^3, \tag{4-8}$$

where ρ_P is Pitzer's density approximation.

$$\rho_P = \frac{PM}{ZRT}, \tag{4-9}$$

and Z is the gas compressibility factor:

$$Z = 1 + \frac{BP}{RT}, \tag{4-10}$$

here, M, B, and T are the molecular weight of CO_2, Pitzer's correlation coefficient, and temperature respectively. The coefficients a_n are function of temperature, and have specific range as shown in Table 4.1, over which equation (4-9) can be used [*Mukhopadhyay et al.* 2012]. Equation (4-10) is the simplified version of Pitzer's correlation when truncated after the second term , while equation (4-8) is the corrected Pizer's correlation to be used at high pressures [*Mukhopadhyay et al.* 2012].

Table 4.1: The coefficients a_n range of values [*Mukhopadhyay et al.* 2012].

T [C^o]	P [atm]	a_0 [M L^{-3}]	a_1 [M L^{-3}atm^{-1}]	a_2 [M L^{-3}atm^{-2}]	a_3 [M L^{-3}atm^{-3}]
45	1-106	-0.0574	0.0660	-0.0083	2.700 E-004
55	1-126	-0.0243	0.0280	-0.0035	1.100 E-004
56	1-138	-0.0209	0.0234	-0.0023	6.090 E-005

Substituting equations (4-9) into equation (4-8) we obtain

$$\rho = P\left[\frac{M}{ZRT} + \frac{a_0}{P} + a_1 + a_2 P + a_3 P^2\right]. \tag{4-11}$$

Substituting equations 4-(10) into equation (4-11) gives

$$\rho = P\left[\frac{M}{RT + PB} + \frac{a_0}{P} + a_1 + a_2 P + a_3 P^2\right]. \tag{4-12}$$

If we substitute equation (4-12) into equation (4-7), we have a highly non-linear equation in *P*. To linearize this problem we follow Al-Hussainy et al [1966] who proposed a pseudo-pressure concept to linearize the general gas diffusivity equation into an equivalent form of a slightly compressible liquid. We define a new variable θ as follows:

$$\theta = \theta_i - \frac{B^2}{MRT}\eta, \tag{4-13}$$

$$\eta = \left[\begin{array}{l}\left(a_0 + \frac{M}{B^2}\right)(P - P_i) + \frac{a_1}{2}\left(P^2 - P_i^2\right) + \\ \frac{a_2}{3}\left(P^3 - P_i^3\right) + \frac{a_4}{4}\left(P^4 - P_i^4\right) - \frac{MRT}{B^2}\ln\left(\frac{P}{P_i}\right)\end{array}\right], \tag{4-14}$$

$$\theta_i = -\left[\frac{BP_i}{RT} + 1 + \ln\left(\frac{MRT}{BP_i + RT}\right) + \sum_1^4 d_n\left(\frac{BP_i + RT}{MRT}\right)^n\right], \tag{4-15}$$

where P_i is the initial gas reservoir pressure and d_n are defined by Mukhopadhyay et al [2012], as follows:

$$d_1 = a_0 B - a_1 RT + \frac{a_2 R^2 T^2}{B} - \frac{a_3 R^3 T^3}{B^2},$$

$$d_2 = M\left[\frac{a_1 RT}{2} + \frac{a_2 R^2 T^2}{B} - \frac{3}{2}\frac{a_3 R^3 T^3}{B^2}\right],$$

$$d_3 = M^2\left[\frac{1}{3}\frac{a_2 R^2 T^2}{B} - \frac{a_3 R^3 T^3}{B^2}\right],$$

$$d_4 = M^3\left[\frac{1}{4}\frac{a_3 R^3 T^3}{B^2}\right].$$

We then define the parameter λ:

$$\lambda = \frac{k(BP+RT)}{\phi\mu}\left[\frac{PM + (BP+RT)(a_0 + a_1 P + a_2 P^2 + a_3 P^3)}{MRT + (BP+RT)^2(a_1 + 2a_2 P + 3a_3 P^2)}\right]. \tag{4-16}$$

If we treat λ as constants, then the problem reduces to a simple linear diffusion equation that is amenable to classical solutions.

$$\frac{1}{r}\frac{\partial}{\partial r}\left(r\frac{\partial\theta}{\partial r}\right) = \frac{1}{\lambda}\frac{\partial\theta}{\partial t}, \tag{4-17}$$

$$\theta(r,0) = 0, \tag{4-18}$$

$$\theta(r_w,t) = -\frac{B^2}{MRT}\eta, \tag{4-19}$$

$$\theta(\infty,t) = 0, \tag{4-20a}$$

$$r\frac{\partial\theta}{\partial r}(r_e,t) = 0. \tag{4-20b}$$

By definition the isothermal gas compressibility is

$$C_g = \frac{Z}{P}\frac{\partial}{\partial P}\left(\frac{P}{Z}\right) = \left(\frac{RT+BP}{PRT}\right)\frac{\partial}{\partial P}\left(\frac{PRT}{RT+BP}\right), \tag{4-21}$$

which can be simplified and rewritten in terms of λ as follows

$$C_g = \frac{k}{\mu\phi}\frac{1}{\lambda}, \tag{4-22}$$

4.4 Solution Development

4.4.1 Non-dimensionlization

The system is scaled by defining the following dimensionless parameters

$$\theta_d = \frac{\theta_i - \theta}{BM},\ r_d = \frac{r}{r_w}, \text{ and } t_d = \frac{\lambda t}{r_w^{\,2}}, \tag{4-23}$$

where the system can be rewritten as follows

$$\frac{1}{r_d}\frac{\partial}{\partial r_d}\left(r_d \frac{\partial \theta_d}{\partial r_d}\right) = \frac{\partial \theta_d}{\partial t_d}, \tag{4-24}$$

$$\theta_d\left(r_d, 0\right) = 0, \tag{4-25}$$

$$\theta_d\left(1, t_d\right) = -\frac{B^3}{RT}\eta, \tag{4-26}$$

$$\theta_d\left(\infty, t_d\right) = 0, \tag{4-27a}$$

$$r_d \frac{\partial \theta_d}{\partial r_d}\left(r_{eD}, t_d\right) = 0. \tag{4-27b}$$

4.4.2 Laplace transform

Taking Laplace transform for equations (4-24) through (4-27b) gives

$$\frac{1}{r_d}\frac{d}{dr_d}\left(r_d \frac{d\bar{\theta}_d}{dr_d}\right) = s\bar{\theta}_d\ , \tag{4-28}$$

$$\bar{\theta}_d\Big|_{r_d \to 1} = -\frac{B^3}{sRT}\eta, \tag{4-29}$$

$$\bar{\theta}_d\Big|_{r_d\to\infty} = 0, \tag{4-30a}$$

$$r_d \frac{d\bar{\theta}_d}{dr_d}\Bigg|_{r_d=r_{ed}} = 0, \tag{4-30b}$$

where "*s*" is the Laplace parameter. Equation (4-28) becomes an ordinary differential equation. Multiplying equation (4-28) by r_d^2, and defining the following scale transformation, $\varepsilon = \sqrt{s} r_d$, we obtain

$$\varepsilon^2 \frac{d^2\bar{\theta}_d}{d\varepsilon^2} + \varepsilon \frac{d\bar{\theta}_d}{d\varepsilon} - \varepsilon^2 \bar{\theta}_d = 0, \tag{4-31}$$

where equation (4-31) is the modified Bessel differential equation, and its general solution is given by Abramowitz and Stegun [1965]

$$\bar{\theta}_d(\varepsilon) = AI_0(\varepsilon) + CK_0(\varepsilon), \tag{4-32}$$

where the functions $I_0(\varepsilon)$ and $K_0(\varepsilon)$ are the modified Bessel functions of zero order and first and second type, respectively. *A* and *C* are coefficients to be determined from the boundary conditions of the problem. Reverting to the radial coordinates, equation (4-32) becomes

$$\bar{\theta}_d(r_d, s) = AI_0\left(\sqrt{s}\, r_d\right) + CK_0\left(\sqrt{s}\, r_d\right). \tag{4-33}$$

In order to solve for *A* and *C*, we have to apply the boundary conditions. Using the chain rule we have

$$\frac{d\bar{\theta}_d}{dr_d} = \frac{d\bar{\theta}_d}{d\varepsilon}\frac{d\varepsilon}{dr_d},$$

and since, $\frac{d\bar{\theta}_d}{d\varepsilon} = A\frac{dI_0(\varepsilon)}{d\varepsilon} + C\frac{dK_0(\varepsilon)}{d\varepsilon} = AI_1(\varepsilon) - CK_1(\varepsilon),$

and $\frac{d\varepsilon}{dr_d} = \sqrt{s}$, we obtain

$$r_d \frac{d\bar{\theta}_d}{dr_d} = A\sqrt{s}\, r_d I_1\left(\sqrt{s} r_d\right) - C\sqrt{s}\, r_d K_1\left(\sqrt{s} r_d\right), \tag{4-34}$$

where functions $I_1(\varepsilon)$ and $K_1(\varepsilon)$ are the modified Bessel functions of first-order and first and second type, respectively

4.4.3 Case-1: Infinite acting reservoir

Applying the boundary condition at the wellbore, by inserting equation (4-29), into equation (4-33) yields

$$-\frac{B^3\eta}{sRT} = AI_0\left(\sqrt{s}\right) + CK_0\left(\sqrt{s}\right). \tag{4-35}$$

Similarly, substituting equation (4-30a) into equation (4-33) gives

$$\lim_{r_d \to \infty}\left(AI_0\left(\sqrt{s}\, r_d\right) + CK_0\left(\sqrt{s}\, r_d\right)\right) = 0. \tag{4-36}$$

Since $I_0\left(r_d \to \infty\right) \approx \infty$, therefore $A = 0$ and solving equation (4-35) for *C* gives

$$C = -\frac{B^3\eta}{sRT}\frac{1}{K_0\left(\sqrt{s}\right)}. \tag{4-37}$$

Substituting equation (4-37) back into equation (4-33), we obtain the particular solution for the infinite-acting reservoir case as follows

$$\bar{\theta}_d\left(r_d, s\right) = -\frac{B^3\eta}{sRT}\frac{1}{K_0\left(\sqrt{s}\right)}K_0\left(\sqrt{s} r_d\right). \tag{4-38}$$

Now equation (4-38) is the solution for the infinite acting reservoir in Laplace domain.

4.4.4 Case-2: Closed reservoir with no flow B.C.

Recall that the no-flow B.C is described by $r_d \left.\frac{d\bar{\theta}_d}{dr_d}\right|_{r_d=r_{ed}} = 0$, where $\bar{\theta}_d$ is described by equation (4-32b), and $r_d \frac{d\bar{\theta}_d}{dr_d}$ is defined by equation (4-34). Thus

$$0 = r_{ed}\sqrt{s}AI_1\left(\sqrt{s}r_{ed}\right) - \sqrt{s}r_{ed}CK_1\left(\sqrt{s}r_{ed}\right), \tag{4-39}$$

Rearranging equation (4-39) and writing "*A*" in terms of *C* gives

$$A = C\frac{K_1\left(\sqrt{s}r_{ed}\right)}{I_1\left(\sqrt{s}r_{ed}\right)}. \tag{4-40}$$

By substituting equation (4-40) back into equation (4-33) and solving for *C*, we obtain

$$C = -\frac{B^3\eta}{sRT}\left[\frac{I_1\left(\sqrt{s}r_{ed}\right)}{K_0\left(\sqrt{s}\right)I_1\left(\sqrt{s}r_{ed}\right) + I_0\left(\sqrt{s}\right)K_1\left(\sqrt{s}r_{ed}\right)}\right], \tag{4-41}$$

$$A = -\frac{B^3\eta}{sRT}\left[\frac{K_1\left(\sqrt{s}r_{ed}\right)}{K_0\left(\sqrt{s}\right)I_1\left(\sqrt{s}r_{ed}\right) + I_0\left(\sqrt{s}\right)K_1\left(\sqrt{s}r_{ed}\right)}\right]. \tag{4-42}$$

Now, we substitute equations (4-41) and (4-42) back into equation (4-33) to have

$$\bar{\theta}_d\left(r_d, s\right) = -\frac{B^3\eta}{sRT}\left[\frac{I_0\left(\sqrt{s}r_d\right)K_1\left(\sqrt{s}r_{ed}\right) + K_0\left(\sqrt{s}r_d\right)I_1\left(\sqrt{s}r_{ed}\right)}{K_0\left(\sqrt{s}\right)I_1\left(\sqrt{s}r_{ed}\right) + I_0\left(\sqrt{s}\right)K_1\left(\sqrt{s}r_{ed}\right)}\right]. \tag{4-43}$$

Since η is constant at the wellbore as $P = P_O$ at the wellbore, an exact solution for $\bar{\theta}$ can be obtained easily from equation (4-43). Equation (4-43) is a particular

solution for a closed reservoir with no flow outer boundary condition. Now, we need to convert equations (4-38) and (4-43) back into real time domain, and then substitute into equation (4-13) to solve for the pressure. Equations (4-38) and (4-43) cannot be inverted back into real time domain analytically, so a numerical inversion is needed. The De Hoog algorithm [*De Hoog et al.* 1982] was implemented in MATLAB to get the solution in real time domain.

4.5 Results and Discussion

Since a numerical scheme is required for the inverse transform, to explore the behavior of pressure in these systems, we must specify an example reservoir. In this example, we will take the initial pressure in that the storage formation to be 9000 kPa. We also assume that the formation porosity is 0.1 and permeability is 10^{-14} m^2. The imposed injection pressure is 11000 kPa and formation temperature is assumed to be 55˚C and surface temperature 22˚C. Assuming a geothermal gradient of 0.03˚C m^{-1} corresponds to a formation depth of 900 m. For the set of results obtained with the proposed solution scheme, the injection pressure, initial and boundary conditions, and the formation properties (thickness, permeability and porosity) are summarized in Table 4.2. The injection process run for hundred years, started at the year 2010 and ended at the year 2110.

Table 4.2: Input data used in gas reservoir computations.

Parameter	Value
A	315 km^2
T	55[C^o]
C_f	7.2 E-005 [bar^{-1}]
H	100[m]
k	10 E-14 [m^2]
P_o	9 [kpa]
p_i	11 [kpa]
r_w	0.1 [m]
r_e	10 [km]
t	100 [year]
μ_c	4.6 E-10-5 [pa s]
ρ_c	610 [kg m^{-3}]
ϕ	0.2 [-]

The pressure buildup within 4.5 km of the well-bore in the infinite acting reservoir is shown at 10 year intervals after injection starts in Figure 4.2. Injection is assumed to be continued at constant pressure for this entire period.

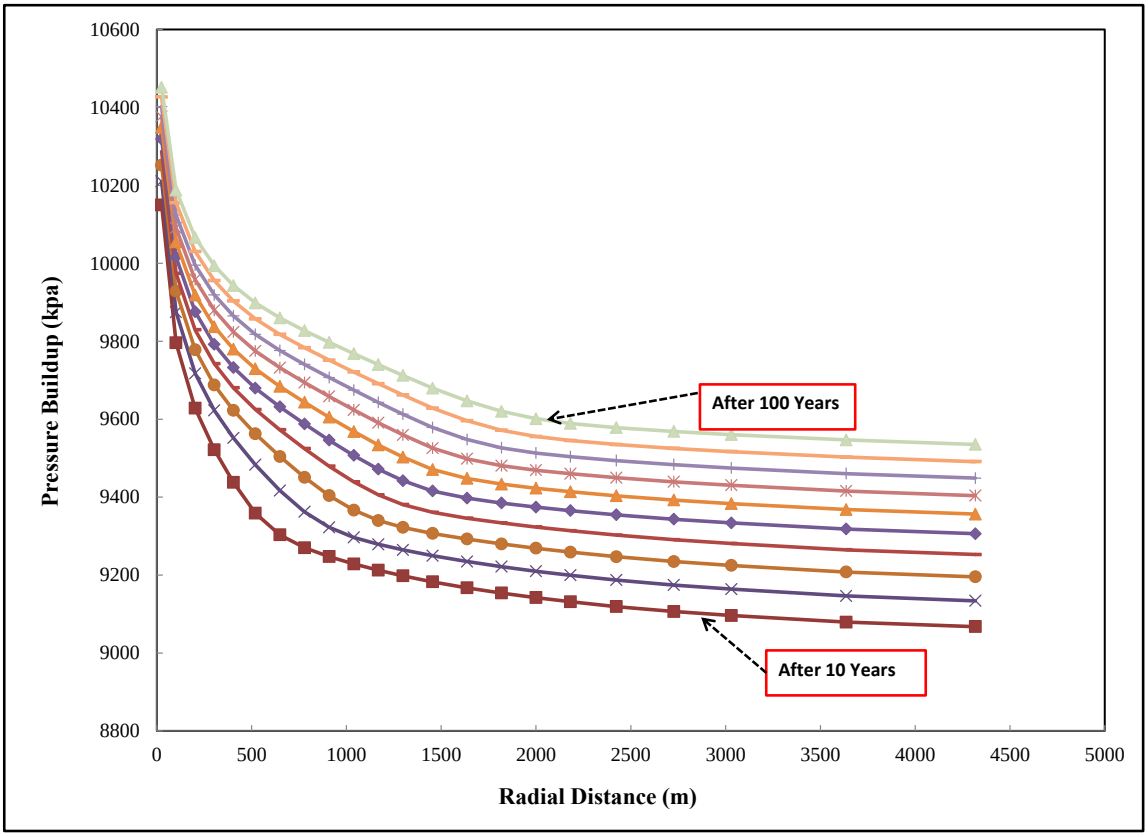

Figure 4.2: Predicted pressure buildup as a function of radial distance at different times (infinite reservoir).

Figure 4.2 shows that pressure increases very rapidly within 500 m of the well, and much more slowly at greater distances. It also shows that as the pressure build up is very high at earlier times and then starts to slow down as time evolves.

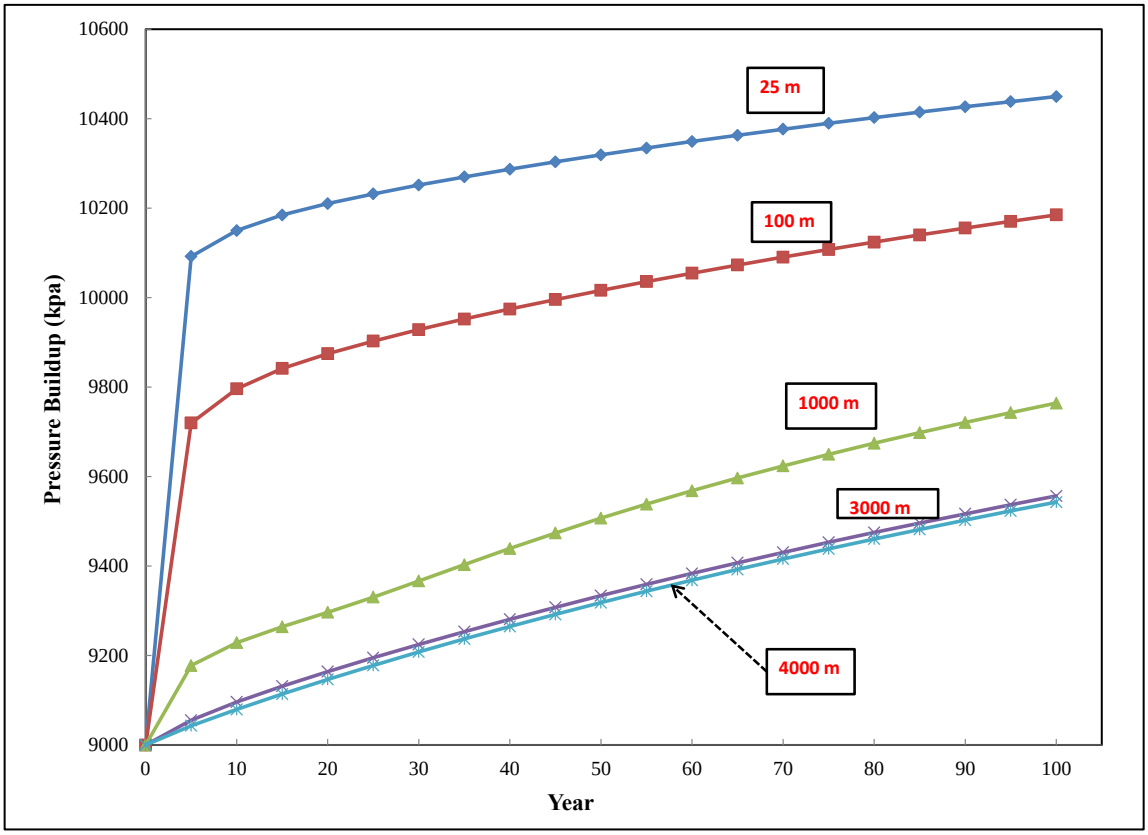

Figure 4.3: Expected pressure buildup vs. time at specific radial distances (r= 25 m, 100 m, 1000 m, 3000 m, and 4000 m).

Figure 4.3 shows the pressure buildup at different radial distances from the wellbore (r = 25, 100, 1000, 3000, and 4000m) were selected to show their pressure change time. These locations are selected to compare the pressure buildup at close (i.e. r=25 and 100m), intermediate (i.e. r= 1000 and 3000m) and at far (i.e. r=4000m) distance from the well. At r=25m, the pressure jumped from 9000kpa to 1100 kpa in very short time (about 5 years), then increased from 1100 kpa to 1500 kpa in the last 95 years of injection. While at r=100, the pressure increased from 9000 kpa to 9700 kpa in about 7 years, then the pressure reached 10200 at the end of injection. The curves at

r=25 and 100m have to different slopes, reflecting two different rates of pressure change. The pressure curves at *r*= 3000 and 4000m have similar slope and the pressure across these curves changed from 9000 kpa to 9500 kpa by the end of injection with a slow rate. The pressure curve at *r*=1000m has changed from 9000 kpa to 9700 kpa with two different rates of changing; the earlier rate was higher than the later one, but still did not change much like the first two curves (i.e. *r*= 25 and 100m).

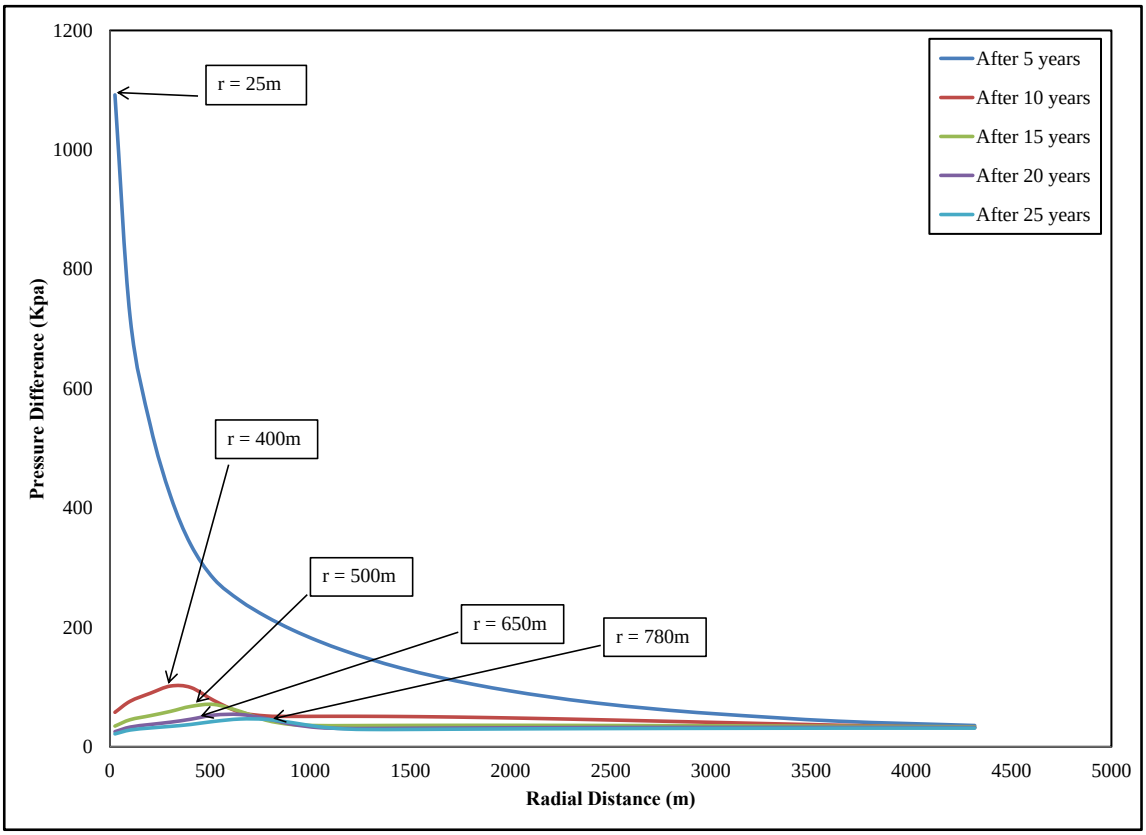

Figure 4.4: Pressure increase over five different 5-year periods (0-5, 5-10, 10-15, 15-20, 20-25 years after beginning of injection) as a function of radial distance. The position of the peak difference, which changes in time, shows the progression of the diffusing pressure front.

Figure 4.4 shows the difference between calculate reservoir pressures separated by 5 years in time; this difference therefore is approximately proportional to the rate of change of pressure. At any given time, the maximum rate of pressure increase will occur at some distance from the wellbore (peaks in Fig. 4.4). The decrease in amplitude and increase in radial distance with time demonstrates the front of pressure diffusing outward from the wellbore as time evolves.

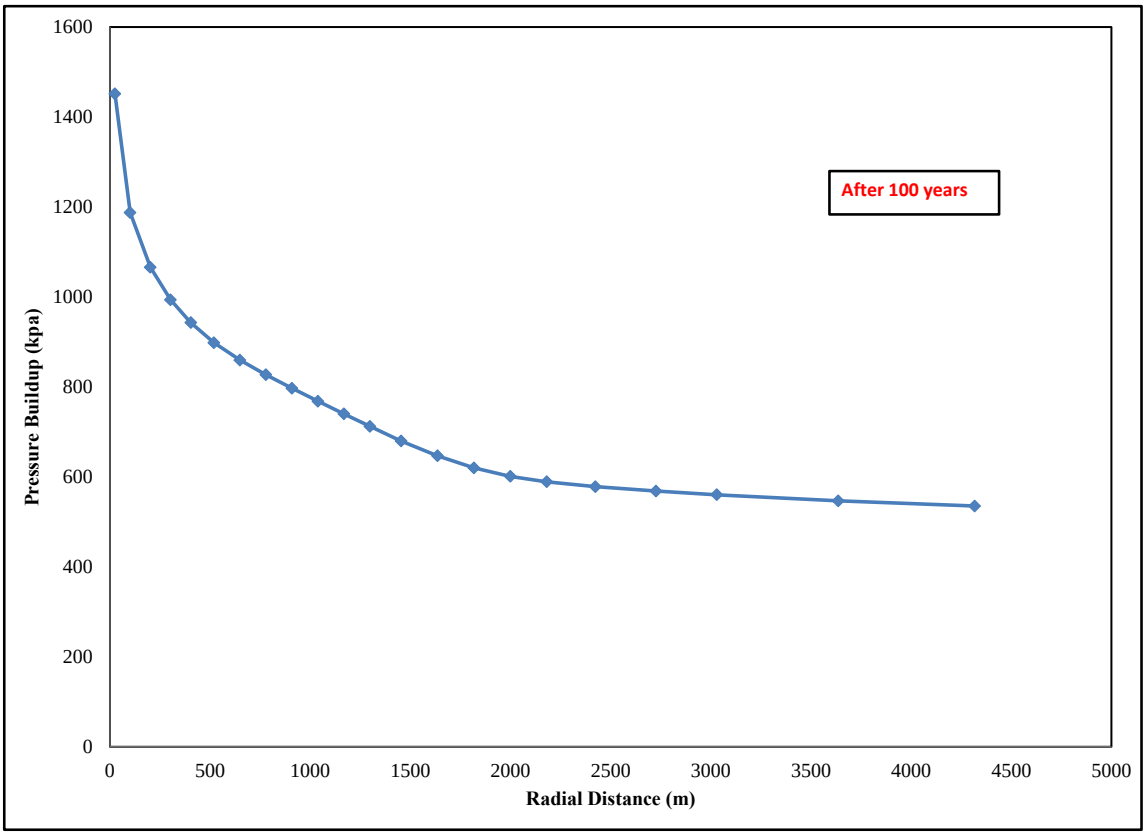

Figure 4.5: Cumulative pressure buildup as a function of radial distance.

Figure 4.5 essentially shows the same results as Figures 4.2 – total change in reservoir pressure after 100 years of injection. It shows that the pressure gradient is very high nearby the injection well and decreases significantly as radial distance increases. At distances greater than 2 km, the pressure has only increased by about one-third of the applied differential pressure at the wellbore.

Knowing the pressure distribution in the reservoir and the wellbore, we can calculate the flux at the wellbore. Figure 4.6 shows the predicted injection rate at the wellbore as a function of time. The injection rate starts very high and then within a few months drops to much lower value. At the beginning of injection, the pressure difference between the injection well and the reservoir is at its maximum, but as injection continues and pressure builds up in the reservoir near the well, the pressure gradient decreases and forces the injection rate to decrease as well. After about 2 years, injection rate decays only very slowly, dropping about 25% over the next 100 years.

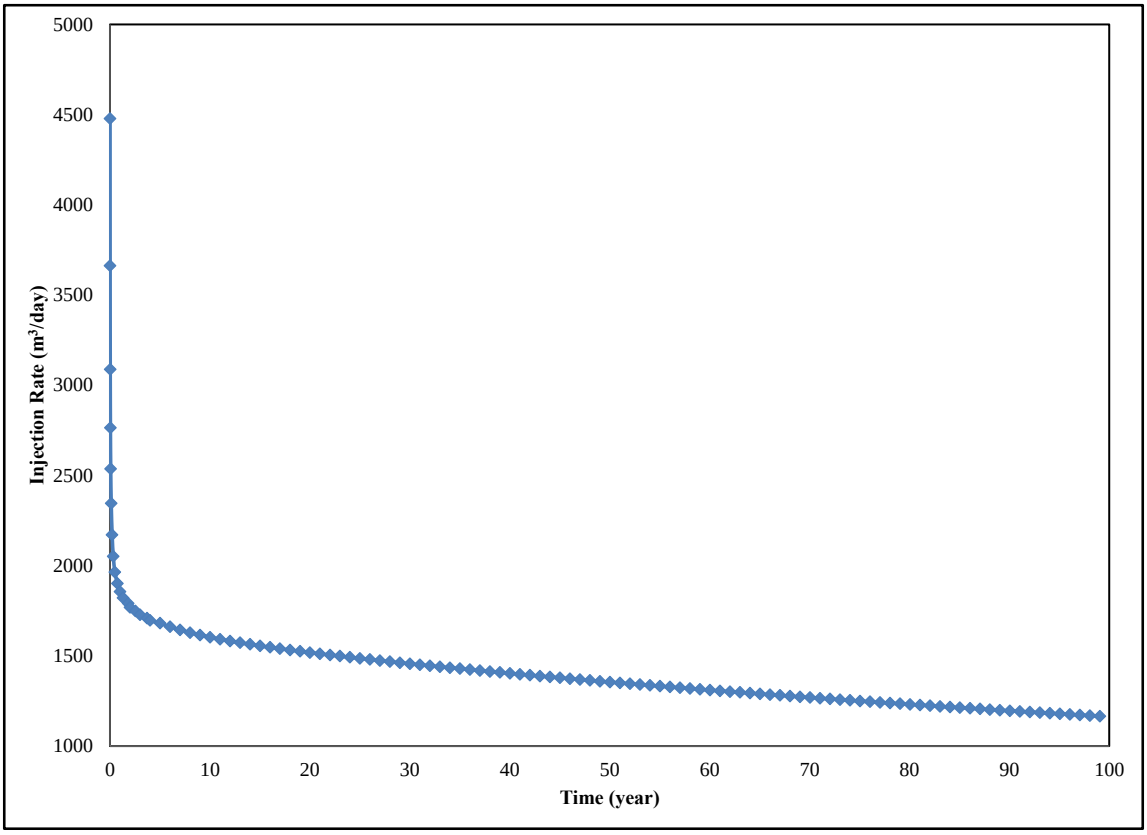

Figure 4.6: Predicted injection rate at the wellbore vs. time.

We can calculate the cumulative injection volume of CO_2 at the wellbore as shown in Figure 4.7. Then by deploying the universal law of gas and the relation between the number of moles of CO_2 and its molecular weight to calculate the cumulative injected mass of CO_2 as shown in Figure 4.8. Cumulative volume and mass of CO_2 increase with time in a near-linear way because the injection rate is only slowly changing over time (the initial very rapid injection rates seen in Fig. 4.6 do not last long enough to the account for much volume).

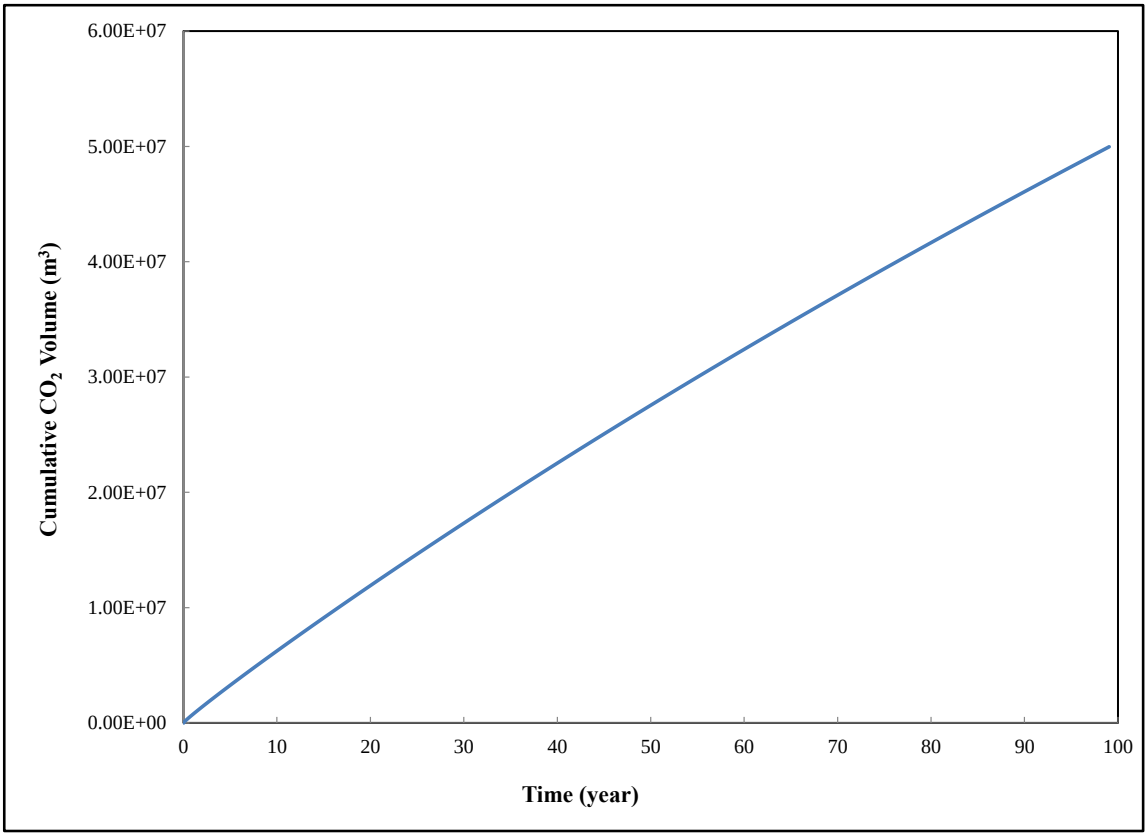

Figure 4.7: Calculated cumulative injected CO_2 volume vs. time.

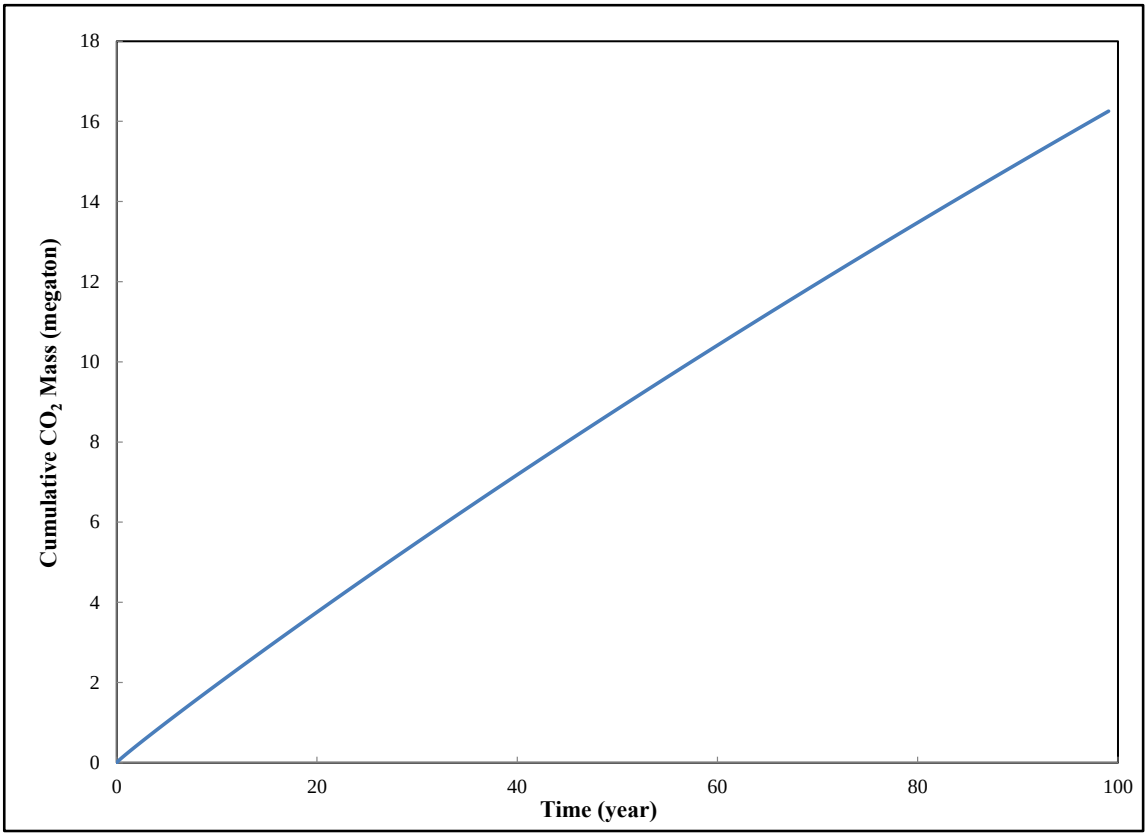

Figure 4.8: Calculated cumulative injected CO_2 mass vs. time.

5. SUMMARY AND CONCLUSIONS

Answers to important practical questions require the availability of practical models that can help to answer those questions. If the problem of CO_2 storage in deep saline aquifers is considered, these questions invariably involve CO_2 plume size, the spatial extent of pressure increases.

The main objective of this dissertation was to build a set of predictive and accurate approximate solutions to study the injection of CO_2 in brine aquifers and gas reservoirs.

This work has described the development of four semi-analytical solutions to model CO_2 injection and geologic storage in infinite and closed brine aquifers and infinite acting and closed gas reservoirs.

Section 2 detailed the mathematical foundation of the model, from the mass balance to the vertically-averaged, two-dimensional governing equations for flow of brine and CO_2 in the aquifers. The method of matched asymptotic expansion was deployed to derive an approximate solution to predict the pressure buildup and the plume extent in infinite aquifers during the injection process. The solution has taken care of both darcyan and non-darcyan flow. In this section we derived a novel closed form

solution for CO_2 sequestration under constant injection pressure. The main results of this section can be summarized as follows:

1- A new closed form solution of CO_2 injection in infinite aquifers under constant injection pressure is introduced.
2- The novel solution is shown to predict the plume extent and the spatial extent of pressure increases.
3- A closed formula for the flux at the wellbore introduced
4- The flux formula used to calculate the cumulative injected volume and mass of CO_2 during the injection.
5- The solution obtained in this section will provide the basis to build the solution in the next section.

Section 3 focused on deploying the solution obtained from the previous section to derive a semi-analytical solution for CO_2 injection problems in closed domains. First a closed form solution was derived for single phase flow. Then the single phase solution obtained in this section was combined with the two phase solution obtained in section 2. The results of this section can be summarized as follows:

1. A novel solution for CO_2 injection in closed domains under constant pressure was developed.
2. The time required for the pressure wave perturbation to reach the outer boundary of the domain was calculated and can be used as a cut off criteria for which solution can be used (i.e. as long as the time required for the pressure

perturbation to reach the outer boundary is less than the injection period, the infinite domain solution can be used for closed domains and vice versa).

3. The newly derived solution is used to predict the pressure buildup distribution as a function of time and radial distance.
4. The cumulative injected CO_2 volume and mass are calculated from the obtained solution.

The topic of section 4 was to derive a semi-analytical solution to CO_2 in depleted gas reservoirs for both infinite acting and closed reservoirs. Laplace transform was used to assist in deriving a solution in Laplace domain then a numerical algorithm [*De Hoog et al.* 1982] was used to invert the solution back in the real time domain. The solution considered gas compressibility as a function of pressure. The main results if this section can be summarized as follows:

1. A new solution for CO_2 injection into gas reservoir (both infinite acting and closed reservoirs) under constant pressure is produced.
2. The solution is used to predict the pressure distribution in the gas reservoir.
3. The cumulative volume and mass of CO_2 are calculated and also the flow rate at the wellbore.

5.1 Contributions

The contribution of this study can be summarized as follows:

1. This dissertation for the first time introduces closed form solutions for CO_2 sequestration under constant pressure injection at the wellbore.
2. These solutions can be used to predict the plume extent and the pressure build distribution while the injection process takes place in order to monitor the injection process.
3. The developed solutions can be extended to predict the leakage through the cap rocks, fractures and/or abandoned wells.
4. It can also be modified to study the post injection behavior of the system.

5.2 Future Work

The solutions presented in this work are applicable only while CO_2 injection is taking place. In order to model the post injection behavior of the system, modifications to the governing equations must be made to account for imbibition of brine into pore space previously occupied by CO_2. These solutions were derived assuming horizontal storage formations; we will extend them to account for dipping systems. Thin formations with large lateral extent may serve as good damping reservoirs for CO_2, and the most efficient way utilize them is to use horizontal wells instead of vertical ones for injections. However, up to now, there is no solution for CO_2 injection through horizontal wells. This idea is considered as a future work.

We finished the derivation of a semi-analytical solution for two dimensional solute transport in multilayered aquifer systems in the Laplace domain. Then, we encountered a problem with one of the boundary conditions and we are planning to change this boundary condition and modify the solution.

NOMENCLATURE

Nomenclature used in Section 2:

A	Formation plan area [L^2]
V	Pore fluid volume [L^3]
b	Forchheimer parameter [L^{-1}]
C_c	Compressibility of CO_2 [$M^{-1}LT^2$]
C_f	Compressibility of geological formation [$M^{-1}LT^2$]
C_w	Compressibility of brine [$M^{-1}LT^2$]
$C_t = C_f + C_w$	Total formation compressibility [$M^{-1}LT^2$]
h	CO_2 brine interface elevation [L]
$h_D = h / H$	Dimensionless interface elevation[-]
H	Formation thickness [L]
k	Permeability[L^2]
P_o	Mass injection pressure [$ML^{-1}1T^{-2}$]
p	Fluid pressure [$ML^{-1}T^{-2}$]
$p_D = p/p_o$	Dimensionless pressure [-]
q_c	CO_2 flux [LT^{-1}]
$q_{cD} = \mu_c r_w q_c / p_o k$	Dimensionless CO_2 flux [-]
q_w	Brine flux [LT^{-1}]

$q_{wD} = \mu_c r_w q_w / p_o k$	Dimensionless brine flux [-]
r	Radial distance [L]
$r_D = r / r_w$	Dimensionless radius [-]
r_w	Well radius [L]
t	Time [T]
$t_D = k p_o t / \phi \mu_c r_w^2$	Dimensionless time [-]
$\alpha = p_o (c_f + c_w)$	Dimensionless [-]
$\beta = b \rho_c p_o k^2 / \mu_c^2 r_w$	Dimensionless Forchheimer parameter [-]
$\gamma = \mu_c / \mu_w$	Viscosity ratio [-]
$\varepsilon = (c_f - c_w) / (c_r + c_w)$	Normalized fluid compressibility difference [-]
μ_c	Viscosity of CO_2 [$ML^{-1}T^{-1}$]
μ_w	Viscosity of brine [$ML^{-1}T^{-1}$]
ρ_c	Density of CO_2 [ML^{-3}]
ρ_w	Density of brine [ML^{-3}]
$\sigma = \rho_c / \rho_w$	Density ratio [-]
ϕ	Porosity [-]

Nomenclature used in Section 3:

A	Formation plan area [L^2]
V	Pore fluid volume [L^3]
b	Forchheimer parameter [L^{-1}]
b_r	Relative Forchheimer parameter [-]
C_c	Compressibility of CO_2 [$M^{-1}LT^2$]
C_f	Compressibility of geological formation [$M^{-1}LT^2$]
C_w	Compressibility of brine [$M^{-1}LT^2$]
$C_t = C_f + C_w$	Total formation compressibility [$M^{-1}LT^2$]
h	CO_2 brine interface elevation [L]
$h_D = h / H$	Dimensionless interface elevation[-]
H	Formation thickness [L]
k	Permeability[L^2]
k_r	Relative permeability[-]
P_o	Mass injection pressure [$ML^{-1}1T^{-2}$]
p	Fluid pressure [$ML^{-1}T^{-2}$]
$p_D = p/p_o$	Dimensionless pressure [-]
q_c	CO_2 flux [LT^{-1}]
$q_{cD} = \mu_c r_w q_c / p_o k_r k$	Dimensionless CO_2 flux [-]

q_w	Brine flux [LT^{-1}]
$q_{wD} = \mu_c r_w q_w / p_o k_r k$	Dimensionless brine flux [-]
r	Radial distance [L]
r_e	Radial extent of reservoir [L]
$r_{eD} = r_e / r_w$	Dimensionless radial extent of aquifer [-]
$r_D = r / r_w$	Dimensionless radius [-]
r_w	Well radius [L]
S_r	Residual brine saturation [-]
t	Time [T]
$t_{ed} = e^{\delta} \alpha r_{eD}^2 / 4\gamma$	Dimensionless time at which the pressure perturbation reaches the aquifer boundary [-]
$t_D = k p_o t / \phi (1 - s_r) \mu_c r_w^2$	Dimensionless time [-]
$\alpha = p_o (c_f + c_w) / k_r (1 - s_r)$	Dimensionless [-]
$\beta = b_r b \rho_c p_o k_r^2 k^2 / \mu_c^2 r_w$	Dimensionless Forchheimer parameter [-]
$\gamma = \mu_c / k_r \mu_w$	Viscosity ratio [-]
$\varepsilon = (1 - s_r)(c_f - c_w) / (c_r + c_w)$	Normalized fluid compressibility difference [-]
μ_c	Viscosity of CO_2 [$ML^{-1}T^{-1}$]
μ_w	Viscosity of brine [$ML^{-1}T^{-1}$]
ρ_c	Density of CO_2 [ML^{-3}]

ρ_w	Density of brine [ML^{-3}]
$\sigma = b_r \rho_c / \rho_w$	Density ratio [-]

Nomenclature used in Section 4:

B	=B'RT [m^3/ mol]
B'	Virial coefficient
k	Permeability [m^2]
L	Thickness of the storage formation
p	Pressure [atm]
p_0	Injection pressure [atm]
p_i	Initial pressure and [atm]
$q_c(t)$	Volume flux of CO_2 [ms^{-1}]
R	Universal gas constant [J $mol^{-1}K^{-1}$]
r	Radial distance from the center of the injection borehole [m]
Δr	Infinitesimal radial distance [m]
s	Laplace parameter
T	Temperature [K]
t	Time [s]
Z	Compressibility factor [-]
z	Vertical distance from the bottom of the storage formation [m]

Δz	Infinitesimal vertical distance, m
ϕ	Porosity of the storage formation [-]
θ	Scaling parameter to linearize the gas diffusivity equation
μ	Viscosity of CO_2 [kg m^{-1} s^{-1}]
ρ	Density of CO_2 as predicted by Altunin's correlations [kg m^{-3}]
ρ_P	Density of CO_2 as predicted by Pitzer's correlations [kg m^{-3}]

REFERENCES

Abramowitz, M., and I. A. Stegun (1965), *Handbook of Mathematical Functions with Formulas, Graph, and Mathematical Tables*, Dover Publications, New York.

Al-Hussainy, R., H. Ramey Jr, and P. Crawford (1966), The flow of real gases through porous media, *Journal of Petroleum Technology*, *18*(5), 624-636.

André, L., P. Audigane, M. Azaroual, and A. Menjoz (2007), Numerical modeling of fluid–rock chemical interactions at the supercritical CO2–liquid interface during CO2 injection into a carbonate reservoir, the Dogger aquifer (Paris Basin, France), *Energy Conversion and Management*, *48*(6), 1782-1797.

Audigane, P., I. Gaus, I. Czernichowski-Lauriol, K. Pruess, and T. Xu (2007), Two-dimensional reactive transport modeling of CO2 injection in a saline aquifer at the Sleipner site, North Sea, *American Journal of Science*, *307*(7), 974-1008.

Audigane, P., J. Lions, I. Gaus, C. Robelin, P. Durst, B. Van der Meer, K. Geel, C. M. Oldenburg, and T. Xu (2009), Geochemical modeling of CO2 injection into a methane gas reservoir at the K12-B field, North Sea.

Bachu, S. (2000), Sequestration of CO2 in geological media: criteria and approach for site selection in response to climate change., *Energy Conversion & Management*, *41*(9), 953-970.

Bachu, S. (2003), Screening and ranking of sedimentary basins for sequestration of CO2 in geological media in response to climate change, *Environ Geol*, *44*(3), 277-289.

Bachu, S. (2008), CO2 storage in geological media: Role, means, status and barriers to deployment, *Progress in Energy and Combustion Science*, *34*(2), 254-273.

Bachu, S., and M. A. Celia (2009), Assessing the potential for CO2 leakage, particularly through wells, from geological storage sites, in *Carbon Sequestration and Its Role in the Global Carbon Cycle*, edited, pp. 203-216, American Geophysical Union.

Bear, J. (1979), *Hydraulics of Groundwater*, McGraw-Hill, New York.

Bennion, B., and S. Bachu (2008), Drainage and imbibition relative permeability relationships for supercritical CO2/brine and H2S/brine systems in intergranular sandstone, carbonate, shale, and anhydrite rocks, *SPE Reservoir Evaluation & Engineering*, *11*(3), 487-496.

Bergmo, P. E. S., A.-A. Grimstad, and E. Lindeberg (2011), Simultaneous CO2 injection and water production to optimise aquifer storage capacity, *International Journal of Greenhouse Gas Control*, *5*(3), 555-564.

Birkholzer, J. T., and Q. Zhou (2009), Basin-scale hydrogeologic impacts of CO2 storage: Capacity and regulatory implications, *International Journal of Greenhouse Gas Control*, *3*(6), 745-756.

Bruant, R. G., A. J. Guswa Jr, M. A. Celia, and C. A. Peters (2002), Safe storage of CO2 in deep saline aquifers, *Environmental science and technology*, *36*(11), 240A-245A.

Celia, M. A., and J. M. Nordbotten (2009), Practical Modeling Approaches for Geological Storage of Carbon Dioxide, *Ground Water*, *47*(5), 627-638.

Celia, M. A., and J. M. Nordbotten (2011), How simple can we make models for CO2 injection, migration, and leakage?, *Energy Procedia*, *4*(0), 3857-3864.

Celia, M. A., S. Bachu, J. Nordbotten, D. Kavetski, and S. Gasda (2006), A risk assessment tool to quantify CO2 leakage potential through wells in mature sedimentary basins, paper presented at Proceedings of the 8th Conference on Greenhouse Gas Technologies.

Dake, L. P. (1978), *Fundamentals of reservoir engineering*, Elsevier Science, Amsetrdam.

De Hoog, F., J. Knight, and A. Stokes (1982), An Improved Method for Numerical Inversion of Laplace Transforms, *SIAM Journal on Scientific and Statistical Computing*, *3*(3), 357-366.

Dentz, M., and D. Tartakovsky (2009a), Response to "Comments on Abrupt-Interface Solution for Carbon Dioxide Injection into Porous Media by Dentz and Tartakovsky (2009)" by Lu et al, *Transport in Porous Media*, *79*(1), 39-41.

Dentz, M., and D. Tartakovsky (2009b), Abrupt-Interface Solution for Carbon Dioxide Injection into Porous Media, *Transport in Porous Media*, *79*(1), 15-27.

Duncan, I. J., J.-P. Nicot, and J.-W. Choi (2009), Risk Assessment for future CO2 Sequestration Projects Based CO2 Enhanced Oil Recovery in the US, *Energy Procedia*, *1*(1), 2037-2042.

Ferronato, M., G. Gambolati, C. Janna, and P. Teatini (2010), Geomechanical issues of anthropogenic CO2 sequestration in exploited gas fields, *Energy Conversion and Management*, *51*(10), 1918-1928.

Forchheimer (1901), Forchheimer P.: Wasserbewegung durch Boden. Z. Ver. Deutsch Ing. 45, 1782–1788 (1901), *45*, 1782–1788.

Gale, J. (2004), Geological storage of CO2: What do we know, where are the gaps and what more needs to be done?, *Energy*, *29*(9–10), 1329-1338.

Gallo, Y., P. Couillens, and T. Manai (2002), CO2 Sequestration in Depleted Oil or Gas Reservoirs, paper presented at SPE International Conference on Health, Safety and Environment in Oil and Gas Exploration and Production.

Gasda, S. E., S. Bachu, and M. A. Celia (2004), Spatial characterization of the location of potentially leaky wells penetrating a deep saline aquifer in a mature sedimentary basin, *Environ Geol*, *46*(6-7), 707-720.

Gasda, S. E., J. M. Nordbotten, and M. A. Celia (2009), Vertical equilibrium with sub-scale analytical methods for geological CO2 sequestration, *Computational Geosciences*, *13*(4), 469-481.

Gasda, S. E., J. M. Nordbotten, and M. A. Celia (2011), Vertically averaged approaches for CO2 migration with solubility trapping, *Water Resources Research*, *47*(5).

Gunter, W. D., B. Wiwehar, and E. H. Perkins (1997), Aquifer disposal of CO2-rich greenhouse gases: Extension of the time scale of experiment for CO2-sequestering reactions by geochemical modelling, *Mineralogy and Petrology*, *59*(1-2), 121-140.

Hawkes, C., P. Mclellan, and S. Bachu (2005), Geomechanical factors affecting geological storage of CO2 in depleted oil and gas reservoirs, *Journal of Canadian Petroleum Technology*, *44*(10), 52-61.

Hepple, R., and S. Benson (2005), Geologic storage of carbon dioxide as a climate change mitigation strategy: performance requirements and the implications of surface seepage, *Environ Geol*, *47*(4), 576-585.

Hesse, M. A., F. M. Orr, and H. A. Tchelepi (2008), Gravity currents with residual trapping, *Journal of Fluid Mechanics*, *611*, 35-60.

Hesse, M. A., H. A. Tchelepi, B. J. Cantwel, and F. M. Orr (2007), Gravity currents in horizontal porous layers: transition from early to late self-similarity, *Journal of Fluid Mechanics*, *577*, 363-383.

Holloway, S. (2005), Underground sequestration of carbon dioxide-a viable greenhouse gas mitigation option, *Energy*, *30*(11), 2318-2333.

Holloway, S., and D. Savage (1993), The potential for aquifer disposal of carbon dioxide in the UK, *Energy Conversion and Management*, *34*(9), 925-932.

Hovorka, S., C. Doughty, P. Knox, C. Green, K. Pruess, and S. Benson (2001), Evaluation of brine-bearing sands of the Frio formation, upper Texas gulf coast for geological sequestration of CO2, paper presented at First National Conference on Carbon Sequestration, May.

IEA (2007), World Energy Outlook 2007: China and India Insights, International Energy Agency, edited by I. E. Agency), Paris, OECD/IEA.

IPCC (2005), Special report on carbon dioxide capture and storage. Prepared by Working Group III of the Intergovernmental Panel on Climate Change*Rep.*, 442 pp, Cambridge University Press, Cambridge, United Kingdom.

IPCC (2007a), The physical science basis. Contribution of Working Group I to the fourth assessment report of the Intergovernmental Panel on Climate Change, edited, pp. 337-383, Cambridge University Press, Cambridge, United Kingdom.

IPCC (2007b), Climate Change 2007: Impacts, Adaptation and Vulnerability: Working Group I Contribution to the Fourth Assessment Report of the Intergovernmental Panel on Climate Change*Rep. 0521880106*, Cambridge University Press.

IPCC (2007c), Climate Change 2007-Mitigation of Climate Change: Working Group III Contribution to the Fourth Assessment Report of the Intergovermental Panel on Climate Change*Rep. 0521880114*, Cambridge University Press.

Johnson, J. W., J. J. Nitao, and K. G. Knauss (2004), Reactive transport modeling of CO2 storage in saline aquifers to elucidate fundamental processes, trapping mechanisms and sequestration partitioning, *Geological storage of carbon dioxide*, *233*, 107-128.

Juanes, R., C. MacMinn, and M. Szulczewski (2010), The Footprint of the CO2 Plume during Carbon Dioxide Storage in Saline Aquifers: Storage Efficiency for Capillary Trapping at the Basin Scale, *Transport in Porous Media*, *82*(1), 19-30.

Kavetski, D., J. Nordbotten, and M. Celia (2006), Analysis of potential CO2 leakage through abandoned wells using a semi-analytical model, paper presented at Proceedings of the 16th International Conference on Computational Methods in Water Resources, Copenhagen Denmark, June 19− 22.

Kevorkian, J. (2000), *Partial differential equations: Analytical solution techniques*, Springer Verlag, New York.

Krey, V., and K. Riahi (2009), Implications of delayed participation and technology failure for the feasibility, costs, and likelihood of staying below temperature targets—Greenhouse gas mitigation scenarios for the 21st century, *Energy Economics*, *31*, S94-S106.

Krooss, B. M., F. van Bergen, Y. Gensterblum, N. Siemons, H. J. M. Pagnier, and P. David (2002), High-pressure methane and carbon dioxide adsorption on dry and moisture-equilibrated Pennsylvanian coals, *International Journal of Coal Geology*, *51*(2), 69-92.

Kuuskraa, V., and R. Ferguson (2008), Storing CO2 with enhanced oil recovery, *National Energy Technology Laboratory. US Department of Energy. Washington, DC, USA*.

Li, S., M. Dong, Z. Li, S. Huang, H. Qing, and E. Nickel (2005), Gas breakthrough pressure for hydrocarbon reservoir seal rocks: implications for the security of long-term CO2 storage in the Weyburn field, *Geofluids*, *5*(4), 326-334.

Li, Z. (2006), *Study of gas diffusion in liquid-saturated porous media for oil recovery and carbon dioxide sequestration*, University of Regina (Canada), Canada.

Li, Z., M. Dong, S. Li, and S. Huang (2006), CO2 sequestration in depleted oil and gas reservoirs—caprock characterization and storage capacity, *Energy Conversion and Management*, *47*(11), 1372-1382.

Mathias, S., P. Hardisty, M. Trudell, and R. Zimmerman (2009a), Approximate Solutions for Pressure Buildup During CO2 Injection in Brine Aquifers, *Transport in Porous Media*, *79*(2), 265-284.

Mathias, S., G. González Martínez de Miguel, K. Thatcher, and R. Zimmerman (2011), Pressure buildup during CO2 injection into a closed brine aquifer, *Transport in Porous Media*, *89*(3), 383-397.

Mathias, S. A., P. E. Hardisty, M. R. Trudell, and R. W. Zimmerman (2009b), Screening and selection of sites for CO2 sequestration based on pressure buildup, *International Journal of Greenhouse Gas Control*, *3*(5), 577-585.

Meinshausen, M., et al. (2011), The RCP greenhouse gas concentrations and their extensions from 1765 to 2300, *Climatic Change*, *109*(1-2), 213-241.

Metz, B., O. Davidson, H. de Coninck, M. Loos, and L. Meyer (2005), IPCC special report on carbon dioxide capture and storage*Rep.*, Intergovernmental Panel on Climate Change, Geneva (Switzerland). Working Group III.

Michael, K., G. Allinson, A. Golab, S. Sharma, and V. Shulakova (2009), CO2 storage in saline aquifers II–Experience from existing storage operations, *Energy Procedia*, *1*(1), 1973-1980.

Michael, K., A. Golab, V. Shulakova, J. Ennis-King, G. Allinson, S. Sharma, and T. Aiken (2010), Geological storage of CO2 in saline aquifers—A review of the experience from existing storage operations, *International Journal of Greenhouse Gas Control*, *4*(4), 659-667.

MIT (2007), The future of coal: options for a carbon-constrained world, edited, The Massachusetts Institute of Technology, Cambridge, MA, USA.

Mukhopadhyay, S., S.-Y. Yang, and H.-D. Yeh (2012), Pressure Buildup During Supercritical Carbon Dioxide Injection From a Partially Penetrating Borehole into Gas Reservoirs, *Transport in Porous Media*, *91*(3), 889-911.

Nordbotten, J., M. Celia, and S. Bachu (2005a), Injection and Storage of CO2 in Deep Saline Aquifers: Analytical Solution for CO2 Plume Evolution During Injection, *Transport in Porous Media*, *58*(3), 339-360.

Nordbotten, J. M. (2004), Sequestration of Carbon in Saline Aquifers Mathematical and Numerical Analysis, 78 pp, University of Bergen, Norway

Nordbotten, J. M., and M. A. Celia (2006a), An improved analytical solution for interface upconing around a well, *Water Resources Research*, *42*(8), W08433.

Nordbotten, J. M., and M. A. Celia (2006b), Similarity solutions for fluid injection into confined aquifers, *Journal of Fluid Mechanics*, *561*, 307.

Nordbotten, J. M., and M. A. Celia (2011), *Geological Storage of CO2: Modeling Approaches for Large-Scale Simulation*, Wiley.

Nordbotten, J. M., M. A. Celia, and S. Bachu (2005b), Injection and Storage of CO2 in Deep Saline Aquifers: Analytical Solution for CO2 Plume Evolution During Injection, *Transport in Porous Media*, *58*(3), 339-360.

Nordbotten, J. M., M. A. Celia, S. Bachu, and H. K. Dahle (2004), Semianalytical Solution for CO2 Leakage through an Abandoned Well, *Environmental Science & Technology*, *39*(2), 602-611.

Nordbotten, J. M., M. A. Celia, H. K. Dahle, and S. M. Hassanizadeh (2008), On the definition of macroscale pressure for multiphase flow in porous media, *Water Resour. Res.*, *44*(6), W06S02.

Obi, E. O. I., and M. J. Blunt (2006), Streamline-based simulation of carbon dioxide storage in a north sea aquifer, *Water Resources Research*, *42*(3), W03414.

Oldenburg, C., and S. Benson (2002), CO2 injection for enhanced gas production and carbon sequestration, paper presented at SPE International Petroleum Conference and Exhibition in Mexico.

Oldenburg, C., and C. Doughty (2011), Injection, Flow, and Mixing of CO2 in Porous Media with Residual Gas, *Transport in Porous Media*, *90*(1), 201-218.

Oldenburg, C., K. Pruess, and S. M. Benson (2001), Process modeling of CO2 injection into natural gas reservoirs for carbon sequestration and enhanced gas recovery, *Energy & Fuels*, *15*(2), 293-298.

Oldenburg, C. M. (2006), Geologic carbon sequestration: CO2 transport in depleted gas reservoirs, in *Gas Transport in Porous Media*, edited, pp. 419-426, Springer.

Oruganti, Y., A. K. Gupta, and S. L. Bryant (2011), Analytical estimation of risk due to pressure buildup during CO2 injection in deep saline aquifers, *Energy Procedia*, *4*(0), 4140-4147.

Pacala, S., and R. Socolow (2004), Stabilization Wedges: Solving the Climate Problem for the Next 50 Years with Current Technologies, *Science*, *305*(5686), 968-972.

Plasynski, S., J. Litynski, H. McIlvried, and R. Srivastava (2009), Progress and new developments in carbon capture and storage, *Critical Reviews in Plant Science*, *28*(3), 123-138.

Rao, A. B., and E. S. Rubin (2002), A technical, economic, and environmental assessment of amine-based CO2 capture technology for power plant greenhouse gas control, *Environmental Science & Technology*, *36*(20), 4467-4475.

Roose, T., A. C. Fowler, and P. R. Darrah (2001), A mathematical model of plant nutrient uptake, *Journal of Mathematical Biology*, *42*(4), 347-360.

Saripalli, P., and P. McGrail (2002), Semi-analytical approaches to modeling deep well injection of CO2 for geological sequestration, *Energy Conversion and Management*, *43*(2), 185-198.

Schnaar, G., and D. C. Digiulio (2009), Computational modeling of the geologic sequestration of carbon dioxide, *Vadose Zone Journal*, *8*(2), 389-403.

Sheppard, M. C., and R. H. Socolow (2007), Sustaining fossil fuel use in a carbon-constrained world by rapid commercialization of carbon capture and sequestration, *AIChE Journal*, *53*(12), 3022-3028.

Shi, J.-Q., and S. Durucan (2005), A model for changes in coalbed permeability during primary and enhanced methane recovery, *SPE Reservoir Evaluation & Engineering*, *8*(4), 291-299.

Stevens, S., J. Pearce, and A. Rigg (2001), Natural analogs for geologic storage of CO2: An integrated global research program, paper presented at Proceedings of the First National Conference of Carbon Sequestration, National Energy Technology Laboratory, Washington, DC, USA.

Stevens, S. H., V. A. Kuuskraa, and J. Gale (2000), Sequestration of CO2 in depleted oil and gas fields: global capacity, costs and barriers, paper presented at Proceedings of the 5th International Conference on Greenhouse Gas Control Technologies (GHGT-5), DJ Williams, RA Durie, P. McMullan, CAJ Paulson and AY Smith (eds.).

Stevens, S. H., V. A. Kuuskraa, D. Spector, and P. Riemer (1999), CO2 sequestration in deep coal seams: pilot results and worldwide potential, *Greenhouse Gas Control Technologies*, 175-180.

Theis, C. V. (1935), *The relation between the lowering of the piezometric surface and the rate and duration of discharge of a well using ground water storage*, US Department of the Interior, Geological Survey, Water Resources Division, Ground Water Branch.

Van der Meer, L. (1992), Investigations regarding the storage of carbon dioxide in aquifers in the Netherlands, *Energy Conversion and Management*, *33*(5), 611-618.

Vilarrasa, V., D. Bolster, S. Olivella, and J. Carrera (2010a), Coupled hydromechanical modeling of CO2 sequestration in deep saline aquifers, *International Journal of Greenhouse Gas Control*, *4*(6), 910-919.

Vilarrasa, V., J. Carrera, D. Bolster, and M. Dentz (2013), Semianalytical Solution for CO2 Plume Shape and Pressure Evolution During CO2 Injection in Deep Saline Formations, *Transport in Porous Media*, *97*(1), 43-65.

Vilarrasa, V., D. Bolster, M. Dentz, S. Olivella, and J. Carrera (2010b), Effects of CO2 Compressibility on CO2 Storage in Deep Saline Aquifers, *Transport in Porous Media*, *85*(2), 619-639.

Whittaker, S., D. White, D. Law, and R. Chalaturnyk (2004), IEA GHG Weyburn CO2 monitoring & storage project. Summary report 2000-2004, in *published in the proceeding of the 7th International Conference on Greenhouse Gas Control Technologies, September*, edited, pp. 5-9.

Wiese, B., and S. A. Mathias (2010), Semi-analytical solution for constant pressure injection of CO2 in saline aquifers, paper presented at International Conference on Greenhouse Gas Technologies (GHGT), Amsterdam.

Wright, I. W. (2007), The In Salah gas CO2 storage project, paper presented at International Petroleum Technology Conference, Dubai, UAE.

Xu, T., and K. Pruess (2001), Modeling multiphase non-isothermal fluid flow and reactive geochemical transport in variably saturated fractured rocks: 1. Methodology, *American Journal of Science*, *301*(1), 16-33.

Xu, T., J. A. Apps, and K. Pruess (2004), Numerical simulation of CO2 disposal by mineral trapping in deep aquifers, *Applied Geochemistry*, *19*(6), 917-936.

Zeidouni, M., M. Pooladi-Darvish, and D. Keith (2009), Analytical solution to evaluate salt precipitation during CO2 injection in saline aquifers, *International Journal of Greenhouse Gas Control*, *3*(5), 600-611.

Zhou, Q., J. T. Birkholzer, and C.-F. Tsang (2009), A semi-analytical solution for large-scale injection-induced pressure perturbation and leakage in a laterally bounded aquifer–aquitard system, *Transport in Porous Media*, *78*(1), 127-148.